SERVICE LIFE ASSESSMENT OF SOLID ROCKET PROPELLANTS CONSIDERING RANDOM THERMAL AND VIBRATORY LOADS

A THESIS SUBMITTED TO
THE GRADUATE SCHOOL OF GRADUATE SCHOOL OF APPLIED SCIENCES
OF
MIDDLE EAST TECHNICAL UNIVERSITY

BY

OKAN YILMAZ

IN PARTIAL FULFILLMENT OF THE REQUIREMENTS
FOR
THE DEGREE OF MASTER OF SCIENCE
IN
MECHANICAL ENGINEERING

AUGUST 2012

Approval of the thesis:

SERVICE LIFE ASSESSMENT OF SOLID ROCKET PROPELLANTS CONSIDERING RANDOM THERMAL AND VIBRATORY LOADS

submitted by **OKAN YILMAZ** in partial fulfillment of the requirements for the degree of **Master of Science in Mechanical Engineering Department, Middle East Technical University** by,

Prof. Dr. Canan Özgen _____
Dean, Graduate School of **Natural and Applied Sciences**

Prof. Dr. Süha Oral _____
Head of Department, **Mechanical Engineering**

Assist. Prof. Dr. Gökhan Özgen _____
Supervisor, **Mechanical Engineering Department**

M. Sc. Bayındır Kuran _____
Co-supervisor, **ROKETSAN**

Examining Committee Members:

Prof. Dr. Suat Kadıoğlu
Mechanical Engineering Department, METU _____

Assist. Prof. Dr. Gökhan Özgen
Mechanical Engineering Department, METU _____

M. Sc. Bayındır Kuran
ROKETSAN _____

Assist. Prof. Dr. Ender Ciğeroğlu
Mechanical Engineering Department, METU _____

Assist. Prof. Dr. Demirkan Çöker
Aerospace Engineering Department, METU _____

Date: _____

I hereby declare that all information in this document has been obtained and presented in accordance with academic rules and ethical conduct. I also declare that, as required by these rules and conduct, I have fully cited and referenced all material and results that are not original to this work.

Name, Last Name: OKAN YILMAZ

Signature :

ABSTRACT

SERVICE LIFE ASSESSMENT OF SOLID ROCKET PROPELLANTS CONSIDERING RANDOM THERMAL AND VIBRATORY LOADS

Yılmaz, Okan

M.S., Department of Mechanical Engineering

Supervisor : Assist. Prof. Dr. Gökhan Özgen

Co-Supervisor : M. Sc. Bayındır Kuran

August 2012, 104 pages

In this study, a detailed service life assessment procedure for solid propellant rockets under random environmental temperature and transportation loads is introduced. During storage and deployment of rocket motors, uncontrolled thermal environments and random vibratory loads due to transportation induce random stresses and strains in the propellant which provoke mechanical damage. In addition, structural capability degrades due to environmental conditions and induced stresses and strains as well as material capability parameters have inherent uncertainties. In this proposed probabilistic service life prediction, uncertainties along with degradation mechanisms are taken into consideration. Vibration loads are accounted by utilizing acceleration spectral density values which are induced during various deployment scenarios of ground, air and sea transportation. Furthermore, thermal loads are represented with a mathematical model being a harmonic function of time. Throughout the finite element analyses, a linear viscoelastic material model is to be used for the propellant. Change in the structural capability of the propellant with time is calculated using Laheru's cumulative damage model. Moreover, to include aging effect of the propellant, Layton model is used. To determine the effects of induced stress and strains under variations and uncertainties in the random loads and material constants, mathematical surrogate models are constructed using

response surface method. Limit state functions are utilized to predict failure modes of the solid rocket motor. First order reliability method is used to calculate reliability and probability of failure of the propellant grain. With the proposed methodology, instantaneous reliability of the propellant grain is determined within a confidence interval.

Keywords: service life, solid propellant, rocket motor, reliability, finite element method

ÖZ

RASTLANTISAL ISIL VE TİTREŞİM YÜKLERİ ALTINDAKİ KATI YAKITLI ROKETLERDE ÖMÜR BELİRLENMESİ

Yılmaz, Okan
Yüksek Lisans, Makine Mühendisliği Bölümü
Tez Yöneticisi : Y. Doç. Dr. Gökhan Özgen
Ortak Tez Yöneticisi : Yük. Müh. Bayındır Kuran

Ağustos 2012, 104 sayfa

Bu tez çalışmasında, rastlantısal çevresel sıcaklık ve taşıma yüklerine maruz kalan katı yakıtlı roket motorlarının servis ömürlerinin belirlenebilmesi için detaylı bir yöntemler dizesi sunulmaktadır. Roket motorlarının depolama ve taşıma safhalarında karşılaşılan kontrolsüz ısıl yükler ve rastlantısal titreşim yükleri katı yakıtlı motorların yakıtlarında gerilme ve gerinim yüklenmesine, dolayısıyla mekanik hasara yol açar. Bunlara ek olarak, malzemenin yapısal kapasitesi çevresel faktörlere ve yüklere bağlı olarak aşınmaya uğramakta ve malzeme özellikleri ile beraber belirsizlik göstermektedir. Bu çalışmada sunulan olasılıksal ömür belirleme yönteminde aşınma mekanizmaları ve belirsizlikler dikkate alınmaktadırlar. Titreşim yükleri, hava, yer ve deniz taşıması gibi taşıma senaryoları göz önünde bulundurularak, bu senaryolar sonucunda elde edilecek ivme spektral yoğunluk değerleriyle hesaba katılmıştır. Isıl yükler için ise zamana bağlı harmonik fonksiyonlardan oluşan bir matematik model oluşturulmuştur. Ömür belirleme kapsamında yapılacak olan sonlu elemanlar analizlerde yakıt için doğrusal viskoelastik malzeme modeli kullanılmıştır. Yakıtın yapısal kapasitesinde görülecek aşınma Laheru'nun birikmiş hasar modeli kullanılarak hesaplanmış, yaşlanma etkisini hesaba katmak için ise Layton modeli kullanılmıştır. Rastlantısal yüklerdeki ve malzeme özelliklerindeki varyasyonları ve belirsizlikleri değerlendirebilmek amacıyla cevap yüzeyi metodu kullanılarak

matematiksel modeller oluşturulmuştur. Yakıt çekirdeğindeki başarısızlık modlarının değerlendirilmesi için sınır durumu fonksiyonları oluşturulmuştur. Birinci derece güvenilirlik yöntemi kullanılarak yakıt çekirdeğinin güvenilirliği ve başarısızlık olasılığı hesaplanmıştır. Bu tez çalışmasında yer alan yöntemler dizesi kullanılarak, yakıtın çekirdeğinin anlık güvenilirliği bir güvenlik aralığı içerisinde belirlenebilmektedir.

Anahtar Kelimeler: servis ömrü, katı yakıt, roket motoru, güvenilirlik, sonlu elemanlar metodu

To my beloved family,

ACKNOWLEDGMENTS

I would like to express my gratitude to my supervisor Assist. Prof. Dr. Gökhan ÖZGEN for his guidance throughout the study. His encouragement, support and suggestions made this long lasting work successful.

My sincere thanks go to my manager and co-supervisor Mr. Bayındır KURAN, who encourage me to choose this topic and work in this field. Without his guidance and valuable feedback, this work would not be possible. He has provided assistance in numerous ways and helped me to shape my interest and ideas.

I would like to thank my colleagues at Structural, Thermal and Dynamical Design Department of ROKETSAN for their valuable support and friendship. Thanks to them, I worked in a productive and friendly environment and excel my knowledge greatly in several fields of engineering. My special thanks go to my chief Mr. Bülent ACAR for enhancing my vision with his vast experience and knowledge. I also thank him for supporting my ideas and goals during the time we have worked together.

In addition, I greatly acknowledge ROKETSAN for supporting the thesis and made this research possible.

I am also grateful to TÜBİTAK for financially supporting me throughout my master studies.

I am deeply and forever indebted to my parents, my brother and my fiancee Elif ERTEM for their love, understanding and encouragement throughout my entire life.

TABLE OF CONTENTS

LIST OF TABLES

TABLES

LIST OF FIGURES

FIGURES

LIST OF ABBREVIATIONS

NATO North Atlantic Treaty Organization

STANAG Standardization agreement

ASTM American Society for Testing and Materials

JANNAF Joint-Army-Navy-NASA-Air Force

WLF Williams-Landel-Ferry

LE Linear elastic

LVE Linear viscoelastic

NLVE Nonlinear viscoelastic

FORM First order reliability method

SORM Second order reliability method

LHS Latin hypercube sampling

FCC Face centered cube

ASD Acceleration spectral density

FEM Finite element method

FFT Fast Fourier transform

FRF Frequency response function

PSD Power spectral density

RSM Response surface method

MVFOSM Mean value first order second moment

E Young's modulus of elasticity

σ Normal stress

ϵ Strain

J Elastic compliance

τ Shear stress

η Viscosity

$E(t)$ Relaxation modulus

τ_r Relaxation time

τ_c Creep or retardation time

$E(\omega)$ Complex modulus

$E'(\omega)$ Storage modulus

$E''(\omega)$ Loss modulus

$G'(\omega)$ Shear storage modulus

$G''(\omega)$ Shear loss modulus

$\eta(\omega)$ Loss factor

$tan(\phi)$ Shear loss tangent

a_T Shift factor

C_1 First constant of WLF shift function

C_2 Second constant of WLF shift function

T_0 Reference temperature

D Damage factor

t_{fi} Time to failure at ith stress level

N Lebesgue form of stress

β Second parameter of the cumulative damage model

k Rate of change of property at any arbitrary age time

E_a Activation energy

R Ideal gas constant

A Arrhenius equation constant

T_M Mean value of the storage temperature

T_Y Yearly storage temperature amplitude

T_D Daily storage temperature amplitude

t_0 Yearly storage temperature phase

t_1 Daily storage temperature phase

G_∞ Equilibrium shear modulus

α Coefficient of thermal expansion

$T_{str,free}$ Stress-strain free temperature of the propellant

T_{cure} Cure temperature of the propellant

$S_j(\omega)$ Spectral density for maximum principal stress

$H_{ja}(\omega)$ Frequency response function for the maximum principal stress

$S_a(\omega)$ Acceleration spectral density

y System output (response values)

X_i Input parameters affecting output

r^2 Coefficient of determination

S_r Sum squares of errors

S_t Sum of squares

$y(X)^L$ Lower bound of the system output

$y(X)^U$ Upper bound of the system output

$D(t)_{total}$ Total damage factor

$D(t)_{th}$ Damage resulting from thermal loads

$D(t)_{vb}$ Damage resulting from vibratory loads

g_1 Limit state function for the stress induced in the propellant grain

g_2 Limit state function for the strain induced in the propellant grain

g_3 Limit state function for the stress induced in the propellant-insulation bondline

σ_{ind} Stress induced in the propellant grain

ϵ_{ind} Strain induced in the propellant grain

σ_{ind}^{bond} Stress induced in the propellant-insulation bondline

σ_{all} Allowable stress of the propellant grain

ϵ_{all} Allowable strain of the propellant grain

g_i Mean for the ith limit state function

g_i^L Lower bound for the ith limit state function

g_i^U Upper bound for the ith limit state function

μ_g Mean value of the limit state function

σ_g Standard deviation of the limit state function

$Var(g)$ Variance of the limit state function

β Reliability (safety) index

ϕ Cumulative distribution function

$\lambda(t)$ Hazard rate

P_{fi} Probability of failure due to ith limit state function

R_i Reliability of the ith limit state function

$P_{f,total}$ Total probability of failure of the system

R_{total} Total reliability of the system

CHAPTER 1

INTRODUCTION

In today's world, solid rocket motors are used as the primary propulsion technology in tactical missiles. Because of this extensive usage, solid rocket motors must be fully functional in different storage and handling environments. The motivation of this study is to predict the service life of the rocket motor under these storage and handling environments in early design phases. With this assessment, the safety and mission performance of rocket motor will be assured under real life storage and transportation conditions through predicted time. To make this prediction, an accurate modeling of the components of the rocket motor system must be made. That is done using material characterization tests and finite element modeling. Analyzing this model, stress-strain response of the system to the real life conditions are determined. However, material properties and real life loads have statistical variations. Hence, the assessment is made in a probabilistic manner and reliability of system over time is determined. Solid rocket motor is analyzed against common failure modes such as formation of surface cracks on the propellant grain and debonding of case-insulation-propellant bondline. A sufficient reliability limit is defined for the system to safely operate under the specified loads and reliability of the system is checked to be over this limit during its service life. Passing below this reliability limit, the system is no more considered as safe.

Hence, an accurate prediction of the service life of the rocket motor has to be made to assure that the rocket motor fulfills its mission at various conditions. In this chapter, general characteristics of solid rocket motors are given to have a sound knowledge of the system considered in this study and details of the scope of this study are to be discussed.

1.1 GENERAL CHARACTERISTICS OF SOLID ROCKET MOTORS

The majority of tactical missiles use solid rocket motors and the rocket motor is a structurally important part which represents nearly %50-60 of the system mass [1]. A solid rocket motor can be divided through five major components as listed below [2]. These components are also illustrated in Figure 1.1.

- Case
- Propellant grain
- Thermal insulation
- Nozzle
- Ignition system

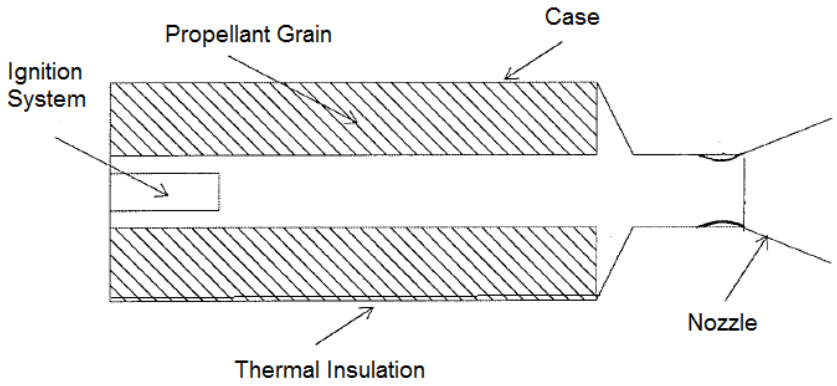

Figure 1.1: Typical rocket motor (Adapted from [1])

1.1.1 Case

The case (or the motor case) of the solid rocket propellant motor is the part the preserve the propellant grain. Apart from storing the propellant grain, it serves as a combustion chamber for high pressure, high temperature burning of the grain while the motor operated. It also provides a structural interface with other motor components, such as nozzle, ignition system

and insulation [3]. The case can be made of metals or composite materials. It acts as a pressure vessel in operation, thus, it must be capable of withstanding the internal pressure which is approximately in range of 3-25 MPa with a sufficiently high safety coefficient [2].

High strength metals and composite materials are the primary choice of materials for the case. Since the motor case part is an inert and non-energy-contributing part, when designing it the primary goal of is to make these part as lightweight as possible, within the bounds of cost and technology [3]. The increasing usage of the composite materials for solid motor cases serves that purpose since with wound composite cases, dramatic weight losses can be obtained with the same level of strength. For example, in a reported study [4], within the use of filament-wound composite cases for solid rocket motors, a propellant mass fraction (ratio of propellant mass to total motor mass) of 90-95% is achieved, which is an impressive value.

1.1.2 Propellant Grain

Propellant grains are to be designed such that adequate thrust can be given to the rocket motor so the motor can fulfill its mission. Grain designers try to meet the thrust profile requirements with material selection and geometrical design for the propellant. At the same time, structural integrity of the propellant grain should be maintained which is the responsibility of structural analysts through the design phase. Hence, to meet the ballistic and structural requirements at the same time, in general, an iterative design process is carried out between the ballistic and structural designers.

There are two types of grain configurations, namely the cartridge-loaded and case-bonded grains [1]. Cartridge-loaded (free-standing) grains are manufactured separately and then assembled to the case. In case-bonded grains, the case is used as mold and the grain is injected to the case where it bonds with the case and insulation. Main advantage of cartridge-loaded grains is that the excessively aged propellants can be replaced. This type of grain configuration is used for rather small tactical missiles. Nevertheless, better performance characteristics are obtained with the case-bonded motors and almost all of larger motors use case-bonded type [5].

Performance characteristics are defined with the material and geometric shape of the propellant grain. Various shapes of propellant grain is used in rocket motors such as star, wagon

wheel, multiperforated, dog bone and dendrite as illustrated in Figure 1.2. Moreover, the use of slots, radial grooves and tube are illustrated in the same figure.

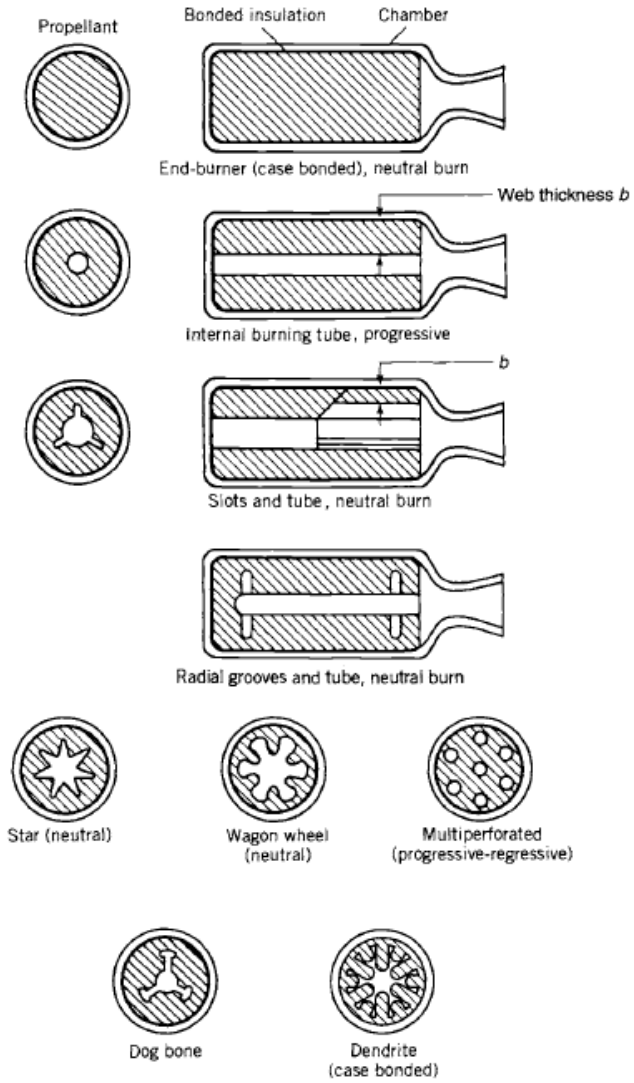

Figure 1.2: Simplified diagrams of various propellant grain configurations [5]

1.1.3 Thermal Insulation

Inside surface of the case requires a means for thermal protection since the combustion temperature of propellant grains ranges approximately from 1500 K to 3500 K [2]. Apart from the protection, structural integrity of case, insulation and propellant must be maintained during the life of the rocket motor. Bonding with case and propellant grain, thermal insulation mate-

rial provides this integrity. For the thermal insulation, generally elastomer materials showing good thermal insulation characteristics are used.

1.1.4 Nozzle

The main function of the nozzle is to channel and control expansion of hot gases coming from the combustion chamber, thus generating the necessary thrust [3]. Nozzles are designed to satisfy various performance criteria such as burning time, operating pressure, weight, space available, expansion ratio, thermal ablation and cost. These performance parameters lead to the design of materials with good thermal insulation and strength characteristics [2].

1.1.5 Ignition System

The ignition system provides the necessary energy to the surface of the propellant to initiate burning [2]. The system has total of three stages which are initiation, booster charging and main charging. A pyrotechnic element transforms the ignition signal to the booster charge where a micro-rocket transmits the flame to the main charge which then ignites the propellant grain.

1.2 SCOPE OF THE THESIS

Determination of the service life of these rocket motors plays an important role especially in early design phases. Service life is defined as the time that the rocket motor is able to operate safely under the real life loads. Since solid rocket motors are expensive and critical designs, several methodologies are developed to accurately determine the service life that the motor fulfils the operation requirements. Conservative service life values are specified for the rocket motor designs without a comprehensive service life study. With an accurate determination of service life, designed rocket motor can be used safely in that specified time with confidence and expensive life extension programs of solid rocket motors may be avoided in the first place. Furthermore, if service life assessment is done in early design phases, slight changes in propellant grain design can be made with using the outputs of this type of study. To sum up, the main goal of service life studies is to provide the most accurate and reliable prediction

of possible system life with assuring safety, effective cost and mission performance [6].

In this study, a service life methodology that takes the storage and transportation loads on solid rocket motors into account is presented. During its life cycle, the rocket motor experiences thermal loads owing to the environment that it is stored and vibratory loads as a result of transportation between the manufacturing site, storage site and forward base. Considering all the loads that the rocket motor may encounter during its life, a prediction of service life is made in this study.

Material behaviour of the solid propellants are explained in detail and a linear viscoelastic material model which have been used for the solid propellant is presented in this study. Material properties have inherent uncertainty, thus, parameters of material model are defined in a specified range or with a mean and a deviation. Apart from the material model used for the solid propellant, cumulative damage and aging mechanisms of the solid propellant are explained in detail.

Thermal loads on the system are due to the variation of environmental temperature with time. To account this variation, an environmental temperature model is utilized using harmonic functions of time. Furthermore, there are vibratory loads owing to transportation between the manufacturing site to the storage site or the forward base. The transportation of solid rocket motors are done by means of trucks, planes or ships. In other words, scenarios for ground, air and sea transportation must be considered to analyze the solid rocket motor system. Several transportation types are accounted using the acceleration spectral density functions. Parameters of the environmental thermal and vibration loads are also defined with some uncertainty like the parameters of the material model. These variable material and loading parameters are then sampled with using different sampling methods to utilize deterministic finite element analysis sets. The term sampling is used in this study in a statistical fashion. It means a selection of subsets of individuals to estimate the behavior of whole population. To estimate the characteristics accurately, this sampling process must be based on verified algorithms and methods. Latin hypercube sampling (LHS) method is used to sample the finite element analysis sets for the thermomechanical storage analysis and face centered cube (FCC) design is used to sample vibration analysis sets for the transportation.

Then, using commercial finite element method tools, namely MSC.Marc and MSC.Nastran, finite element analyses are conducted. MSC.Marc is used to conduct thermomechanical

analyses and for the vibration analyses MSC.Nastran is used. Stress-strain response of the propellant grain in thermomechanical analysis is decomposed using fast Fourier transform (FFT). With this decomposition, mathematical models for the thermomechanical stress-strain response of the propellant grain can be utilized. Moreover, a power spectral density analysis is done using the acceleration spectral density of various transportation scenarios and frequency response function outputs of the vibration analysis.

Using the results of FFT and PSD analyses, mathematical models for the storage and transportation scenarios are utilized using response surface methodology with a specified confidence interval. In other words, results of the analyses are fitted into a mathematical response surface. Determining a mathematical response expression for both thermomechanical and vibratory responses, mechanical damage accumulated on the system is combined using damage factor approach method. Then, limit state approximation is used to predict the failure. Two different failure modes are defined for the solid rocket motor in this study. First failure mode is the formation of surface cracks in the propellant grain and second is the separation of case-insulation-propellant bondline. To predict the modes which will lead to failure of the system, limit state (performance) functions are utilized. These limit state functions are a comparison of induced stress and strain in the propellant and propellant bondline against the allowable strain and stress values of the propellant. Finally, using these performance function which states our failure criteria, probability of failure and reliability of the system can be obtained using first order reliability method (FORM). An assessment of reliability in a specified confidence interval limit is made and a life prediction based on a specific reliability allocation value is presented at the end of this study.

General methodology that has been followed in this study is presented in Figure 1.3.

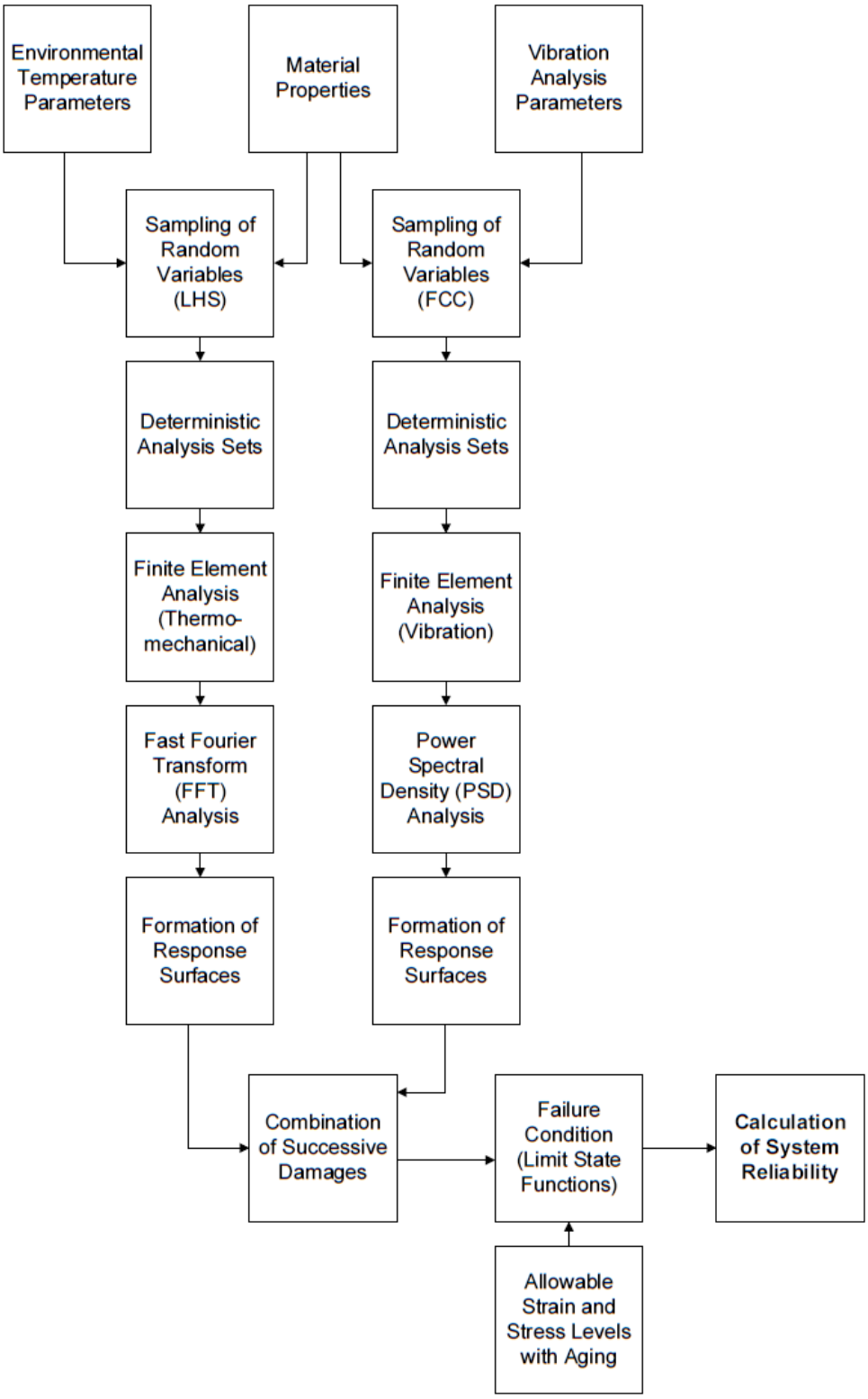

Figure 1.3: Methodology of the service life assessment

1.3 ORGANIZATION OF THE THESIS

In this chapter, a brief introduction about solid rocket motors is given and general characteristics are explained. Also, detailed information about the scope of the study is introduced.

In Chapter 2, which is reserved for literature survey on the subject manner, viscoelastic behavior of solid propellant is explained with the concepts of stress relaxation and creep. After the introduction of viscoelastic solids, material characterization of solid propellants are demonstrated which is done with conducting several material tests. Construction of master curves are described and thermorheologically simple behavior of solid propellants are introduced. Apart from the utilization of linear viscoelastic model for the solid propellant, aging and cumulative damage mechanisms are introduced. At the end of this chapter a survey for the service life studies in the literature is presented.

Chapter 3 consists of the physical aspects of the solid rocket motor system and definition of material and loading models. Loads in the solid rocket motor's life cycle have been determined and failure modes of the solid rocket motor are demonstrated. Then, environmental temperature model and acceleration spectral density values for the transportation scenarios are explained in detail. Sampling algorithms which has been used to utilize deterministic finite element analysis sets are also introduced in this chapter.

In Chapter 4, finite element analyses that have been used in this study are explained in detail. Boundary conditions, stress-strain response of the system and frequency response function outputs are illustrated. Furthermore, interpretation of these results are given. Fast Fourier transform and power spectral density analyses are explained in detail and results are presented.

Reliability assessment of the solid rocket motor system is demonstrated in Chapter 5. At the beginning of this chapter, formation of response surfaces in a confidence interval are explained. The effect of degradation mechanisms, cumulative damage and aging is illustrated with figures. Then, the limit state functions are introduced and using the first order reliability method, total reliability and probability of failure of the system is determined.

Chapter 6 summarizes the service life assessment study. A discussion of the outputs of this study is introduced. Furthermore, some recommendation for the future work are given at the end of this chapter.

CHAPTER 2

LITERATURE SURVEY

Literature survey is made up of two sections. The first section is about the material behaviour of solid propellants and other section summarizes the service life prediction studies of solid propellant rocket systems. Selecting the constitutive material model for the solid propellant is important for the structural analysis, since failure prediction in the system is made from the stress and strain response of the finite element model. There is a continuing research in the material modeling of solid propellants and a variety of material models are used from simple linear elastic models to complex nonlinear viscoelastic models. As mentioned above, the second major section in this chapter is devoted to service life studies of solid propellant rocket motors. Different methodologies have been developed for the evaluation of critical missile systems over time, from crude deterministic approaches to detailed probabilistic analysis. These approaches will be summarized in the second part.

2.1 PROPELLANT BEHAVIOR

The components found in solid rocket motors have complex behaviour under even simple loading conditions (propellant grain, insulation and in some designs, composite cases). This complex material behaviour, under various loading conditions, has not been completely described by any single material constitutive law yet [1].

The constitutive model for the propellant grain can be considered in a variety of forms. For a time varying approach, a linear viscoelastic material definition can be used [1]. Considering the experience and widespread usage of the linear viscoelastic model in the literature, this type of material model will be used in this study. To understand the viscoelastic nature of the pro-

pellants better, this section is devoted to viscoelastic solids and the material characterization of the solid propellants.

2.1.1 Viscoelastic Solid

For small strains, Hooke's law of linear elasticity is used to describe materials where stress is proportional to strain with a constant, E, namely Young's modulus.

$$\sigma = E \cdot \epsilon \tag{2.1}$$

Moreover, inverse of the modulus can be expressed as the elastic compliance, J.

$$J = \frac{1}{E} \tag{2.2}$$

In difference to elastic materials, viscous fluids under shear strains are described using Newton's law of viscosity, where viscosity is denoted by η.

$$\tau = \eta \cdot \frac{d\epsilon}{dt} \tag{2.3}$$

In reality, all materials show deviation from Hooke's law in different ways. Viscoelastic materials are those for which the relationship between stress and strain depends on time [7]. Some important phenomena that is typical in viscoelastic materials are creep and stress relaxation. Increasing strain under a constant load is named as creep behaviour, where a decreasing stress under a constant elongation load is addressed as stress relaxation. Forthcoming sections are devoted to explain these phenomena.

2.1.1.1 Creep

Creep behaviour can be defined as a slow, progressive deformation of a material under a constant load [7]. Considering a constant load, elastic compliance of a viscoelastic material as a function of time can be written as follows,

$$J(t) = \frac{\epsilon(t)}{\sigma_0} \tag{2.4}$$

Considering a step input of stress, strain history of a viscoelastic solid can be illustrated as in Figure 2.1 . Whereas elastic materials show an immediate recovery from creep, viscoelastic materials recover after sufficient time passes. Viscous materials show no recovery behaviour.

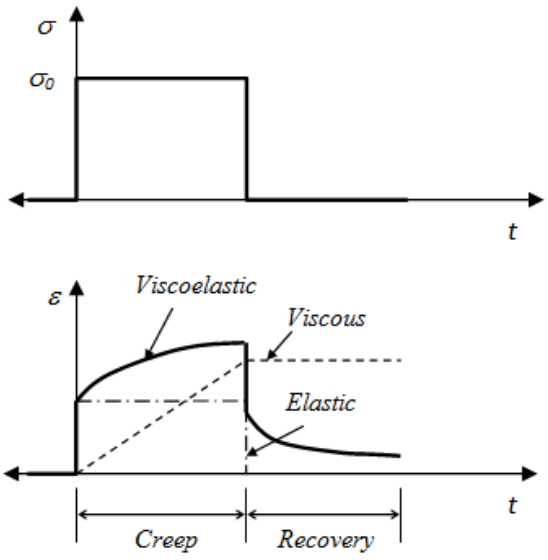

Figure 2.1: Creep and recovery phenomena in viscoelastic solids [8]

2.1.1.2 Stress Relaxation

Stress relaxation behaviour is defined as the gradual decrease of the stress when the material is held at constant strain [7]. Considering a elongation load, Young's modulus of a viscoelastic material as a function of time can be written as follows, and called relaxation modulus. In linear materials, the relaxation modulus do not change with the strain level, so it is a function of time only.

$$E(t) = \frac{\sigma(t)}{\epsilon_0} \tag{2.5}$$

Considering a step input of strain, stress history of a viscoelastic solid can be illustrated as in Figure 2.2. Similar to creep, elastic materials show an immediate recovery from relaxation

and viscoelastic materials recover after sufficient time passes.

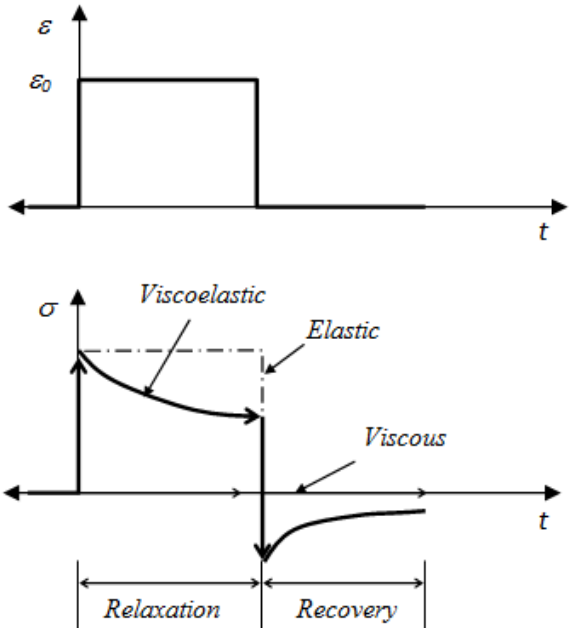

Figure 2.2: Stress relaxation and recovery phenomena in viscoelastic solids [8]

2.1.1.3 Mechanical Material Models

To develop mathematical models for materials, usage of mechanical analogies is a common practice. For example, consider a linear elastic material obeying Hooke's law. This material can be represented using an ideal spring only as shown in Figure 2.3. In this model, strain is analogous to displacement and the stress is analogous to force. Hence, Young's modulus is the spring constant in this model.

To introduce the effect of viscous behaviour, ideal dampers are used and spring-dashpot model which is seen in Figure 2.4 is called Maxwell model [7]. In this model, the equation relating the strain to stress becomes:

$$\frac{d\epsilon}{dt} = \frac{1}{E} \cdot \frac{d\sigma}{dt} + \frac{\sigma}{\eta} \tag{2.6}$$

Figure 2.3: Mechanical analogy of Hooke's law

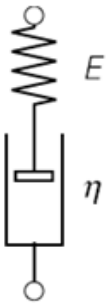

Figure 2.4: Maxwell material model

A variable called relaxation time, τ can be introduced at this point.

$$\tau = \frac{\eta}{E} \tag{2.7}$$

If a step strain is given to the Maxwell element, the relaxation response will become:

$$E(t) = E_0 \cdot exp(\frac{-t}{\tau}) \tag{2.8}$$

However, if a step stress is given, the creep response will be in the form of Equation 2.9 which is linear with respect to time and rather unrealistic considering the experimental creep behaviour.

$$J(t) = \frac{1}{E} + \frac{t}{\tau} \tag{2.9}$$

Hence, Kelvin-Voigt material model is introduced to model creep more realistically in which

the spring and dashpot are connected in parallel [7]. This material model can be seen in Figure 2.5.

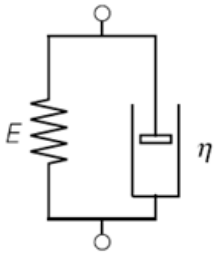

Figure 2.5: Kelvin-Voigt material model

Creep response of a Kelvin-Voigt model becomes:

$$J(t) = \frac{1}{E} \cdot (1 - exp(\frac{t}{\tau})) \tag{2.10}$$

Although the model gives a good representation of creep behaviour, relaxation response is unrealistic. To have realistic behaviour in both creep and relaxation, standard linear model can be used [7]. The model is illustrated in Figure 2.6.

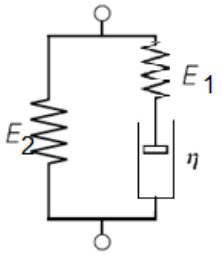

Figure 2.6: Standard linear material model

Using this model one will get the relaxation response as,

$$E(t) = E_2 + E_1 \cdot exp(\frac{-t}{\tau_r}) \tag{2.11}$$

where $\tau_r = \tau$, and called as relaxation time. Similarly, creep response of the standard linear

model can be written as

$$J(t) = \frac{1}{E_2} + \frac{E_1}{E_2 \cdot (E_1 + E_2)} \cdot exp(\frac{-t}{\tau_c}) \tag{2.12}$$

where τ_c is named creep or retardation time and denoted as:

$$\tau_c = \tau_r \cdot \frac{(E_1 + E_2)}{E_2} \tag{2.13}$$

Another material model that is being used frequently is generalized Maxwell model, in which N number of Maxwell elements are connected in parallel as seen in Figure 2.7 [8].

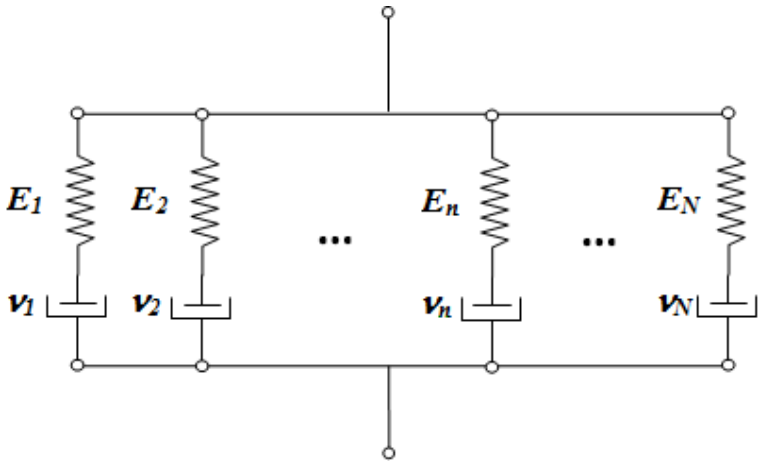

Figure 2.7: Generalized Maxwell material model [8]

Relaxation response in this material model becomes:

$$E(t) = \sum_{i=1}^{N} E_i \cdot exp(\frac{-t}{\tau_i}) \tag{2.14}$$

However, in this material model, relaxation modulus goes to zero as time goes to infinity. It is known that in viscoelastic solids, relaxation modulus approaches a non-zero value. Hence, modified generalized Maxwell model is built with connecting an elastic element as illustrated in Figure 2.8.

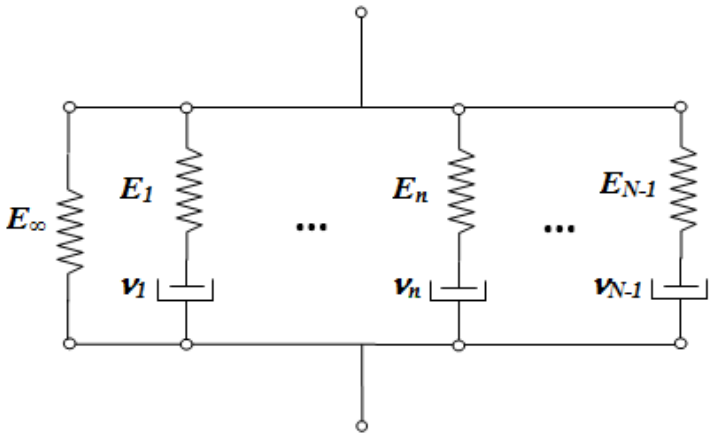

Figure 2.8: Modified generalized Maxwell material model

Now, the relaxation modulus of viscoelastic solids can be expressed in a more realistic way using modified generalized Maxwell model.

$$E(t) = E_\infty + \sum_{i=1}^{N} -1E_i \cdot exp(\frac{-t}{\tau_i}) \tag{2.15}$$

The form of given series has the same form with the mathematical expression called Prony series, and it is a common way of representing the relaxation modulus of viscoelastic solids.

2.1.1.4 Dynamic Behaviour

Viscoelastic materials in general show good damping characteristics and they are widely used in passive vibration isolation systems. Since propellant grain of solid rocket motor is a viscoelastic material, its damping characteristics must be determined.

For a linear elastic material, stress-strain relationships can be written as,

$$\tau = G \cdot \phi \tag{2.16}$$

$$\sigma = E \cdot \epsilon \tag{2.17}$$

where shear deformation is denoted by ϕ and extensional deformation is expressed by ϵ [9].

However, for most engineering problems, it is more convenient to work in frequency domain when studying the mechanical vibrational behavior of viscoelastic materials at which case the stress-time and strain-time history are both harmonic [9]. To describe the relationship between stress and strain for harmonic excitation, complex modulus relationships can be used. For shear and extensional deformation, these relationships are

$$\tau = G \cdot (1 + i\eta) \cdot \phi \tag{2.18}$$

$$\sigma = E \cdot (1 + i\eta) \cdot \epsilon \tag{2.19}$$

where again shear deformation is denoted by ϕ, extensional deformation is expressed by ϵ and loss factor is denoted by η [9].

Complex modulus can be expressed alternatively as,

$$E(i\omega) = E'(\omega) + iE''(\omega) \tag{2.20}$$

where E' is denoted as storage modulus and E'' is named loss modulus and they are both functions of frequency. Same relationships can be written for shear modulus also. Moreover, loss factor is expressed as

$$\eta(\omega) = \frac{E''(\omega)}{E'(\omega)} \tag{2.21}$$

Typical frequency domain distributions of modulus and loss factor for viscoelastic solids are illustrated at Figure 2.9. It is seen that at the rubbery region the modulus value is at its minimum and increasing slowly as it enters the transition region. The value of modulus for viscoelastic solids is maximum at glassy region. Loss factor shows a different behaviour. It is at its maximum in transition region and decreases as the viscoelastic materials enters rubbery or glassy regions.

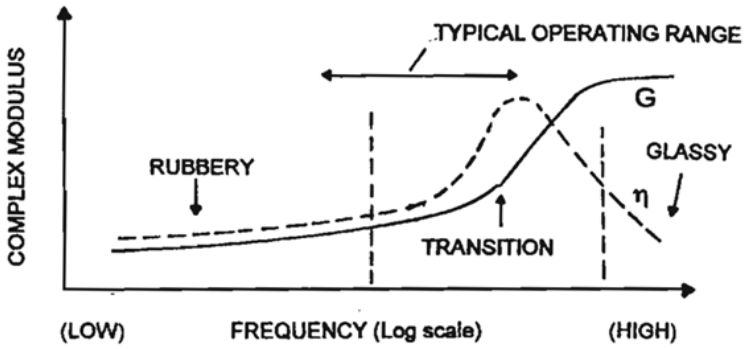

Figure 2.9: Typical modulus and loss factor distributions for viscoelastic solids [9]

2.1.2 Solid Propellant Material Characterization

The propellant behaviour is characterized by failure properties and response to deformation which is a function of the independent relationships of stress, strain, time and temperature. In other words, solid propellants can be named as thermoviscoelastic materials [10]. To characterize these independent relationships, one must conduct various material characterization tests which will be explained in this section.

Material properties that have to be determined in order to generate the input parameters for the structural analysis computations are stress-strain relationship, Poisson's ratio or bulk modulus, density, coefficient of linear thermal expansion, and thermal properties such as specific heat capacity and thermal conductivity [1]. In addition, storage modulus and loss factor is to be determined for the vibration analysis of solid rocket motor.

To determine the stress-strain relationship of a linear viscoelastic material, a series of stress relaxation tests and uniaxial tensile tests are needed to be performed. The propellant can be assumed as an incompressible material. Hence, Poisson's ratio can be taken as 0.5 [1]. For the coefficient of linear thermal expansion, thermomechanical analysis (TMA) is to be done. Moreover, to obtain the specific heat capacity of the propellant, differential scanning calorimetry (DSC) is used. Last, for the vibration parameters of the propellant, dynamic mechanical analysis (DMA) method is used.

Following sections are devoted to explain the test methods need to be followed for determi-

nation of material properties.

2.1.2.1 Stress Relaxation Tests

In this mechanical characterization test, the propellant specimen is subjected to a constant elongation and the stress is calculated over time. Stress relaxation tests are conducted using a NATO standard named STANAG 4507 that is prepared for obtaining the mechanical properties of the explosives materials [11]. Typical specimen arrangements in the specified standard are illustrated in Figure 2.10. It is mandatory to use wood or metal tabs if there is no direct strain control. In this study, untabbed specimens are used with the proposed arrangement with extensometers. Dimensions of the specimen are given in Figure 2.11.

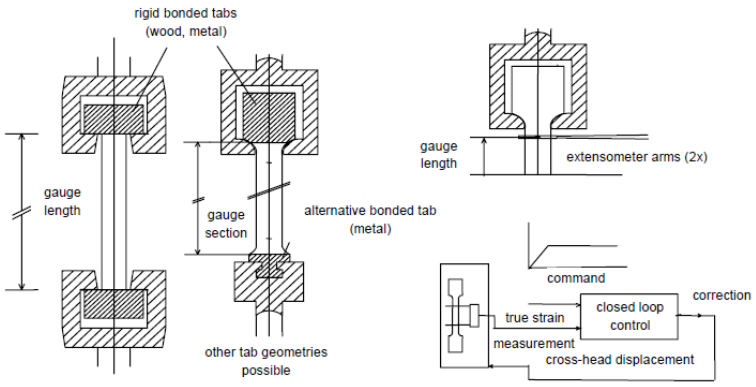

Figure 2.10: Typical test arrangements for tabbed and untabbed specimens [11]

Relaxation modulus is expressed by the ratio of stress calculated over applied strain.

$$E_{rel} = \frac{\sigma(t)}{\epsilon_{app}} \tag{2.22}$$

To characterize the relaxation in solid propellant, tests are conducted at various temperatures, namely at -55 °C, -40 °C, -20 °C, 0 °C, 20 °C, 40 °C, and 60 °C. Normalized results of these tests are shown in Figure 2.12 and they will be used in constructing the master curves of the propellant as explained in Section 2.3.

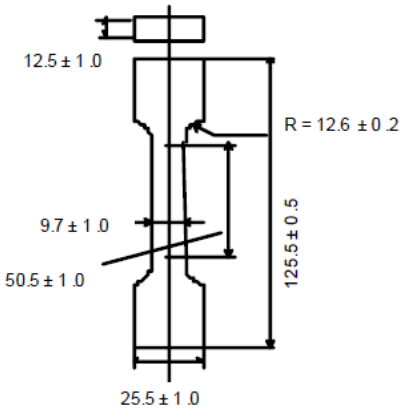

Figure 2.11: Dimensions of untabbed specimen [11]

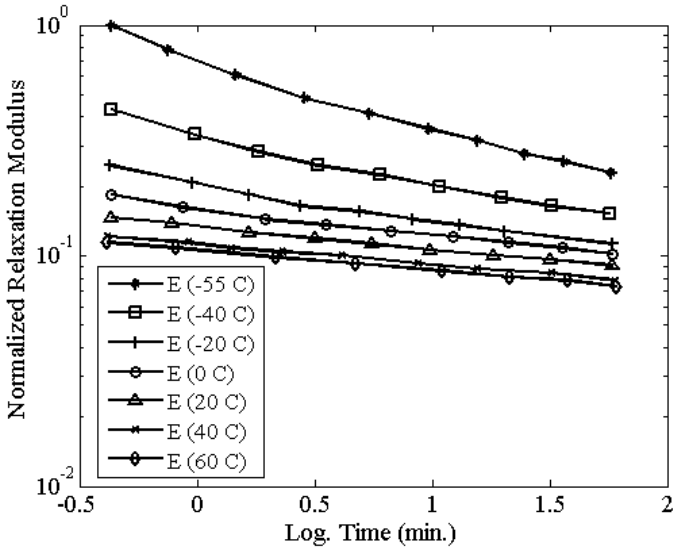

Figure 2.12: Normalized relaxation modulus values at different temperatures

2.1.2.2 Uniaxial Tensile Tests

These tests are conducted at different temperatures and cross-head speeds. The specimen is conditioned at a pre-specified constant temperature and then, subjected to a constant cross-head speed. Stress-strain curves of the propellant specimen are recorded for output.

Uniaxial tensile tests are done using the NATO standard STANAG 4506 which is define a specific test technique for evaluating the tensile properties of solid propellants [12]. Spec-

imen dimensions are standardized by JANNAF (Joint-Army-Navy-NASA-Air Force) and is illustrated in Figure 2.13.

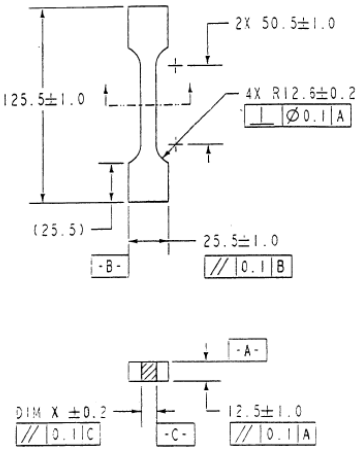

Figure 2.13: Specimen configuration in the uniaxial tensile test [12]

A typical stress-strain curve of the propellant resulting from a constant strain rate uniaxial tensile test is illustrated in Figure 2.14. Both maximum or rupture (break) stress or strain values can be used as the allowable limit of the material. In this study, rupture stress and rupture strain values are used as allowable limits.

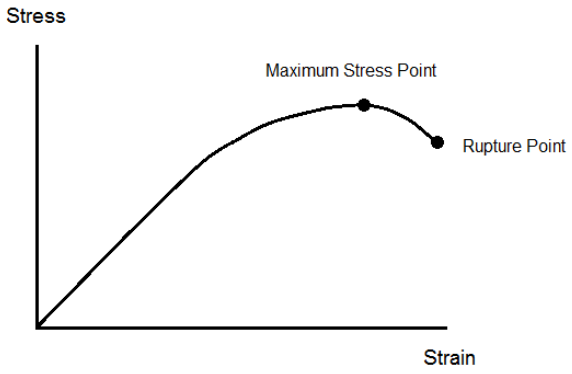

Figure 2.14: Typical stress-strain curve for a solid propellant

As it is mentioned above, tests are conducted at various temperatures and cross-head speeds. In this study tests are conducted in a temperature range varying from -55 °C to 60 °C, and in

a cross-head speed range of 1 mm/min to 500 mm/min. Normalized test results are given in Section 2.1.4 as allowable stress and allowable strain master curves.

From these tests, master curves are prepared for rupture stress and rupture strain parameters. These parameters are used in detecting the failure modes in the solid rocket motor systems explained in Chapter 3.

2.1.2.3 Thermomechanical Analysis (TMA)

Thermomechanical Analysis (TMA) can be defined as the measurement of the length or volume of a specimen as a function of temperature while it is subjected to a constant mechanical load. Using the method, linear thermal expansion coefficient of the solid propellant can be obtained with monitoring the length as a function of temperature.

Coefficient of thermal expansion (CTE) is a parameter of great importance in structural analysis since the temperature differences in solid rocket motors affect the stress and strain states greatly.

The test is conducted using an ASTM standard, named ASTM E 831 [13]. Heating the specimen with a constant heat rate, an expansion versus temperature graph is obtained as shown in Figure 2.15. From this graph, linear coefficient of thermal expansion can be calculated as in the equation below.

$$\alpha = \frac{\Delta L}{\Delta T} \tag{2.23}$$

where the coefficient of linear thermal expansion is denoted with α, change in specimen length and temperature is shown with ΔL and ΔT respectively.

2.1.2.4 Differential Scanning Calorimetry (DSC)

This technique is used to find the specific heat capacity of the propellant. Test method consists of heating the test material at a controlled rate in a controlled atmosphere through the region of interest. The difference in heat flow into the test material and a reference material or blank

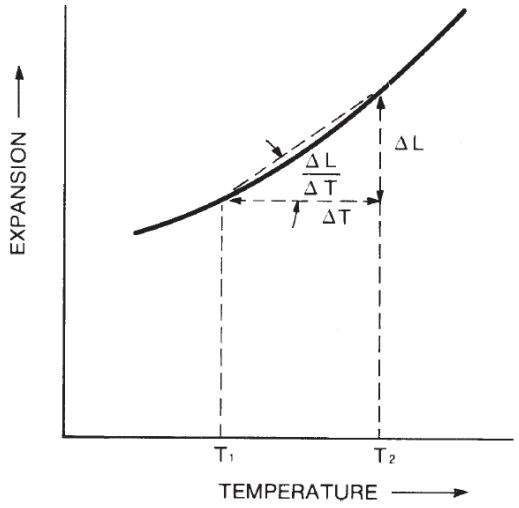

Figure 2.15: Typical expansion vs. temperature graph in TMA [13]

due to energy changes in the material is continually monitored and recorded. The test is conducted using an ASTM standard, named ASTM E 1269 [14].

2.1.2.5 Dynamic Mechanical Analysis (DMA)

Dynamic Mechanical Analysis (DMA) is a dynamic test method for characterization of viscoelastic materials as a function of temperature, frequency or time. The method is based on measurement of sample deformation under a sinusoidal load or load measurement under a sinusoidal deformation.

The test is commonly used to characterize vibration parameters of a viscoelastic materials. A NATO standard, STANAG 4540 is available for the procedure [15]. A typical output of a DMA test can be seen in Figure 2.16.

2.1.3 Thermorheologically Simple Behaviour

Empirical studies on viscoelastic materials show that time, temperature and frequency have similar effects on viscoelastic materials. With this property, these similar effects can be combined and so-called master curves that represent time domain or frequency domain material properties where temperature dependency is embedded into a reduced frequency or a reduced

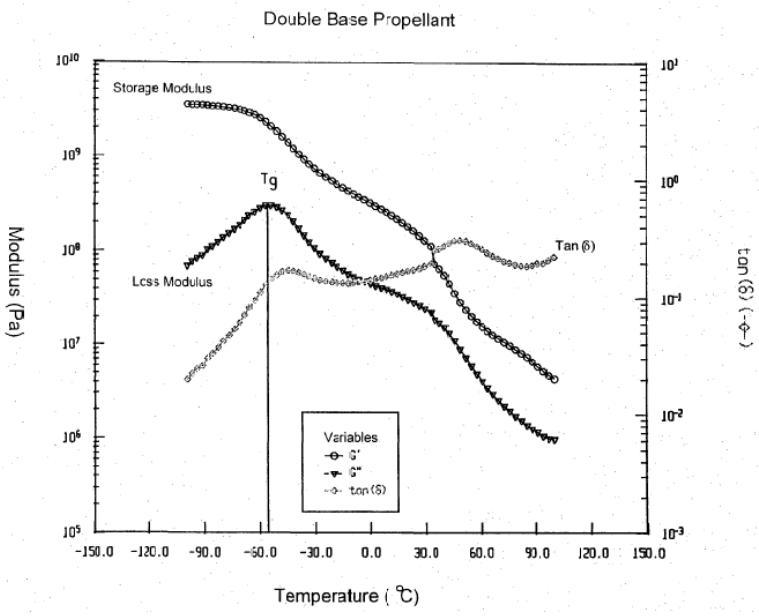

Figure 2.16: Typical output of a DMA test [15]

time variable can be constructed. These reduced variables show the superposed effect of combined phenomena. Following sections touch upon the effects of temperature and frequency on viscoelastic materials. The materials that this empirical time-temperature or frequency-temperature superposition is valid are called thermorheologically simple materials.

2.1.3.1 Effect of Temperature

Viscoelastic material mechanical properties depend on temperature as well as time. Temperature dependency originates from a molecular rearrangement for viscoelastic materials, almost all of which are polymers, which occurs under stress, or from a diffusion process under stress. The speed of such processes depend on the speed of molecular motion for which temperature is a measure [7]. Hence, a temperature rise is a factor to accelerate that molecular motion. In that manner, relaxation modulus can be written in that manner as

$$E = E(t,T) = E(\zeta, T_0) \; with \; \zeta = \frac{t}{a_T(T)} \tag{2.24}$$

where ζ is called the reduced time, T_0 is the reference temperature and $a_T(T)$ is called the shift

factor. Materials showing this time-temperature superposition property are called thermorheologically simple materials. It is the case with these materials that some temperature shift is equal to a some shift in time axis. Increasing temperature, it is observed that the modulus and stress of viscoelastic material decreases.

In this study, master curves for relaxation modulus, allowable stress and allowable strain of the propellant is constructed using time-temperature superposition concept.

2.1.3.2 Effect of Frequency

Effect of frequency is somewhat the inverse of temperature. At constant temperature, with increasing frequency, amplitude of complex modulus increases. Likewise, with decreasing frequency, one can observe that amplitude of complex modulus decreases.

Like it is the case in time and temperature superposition, temperature and frequency can be superposed. In other words, several decades of frequency change similar to a change of a few degrees of temperature. Using this superposition principle, master curves for the complex modulus and loss factors are constructed.

2.1.3.3 Williams-Landel-Ferry (WLF) Shift Function

The superpositions that referred at preceding section can be done using Williams-Landel-Ferry (WLF) shift function which is given as below.

$$log(a_T) = \frac{C_1(T - T_0)}{C_2 + (T - T_0)} \tag{2.25}$$

where T_0 is the reference temperature and C_1 and C_2 are empirical constants. Reference temperature is generally taken as room temperature or glass transition temperature. In this study, room temperature is used as reference temperature.

This equation is introduced as an empirical expression for a general curve $a_T(T)$ in which many different polymers had been reduced to standard states [16]. Master curves for the propellant which are illustrated at next section are constructed using WLF shift function.

2.1.4 Master Curves of the Solid Propellant

As it is mentioned in previous section, time-temperature and frequency-temperature superpositions can be done in viscoelastic materials. With this property, master curves can be utilized with introducing reduced variables for the superposed phenomena. In this study, master curves are prepared for relaxation modulus, allowable stress, allowable strain, storage modulus and loss factor.

Like relaxation modulus, allowable stress and allowable strain is also time dependent as the failure of the specimens tested at different time rates occurs at different time values. Allowable stress and allowable strain is plotted against the reduced time required for the failure to occur [17].

2.1.4.1 Relaxation Modulus

In Figure 2.17, unshifted relaxation modulus values are shown. These curves are shifted using the Williams-Landel and Ferry (WLF) shift function and master curve for relaxation modulus is given in Figure 2.18. This master curve is used to determine the modulus of the propellant at different temperature and time values.

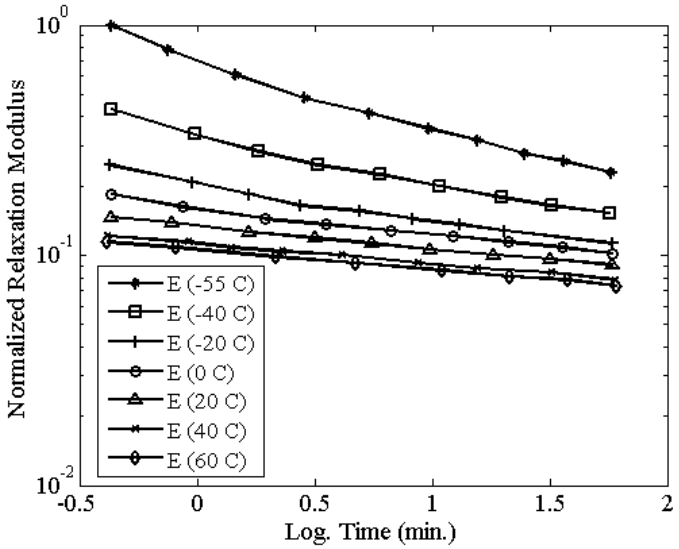

Figure 2.17: Normalized relaxation modulus values at different temperatures

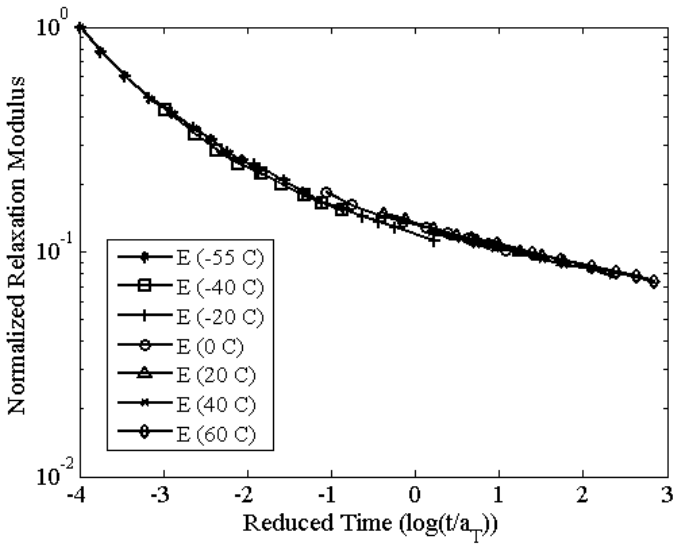

Figure 2.18: Master curve of the relaxation modulus

2.1.4.2 Allowable Stress and Strain

For some propellants, the shift factors found from the shifting of relaxation modulus data and stress resulting from the uniaxial test data are identical as it is the case in this study [2]. Using the results of uniaxial tensile tests and same shift constants, master curves for allowable stress and allowable strain are prepared. These master curves are illustrated in Figure 2.19 and Figure 2.20 respectively. Analytical models are fitted to the experimental values as seen in this figures. For the analytical models, exponential, polynomial or Gaussian curves may be used. As seen in the figures, an exponential curve is used to represent the allowable stress and a third degree polynomial curve is used to represent the allowable strain. Allowable stress and strain values of the propellant is used as failure limits for the propellant grain.

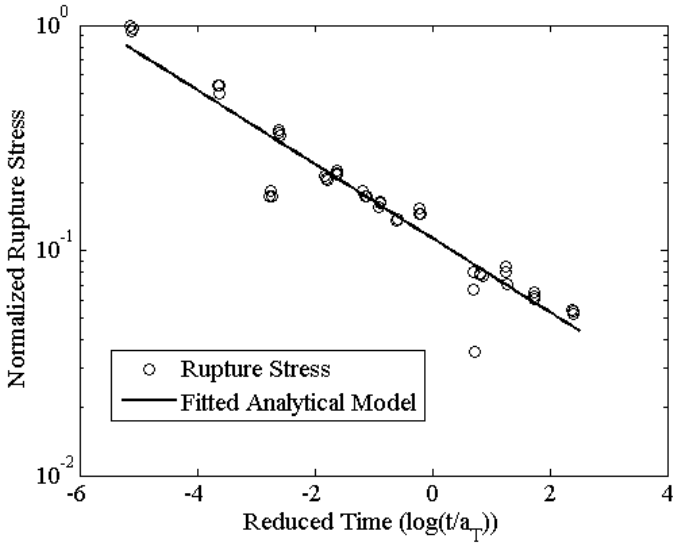

Figure 2.19: Master curve of allowable stress of propellant

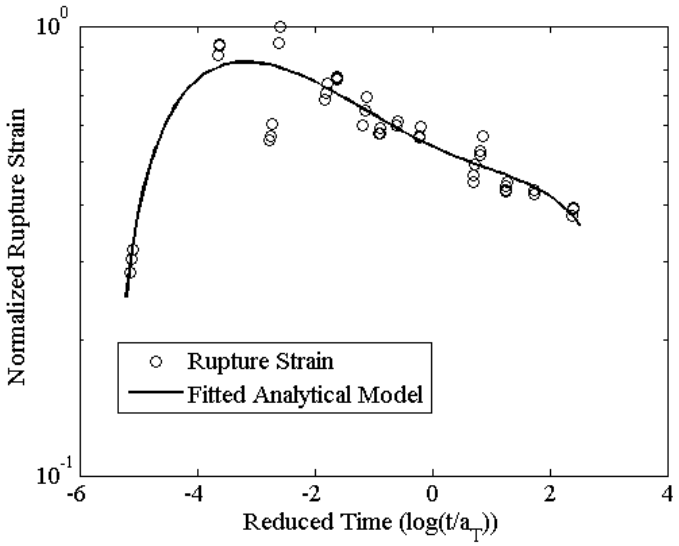

Figure 2.20: Master curve of allowable strain of propellant

2.1.4.3 Storage Modulus and Loss Factor

Also, for the modulus and loss factor parameters, temperature-frequency shifting is done and master curves are constructed. For the temperature shift, again the WLF shift function is used with different shift constants. Master curves for the modulus and loss factor are given in Figure 2.21 and Figure 2.22 respectively. Complex modulus and loss factor at different frequency and temperature values are used in the vibration analysis of the system.

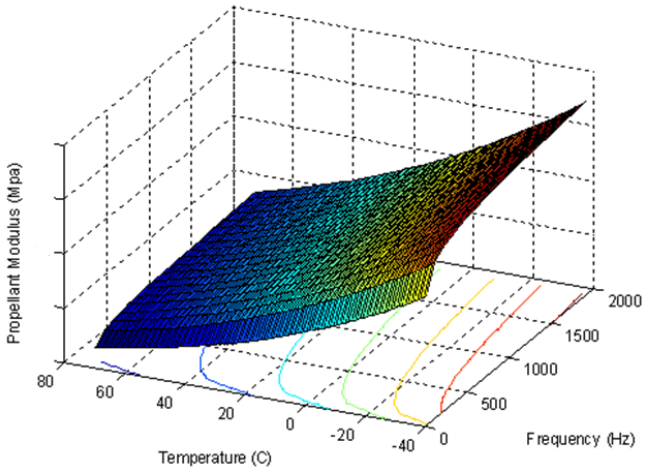

Figure 2.21: Master curve of modulus of propellant

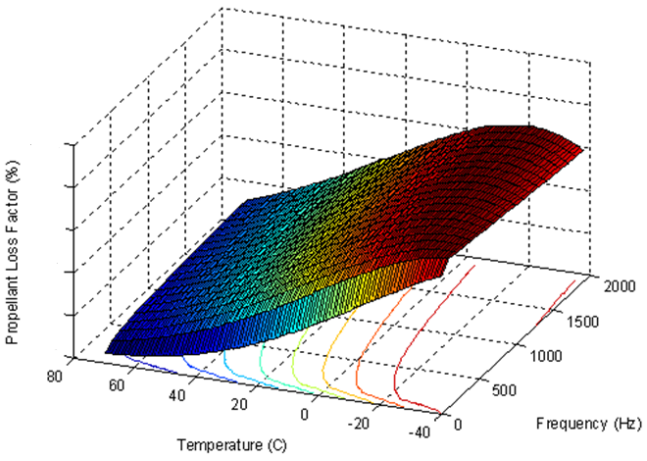

Figure 2.22: Master curve of loss factor of propellant

2.1.5 Cumulative Damage

Application of a dynamic load to a solid propellant results in mechanical damage, even though the damage may not be readily detectable [17]. Successive loading will increase the damage, which will result in a structural failure of the system. To predict the cumulative damage response, various theories are discussed in literature. The most common theory that is being used and widely accepted is the classical Miner's law [18]. This law is widely used in structures that has been subjected to repetitive and fatigue loads, and can be expressed as,

$$\sum D_k = \sum \frac{n_k}{N_k} \tag{2.26}$$

where D_k is the damage fraction added by the application of the k$^{\text{th}}$ load level, n_k is the number of cycles at the k$^{\text{th}}$ load level, and N_k is the number of cycles measured for failure at the k$^{\text{th}}$ load level [17].

For propellants, this formulation is changed slightly based on time to failure under stress [17]:

$$P \sum D_i = \sum_{i=1}^{n} \frac{\Delta t_i}{t_{fi}} \tag{2.27}$$

where P is the probability distribution function (PDF) observed during failure tests, D_i is the damage fraction added by the application of the i$^{\text{th}}$ stress level, Δt_i is the time that specimen is exposed i$^{\text{th}}$ stress level and t_{fi} is the mean time to failure if specimen only experienced i$^{\text{th}}$ stress level [17].

Time to failure parameter can be written as below as Bills proposed considering the experimental observations [19], [1].

$$t_{fi} = t_0 a_T(T_i) \left(\frac{\sigma_0}{\sigma_i} \right)^{\beta} \tag{2.28}$$

where β is the negative inverse slope of the log-log plot of stress versus time, a_T is the shift factor at the temperature T_i, σ_0 is the reference stress value and t_0 is time to failure under the reference stress value. Combining Equations 2.27 and 2.28, a general cumulative damage law in terms of an arbitrary discrete stress state is obtained.

$$D = \sum_{i=1}^{n} D_i = \sum_{i=1}^{n} \left[\frac{\Delta t_i}{a_T(T(t_i))t_0} \cdot \left(\frac{\sigma_i}{\sigma_0} \right)^{\beta} \right] \tag{2.29}$$

To determine the cumulative damage characteristics, σ_0 and β, a series of constant stress tests are needed to be carried out. However, in the method Kunz proposed in his article, constant strain rate tests can be used in determining these constants [20].

In this study, Laheru's linear cumulative damage model is used [21]. This cumulative damage model is also based on Miner's rule. The model is linear since it hypothesizes that the damage accumulates linearly with time at a specific level of stress [20]. Hence, time to failure can be determined using the following relation.

$$\int_0^{t_f} \frac{dt}{t(\sigma(t))} = 1 \tag{2.30}$$

where $t(\sigma(t))$ is the to failure under constant stress, σ and t_f is the time to failure under a time varying stress $\sigma(t)$. Using the experimental observations that are explained above, time to failure can be written as,

$$t_f = t_0(\sigma_0)\left(\frac{\sigma_0}{\sigma} \right)^{\beta} \tag{2.31}$$

where σ_0 is the stress level to cause failure at time t_0 and β is an experimentally determined variable. Laheru's cumulative damage model combines Equations 2.30 to 2.31 to define a Lebesgue form of stress, which is a characteristic failure parameter which has the physical interpretation as the constant stress which would cause the material to fail in unit time [20].

$$N = \left[\int_0^{t_f} \sigma(t)^{\beta} dt \right]^{\frac{1}{\beta}} \tag{2.32}$$

Since constant stress tests are experimentally difficult, constant strain tests are used to find the damage parameters. Integrating the stress history in Equation 2.32 over time, equivalent creep strain is obtained and shown as $\bar{\sigma}$,

$$N = \bar{\sigma} t_f^{\frac{1}{\beta}} \tag{2.33}$$

Combining Equations 2.32 and 2.33, equation is solved for the equivalent creep stress.

$$\bar{\sigma} = t_f^{\frac{1}{\beta}} \left[\int_0^{t_f} \sigma(t)^{\beta} dt \right]^{\frac{1}{\beta}} \tag{2.34}$$

To determine the cumulative damage parameters N and β, an iterative approach has to be used. Consider that, M constant strain tests are used to find the parameters. The method suggest to estimate an initial β from log-log plot of time to failure, and the stress at failure. Such a plot is shown in Figure 2.23.

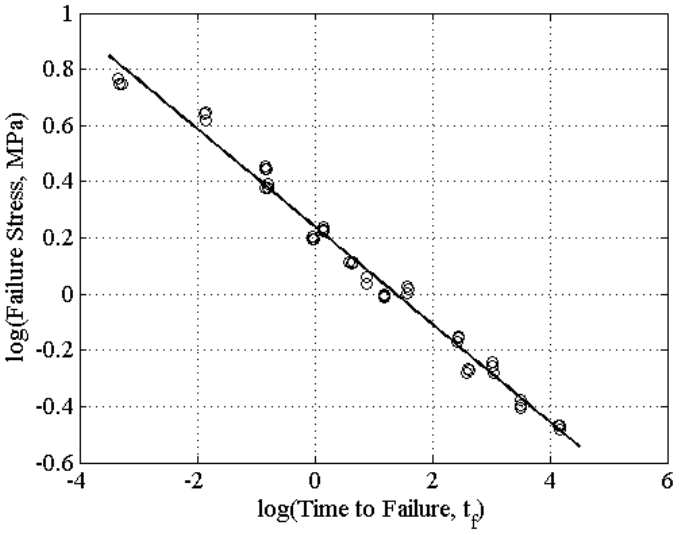

Figure 2.23: Determination of the Initial Value of β

Then, an initial estimate of β is obtained using the slope and correlation coefficient, R.

$$\beta_0 = -\frac{R_0}{m} \tag{2.35}$$

where m denotes the slope of the line. For all M specimens, equivalent creep stress can be calculated with the given formula

$$\bar{\sigma}_{i0} = t_{fi}^{\frac{1}{\beta_0}} \left[\int_0^{t_{fi}} \sigma(t)_0^{\beta} dt \right]^{\frac{1}{\beta_0}}, i = 1, ..., M \tag{2.36}$$

Using the found equivalent creep stress values for M specimens, $\log(\bar{\sigma}_{i0})$ vs. $\log(t_{fi})$ graph is made again, and from the slope and correlation coefficient, another β value is obtained. Using the equivalent creep stress and β values, this process is repeated until a convergence is achieved.

Apart from determining the margin of safety of the system, damage accumulation can also be assumed to be equivalent to a linear strength reduction [28]. This strength reduction can be illustrated with a formula as shown below.

$$S(t) = S_0 \cdot (1 - D(t)) \tag{2.37}$$

where D(t) is the damage factor, S is the mechanical strength of the material and S_0 is the mechanical strength at t=0.

2.1.6 Aging

Aging of propellants in rocket motors refers to their deterioration in the physical properties with time. There are two types of aging in solid propellants; mechanical and chemical aging. Mechanical aging is caused by the damage done to the grain during storage, handling, or transport. Chemical aging is characterized by the chemical changes with time, such as the gradual depletion (evaporation) of certain liquid plasticizers or moisture absorption. [5]. To consider the aging effect, a mathematical model can be used. In this study, Layton model [22] will be used which is an aging model used that has been used widely in literature [23], [24]. Any mechanical property at time t can be expressed with the mathematical aging model given in Equation 2.38.

$$S(t) = S_0 + k \cdot log(t) \tag{2.38}$$

where S is the mechanical property at any arbitrary age time, S_0 is the mechanical property at the end of cure, k is the rate of change of the property and t is the aging time. This rate of change can be found with using Arrhenius equation [24].

$$k = A \cdot exp\left(\frac{-E_a}{RT}\right) \tag{2.39}$$

where A is the Arrhenius constant, R is the universal gas constant, E_a is the activation energy and T is temperature. Using the specimens that are artificially aged at different temperatures, uniaxial tensile tests are performed. Using the results, S(t)-log(t) graphs are constructed and k parameter is calculated from the slope of these curves with a simple regression analysis. Unit of time must be consistent with the unit of time in Equation 2.38 Using the k values that are found for different temperatures, ln(k)-1/T graph is formed and using regression again, A and E_a parameters are calculated [24].

An example for the determination of k from a series of accelerated aging test is illustrated in Figure 2.24. To set an example, accelerated aging data at one temperature is shown.

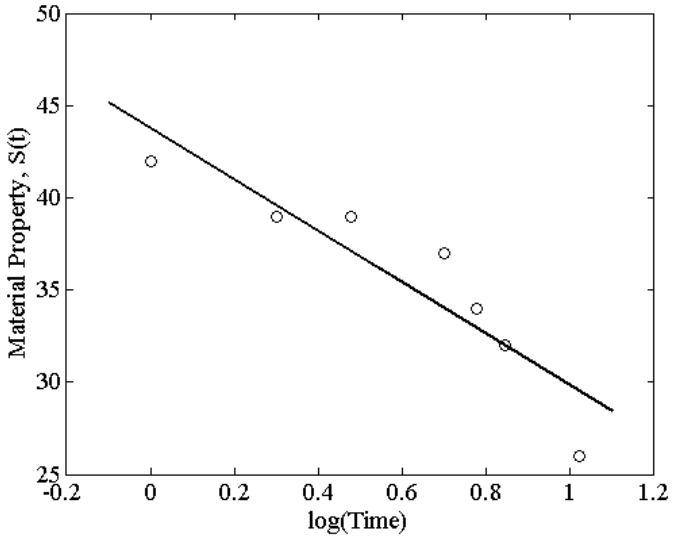

Figure 2.24: Determination of k parameter from accelerated aging tests at a constant temperature

Finding different k values from the slopes of different accelerated aging temperatures, one may utilize the graph ln(k) vs. 1/T as seen in Figure 2.25. From the trendline of the data, aging parameters in Arrhenius equation, namely A and E_a are determined.

With the proposed method, different aging constants are calculated for different mechanical properties. Uniaxial tensile tests are performed at room temperature.

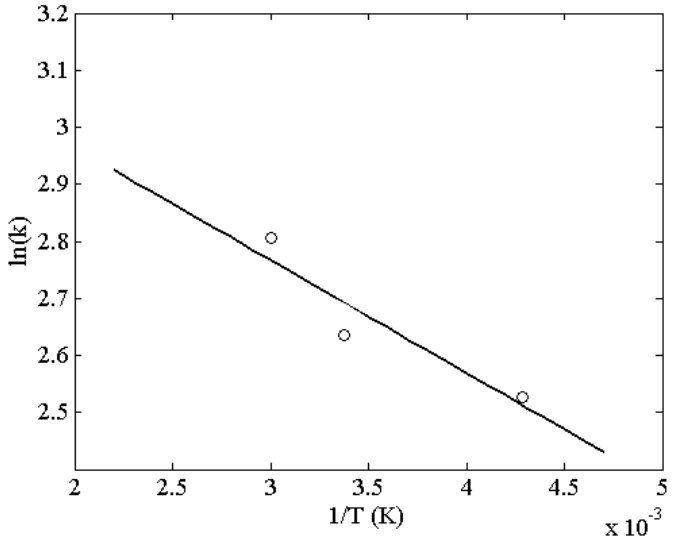

Figure 2.25: Determination of aging parameters in Arrhenius equation

2.2 SERVICE LIFE ASSESSMENT OF SOLID ROCKET MOTORS

Solid propellant rocket motors are the most widely used propulsion technology used in tactical missiles. They must be designed with narrow performance boundaries and increasingly extended shelf life. Hence, their life cycles need to be predicted under the loads that the systems will encounter during their life spans. These loads consist of handling, storage and deployment loads under varying conditions. The complexity of these loads makes the service life assessment indeed a difficult task [6]. In literature, there are various studies which develop alternative techniques to predict the service life of solid propellant rocket systems.

One of the first studies in the service life prediction area is conducted by Chappell and Jensen [25]. In their study, a probability of failure value for the corresponding rocket system is calculated using Monte Carlo method. The finite element analysis is conducted using a simplified two dimensional plane strain model, which is a common practice till 1990's since computational power of the finite element tools was not enough to build and solve complex three dimensional models. In predicting the failure, cumulative damage in the propellant grain is taken into consideration. Also, the cumulative damage and margin of safety values are extrapolated as a function of propellant age.

Environmental temperature effects are widely studied by Heller's studies [26], [29], [28], [30],

[31]. In the study conducted with Kamat and Singh [26] random environmental temperature is characterized and a mathematical model is proposed. The model is basically consists of seasonal and diurnal temperature cycles with cycle amplitudes having normal distributions. Using this mathematical model, probability of failure of the system is calculated for a year. This probability of failure value is found by summing the daily probabilities of failure. For the propellant grain, an elastic material model is used.

Thrasher had estimated the structural service life of the reduced-smoke Maverick rocket motor in his study [27]. The motor is analyzed under the thermal and pressurization loads accelerated laboratory tests are conducted to simulate the mechanical and chemical aging effects. Total of three two-dimensional finite element models are prepared to analyze the rocket motor. An axisymmetric model of the whole motor, a plane strain model, and an axisymmetric model of the center section is built and TEXGAP-2D computer code is used in the simulation. A linear viscoelastic material model is used throughout the study.

In another study, Heller and Singh improved the material model of propellant grain to a linear viscoelastic one [28]. Furthermore, chemical aging and stress-dependent cumulative damage mechanisms of propellant are taken into account in this work. Thermal stress analysis is conducted again using a plane strain finite element model and progressive probability of failure is estimation is extended to more than ten years time.

Zibdeh and Heller has used a different technique called first passage method in estimating the service life in their work [29]. Environmental conditions and mechanical properties are taken as variable parameters and the results of Poisson and Markov models are compared.

Different from these studies, Janajreh, Heller and Thangjitham have developed a safety index approach to predict the storage life of rocket motors [30]. In this study, first-order second-moment (FOSM) reliability method is used instead of Monte Carlo simulations. Progressive probability of failure is obtained for variables with various statistical distributions. A service life analysis methodology based on stress-strength interference is also developed by them [31].

Margetson and Wong had also developed a methodology for the service life prediction of solid rocket motors [32]. In this study a comparison between a probabilistic approach and deterministic structural analysis is made and different failure criteria (strain and stress based)

are taken into account. Moreover, a bondline measuring data monitor system is used and bondline stresses are measured experimentally.

All these studies listed above had used linear elastic or linear viscoelastic material models for propellant grain. However, in Collingwood, Clark and Becker's approach, a nonlinear viscoelastic material model is used with a probabilistic service life prediction technique [33]. Furthermore, in the analysis, various models are used to simulate damage and dilatation of solid propellant.

Akpan and Wong had used a probabilistic sensitivity analysis method in their study [34]. Using first order reliability method (FORM) and Monte Carlo simulation, instantaneous reliability of the missile structure is calculated. With a probabilistic sensitivity analysis, importance of measurable experimental parameters are also determined.

In another study that Akpan et. al conducted, probabilistic assessment is expanded to second order reliability methods [35]. A methodology for the calculation of progressive reliability is proposed and service life predictions of a motor at different storage sites are compared.

Marotta, et. al. discussed the use of probabilistic analyses in predicting the reliability of tactical missiles [36]. In this study, an application of an integrated health monitoring system and the usage of probabilistic engineering methods to analyze the monitoring system data is discussed.

Hasanoğlu has made a storage reliability analysis of solid rocket motors considering the environmental storage loads in his thesis [37]. Cumulative damage methods are used in predicting the failure and parametric finite element analyses are carried out using three dimensional finite element models.

Yıldırım and Özüpek considered the structural assessment of a solid propellant rocket motor under the effects of aging and damage [39], [40]. Using the aged and unaged propellant data, structural analysis of solid rocket motor is carried out and it is indicated that using the results, an estimation of service life can be made. A nonlinear viscoelastic material model is used for the solid propellant in this study and for the finite element analysis, a two dimensional axisymmetric model is used.

The studies that are found in the literature are generally take only the storage loads into ac-

count. However, Kuran et. al. have considered the vibration exposure to the rocket motors [38]. In this study, different transportation scenarios are investigated and mathematical models for the structural analysis is generated using response surface method. Cumulative damage analysis is done to assess the damage in the propellant grain.

One of the most recent works in this are belongs to Gligorijevic et. al., where a procedure for the structural analysis of case bonded solid propellant grain is proposed [41]. Natural aging data is used to predict the effect of chemical aging and cumulative damage laws are used to predict the damage accumulated in the propellant grain. It is indicated in the study that, the mathematical model is verified since the results are coincided with the time of failure appearance on real grains.

A table is prepared for summarizing the scope of these studies in Table 2.1. In the table, material models used for solid propellants, finite element models, cumulative damage and aging effects and failure prediction methods are summarized. It is seen that for the failure prediction, probabilistic methods are used nearly in all of the studies and linear viscoelastic material models are used in general.

Table 2.1: Summary of the service life studies in the literature

Author	Mat. Model	FE Model	Cum. Damage	Aging	Failure Prediction
Chappell (1967)	LVE	2D	Yes	Yes	Monte Carlo Method
Heller (1979)	LE	2D	No	No	Probabilistic Approach
Thrasher (1981)	LVE	2D	No	Yes	Deterministic Approach
Heller (1983)	LVE	2D	Yes	Yes	Probabilistic Approach
Zibdeh (1989)	LVE	2D	Yes	Yes	First-Passage Method
Janajreh (1994)	LVE	2D	Yes	Yes	FORM
Heller (1996)	LVE	2D	Yes	Yes	FORM
Margetson (1996)	-	-	Yes	Yes	Experimental
Collingwood (1996)	NLVE	3D	Yes	Yes	Statistical Model
Akpan (2002)	LVE	-	No	No	FORM
Akpan (2003)	LVE	-	No	No	SORM
Yıldırım (2011)	NLVE	2D	Yes	Yes	-
Gligorijevic (2011)	LVE	-	Yes	Yes	Probabilistic Approach

CHAPTER 3

PHYSICAL, MATERIAL AND LOADING MODELS FOR SERVICE LIFE ASSESSMENT

In this chapter, the system considered in this study is explained briefly. Starting with physical aspects of the system, random nature of the environment that the system is exposed to be discussed. Failure modes that has to be avoided in solid propellants are explained in detail. In literature survey part, it is emphasized that probabilistic loading models play an important role in service life assessment of solid propellant rocket motors. Using statistical approaches, capability variations due to manufacturing process, material reproducibility, mechanical testing, aging, etc. and induced stress/strain variations due to the uncertainties of boundary conditions can be assessed with an estimation of reliability [2]. Hence, probabilistic models are built to account the randomness in both the material itself and environmental effects, and are presented in this section.

3.1 PHYSICAL PROPERTIES OF THE SYSTEM

During its life cycle solid rocket motors are exposed to different kind of loads like environmental temperature and transportation vibration. These loads induce stress and strain in propellant grain, and failure may occur. There are several failure modes like crack formation in propellant grain or debonding of grain-insulation-case interfaces. In this part, loads that the solid rocket motor are exposed to and failure modes in solid propellant grains are explained in detail with schematics.

3.1.1 Exposure to Environmental Temperature and Vibration

Solid propellant rocket motors are deployed from manufacturing site to storage sites or forward bases by means of ground, air or sea transportation. Hence, in this transportation periods, a certain level of vibration is experienced. Main causes of this vibration loading can be listed as follows [42].

- Condition of the roads, bumps and potholes in ground transportation
- Engine caused in-flight vibration in air transportation
- Wave induced vibration in sea transportation

Solid rocket motors may be stored in both temperature controlled rooms and temperature uncontrolled environments with basic sheltering. Storage in temperature uncontrolled environments makes the rocket motor to experience varying environmental temperatures which will provoke mechanical damage. In Figure 3.1, the vibration and thermal loads that solid rocket motor experience during its life is shown.

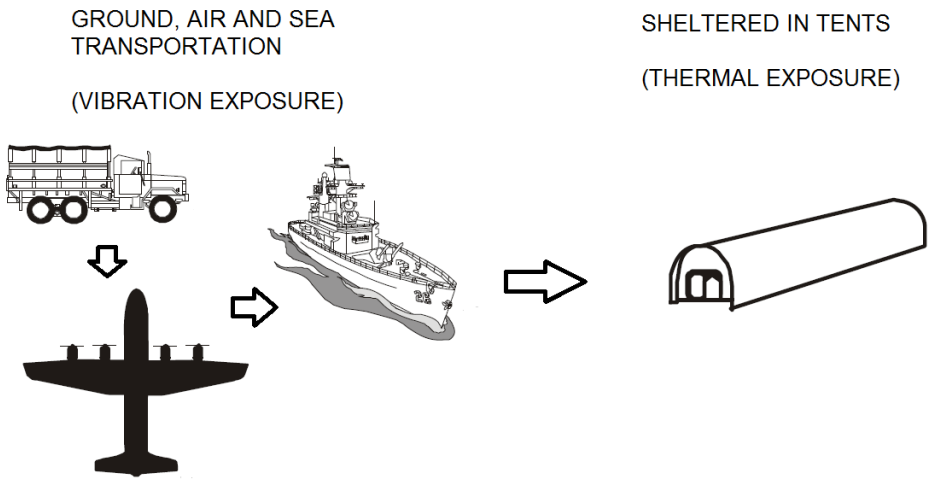

Figure 3.1: Loads solid rocket motor exposed to during its life cycle

To analyze, a certain transportation and storage pattern is considered in this study. This pattern can be enumerated as follows.

1. Ground transportation for 50 hours
2. Air transportation for 2 hours
3. Stored in a ship for 4 years (temperature uncontrolled environment)
4. Ground transportation for 50 hours
5. Air transportation for 2 hours
6. Stored in a temperature uncontrolled storage site for 4 years

and this pattern continues till the operation, in other words, firing of the rocket motor.

3.1.2 Failure Modes in Solid Propellant Rocket Motor Systems

Failure in the propellant grain can be expressed any malfunctioning preventing the system from fulfilling its mission. To determine whether failure will occur or not, comprehensive analysis has to be done and system should be checked against common failure modes. This part is devoted to explain these failure modes in detail. Failure modes that are seen in propellant grain can be listed as in Reference [1].

- Surface cracks
- Debonding of interfaces
- Dewetting (Dilatation)
- Excessive deformation

In this study, detailed analysis is done to explore the modes of surface cracking and debonding of interfaces since they are the most common types of failure. Also, it is seen that in the service life studies listed in literature survey examine the surface cracking and interface debonding failure types to predict failure. Strain and stress based criteria are used to detect the failure in propellant grain and stress based failure criteria are used in detecting the failure in bondline [1].

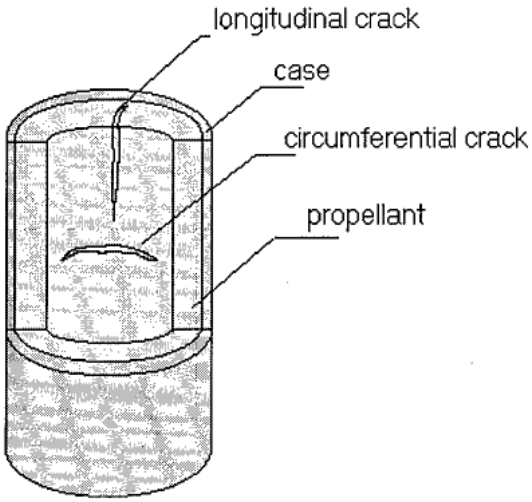

Figure 3.2: Schematic of surface crack in propellant grain [1]

Schematics for surface crack and debonding of interfaces are given in Figure 3.2 and 3.3 respectively.

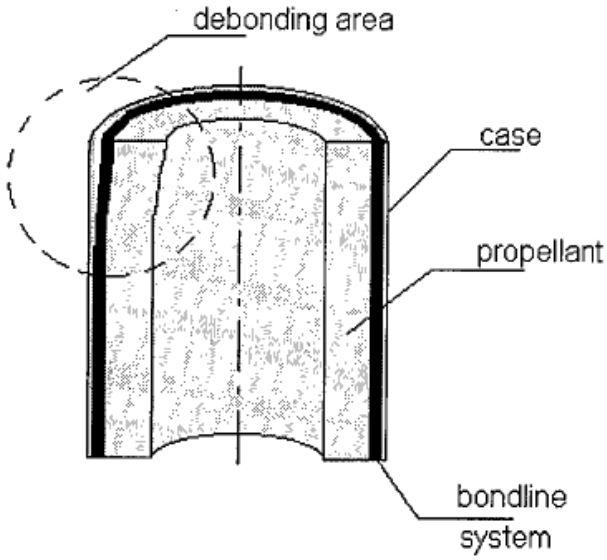

Figure 3.3: Schematic of debonding of interface [1]

3.1.2.1 Surface Cracks

As load exceeds a certain level that propellant material withstand, cracks will start to form in the propellant grain. Cracks in grain can grow as a result of loading history. As a consequence, the effective burning surface of the grain is unintentionally increased during motor operation which may result in an abnormal pressure and thrust history [1]. An uncontrollable pressure rise may even be the cause of explosion of the motor case.

This failure mode is checked against strain capabilities of the propellant. Consequently, strain properties of the solid propellant have to be determined for the structural analysis.

An experimentally observed crack is illustrated in Figure 3.4.

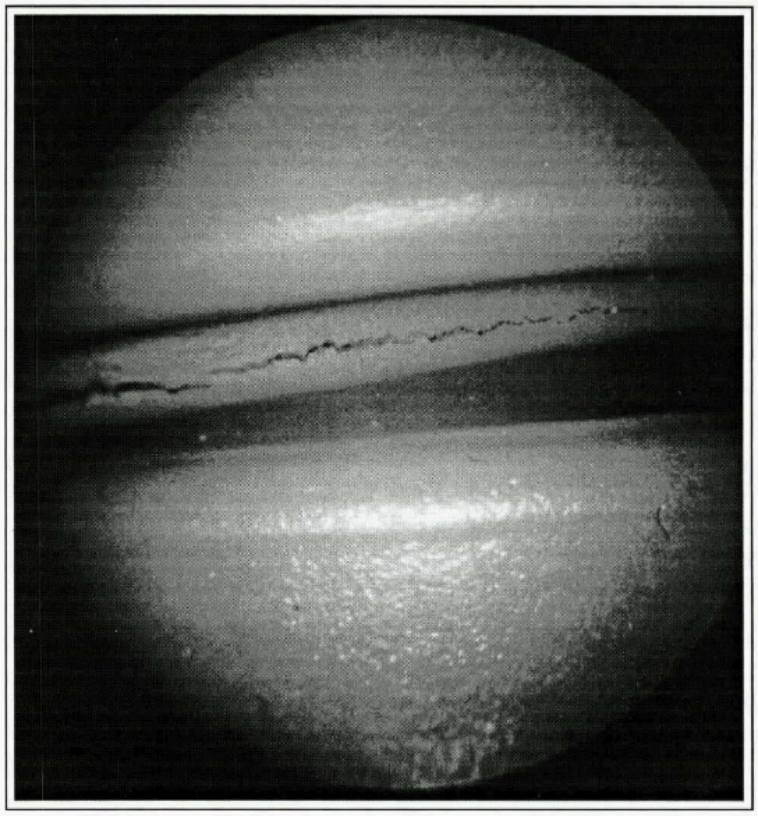

Figure 3.4: Experimentally observed crack [1]

A crack does not always mean that a failure will occur in the system. If sufficient data is available, detailed analysis of a crack can be done using fracture mechanics principles, and crack can be controlled for unstable growth.

3.1.2.2 Debonding of Interfaces

Because of the difference between the thermal expansion coefficients of case, insulation and the propellant grain, shear stresses are developed at the case-insulation-propellant interfaces. To give an idea, the difference between thermal expansion coefficients of case and propellant is approximately a factor of ten between metallic bond cases and composite propellants [10].

Debonding in a real application is illustrated at Figure 3.5.

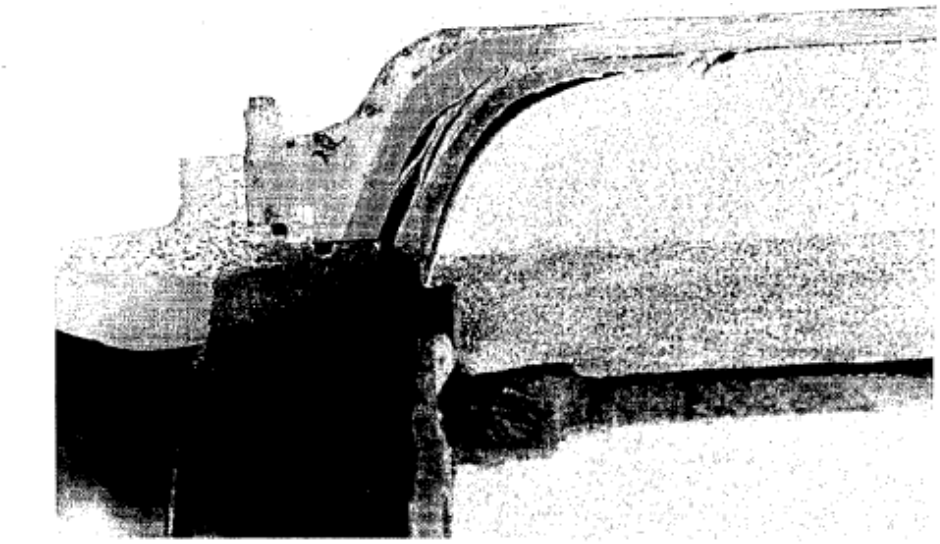

Figure 3.5: Debonding in a real application [1]

3.2 LOADING MODELS

Analyzing the loads that solid rocket motors are subjected to during their service life, namely the environmental temperature and transportation, it is seen that these loads are highly random. Thus, these loads need to be characterized using random parameters. Random parameters are selected so that they dominate loading characteristics. In this section, these parameters are presented and their extremes will be given.

Our system is to experience two main types of loading, which are thermal exposure and transportation vibration respectively. For storage loads, an environmental temperature model is prepared and for transportation loads, experimental vibration profiles are used.

3.2.1 Environmental Temperature

The loads induced during the storage phase of the life cycle are represented by random variables. Time dependent thermal environment which the solid rocket motor is subjected to is defined in terms of long term mean temperature, yearly and daily temperature amplitudes. In literature, thermal loads in the storage conditions in which large percentage of rocket life is spent, are considered as listed in the literature survey part. As seen in these studies, change in temperature of the motor case outer surface can be taken as a harmonic function of time.

$$T(t) = T_M + T_Y sin\left(\frac{2\pi}{8760}\right)(t - t_0) + T_D sin\left(\frac{2\pi}{24}\right)(t - t_1) \tag{3.1}$$

where, T_M is the mean value of yearly storage temperature, T_Y is the yearly temperature amplitude, T_D is the daily temperature amplitude, t_0 is the yearly temperature phase, and t_1 is the daily temperature phase.

If the change in temperature of the store is known or stored in a database, the parameters given above will be determined easily. However, hourly changes in temperature may not be kept during long years so that such uncertainties should be considered in calculation of the service life.

To find the parameters mentioned above, meteorologic data of the places, Ankara, Diyarbakir, Edirne, Hakkari, Istanbul, Konya, Tekirdag and Cyprus are used [43]. Using the temperature data corresponding last 30 years, parameters of the temperature model are calculated as listed on Table 3.1.

Table 3.1: Parameters of the temperature model

Parameter	Value
T_M, Mean Value of the Storage Temperature	9°C - 19°C
T_Y, Yearly Temperature Amplitude	10°C - 35°C
T_D, Daily Temperature Amplitude	2°C - 5°C
t_0, Yearly Temperature Phase	2920 hours
t_1, Daily Temperature Phase	9 hours

Using the mean values of the variables, a sample temperature distribution over a year can be plotted as in Figure 3.6. To illustrate the daily sinusoidal harmonic behaviour, a zoom window

is used in the figure.

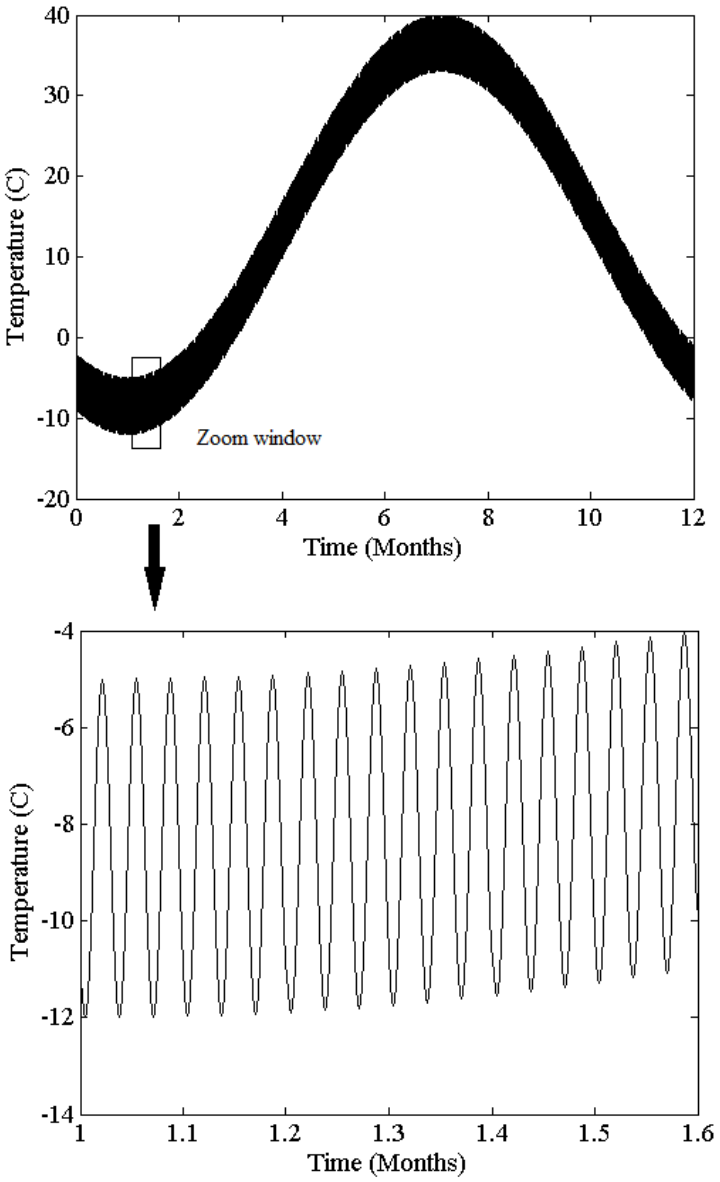

Figure 3.6: Sample temperature distribution over a year (Total and zoomed)

3.2.2 Transportation

In order to account for transportation loads, acceleration spectral density functions are produced using an in-house code using the available profiles in References [42] and [44]. A deviation of %30 is considered in the acceleration spectral density functions. The upper and

lower limits of spectral densities are shown in Figures 3.7-3.11 for ground, air and sea transportation. For ground transportation, three different envelopes exist which correspond to excitations in longitudinal, vertical and transverse excitations. For air and sea transportation, acceleration spectral density envelopes are available for vertical excitations. Vibrations loads are assumed to be stationary and they are uncorrelated in three mutually perpendicular axes. In Table 3.2, RMS levels that are used in the computations are listed.

Table 3.2: RMS Vibration Levels

Type	Lower Limit	Upper Limit
Ground Vertical	1.233	1.680
Ground Transverse	0.931	1.269
Ground Longitudinal	1.154	1.572
Air	2.859	3.896
Sea	0.003	0.004

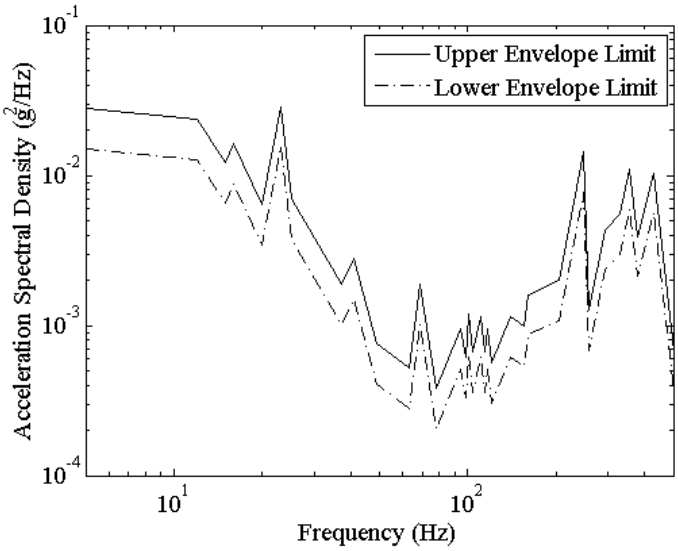

Figure 3.7: Upper and lower envelope limits of ground transportation (Longitudinal Axis)

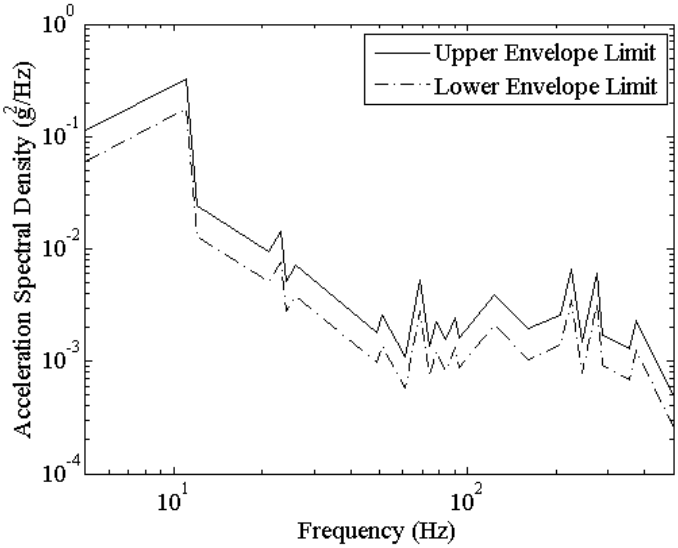

Figure 3.8: Upper and lower envelope limits of ground transportation (Vertical Axis)

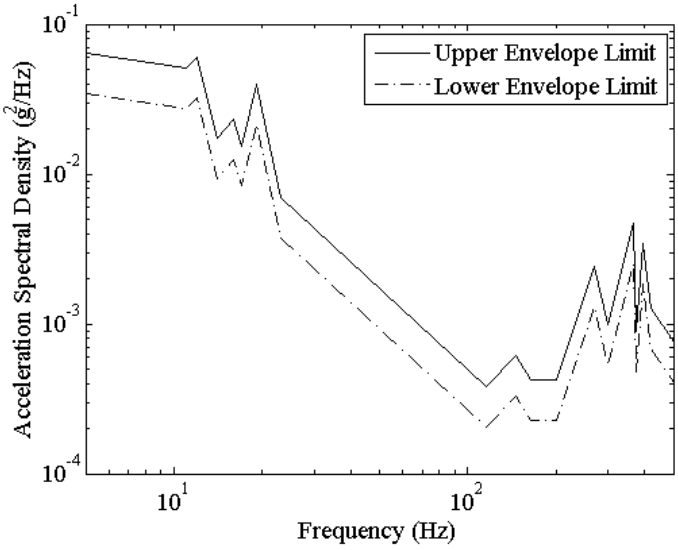

Figure 3.9: Upper and lower envelope limits of ground transportation (Transverse Axis)

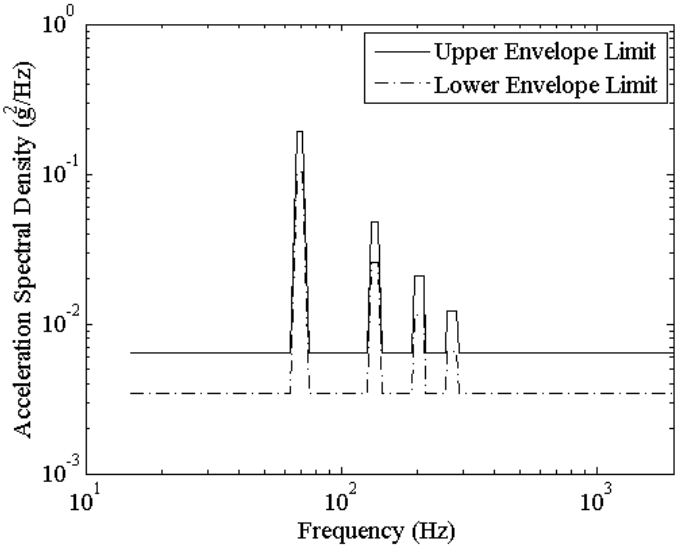

Figure 3.10: Upper and lower envelope limits of air transportation (Vertical Axis)

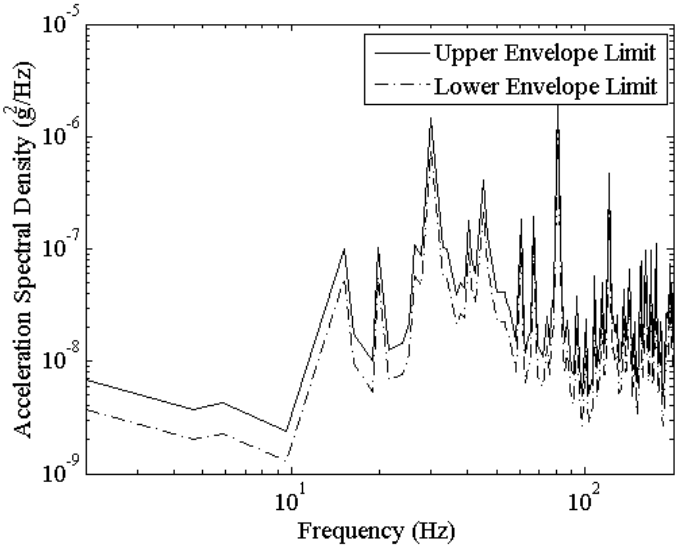

Figure 3.11: Upper and lower envelope limits of sea transportation (Vertical Axis)

3.3 MATERIAL MODEL

Material properties of solid propellants have inherent uncertainties due to manufacturing process, material reproducibility and mechanical testing. Variability can even be observed be-

tween different mixes of same formulation of propellant and in experiments. Hence, uncertainties for the material properties of solid propellants are defined.

A complete list of parameters showing variability and non-variability is given in Table 3.3. For modulus, coefficient of thermal expansion coefficient and loss factor, variability is defined considering the experimental values. Modulus and thermal expansion coefficient are selected to have uncertainty since these material properties are dominant in the stress-strain response of the propellant grain to environmental thermal loads [34]. Also, loss factor is selected to have variability since it is an important parameter which determines the vibration characteristics of the propellant. Material properties that do not have any statistical variation are listed in Appendix A.

Table 3.3: Parameters having variability

Parameter	Uncertainty (Yes/No)
Modulus of Propellant	Yes
Poisson Ratio of Propellant	No
Coefficient of Thermal Expansion of Propellant	Yes
Thermal Conductivity of Propellant	No
Heat Capacity of Propellant	No
Loss Factor of Propellant	Yes
Modulus of Case	No
Poisson Ratio of Case	No
Coefficient of Thermal Expansion of Case	No
Thermal Conductivity of Case	No
Heat Capacity of Case	No
Modulus of Insulation	No
Poisson Ratio of Insulation	No
Coefficient of Thermal Expansion of Insulation	No
Thermal Conductivity of Insulation	No
Heat Capacity of Insulation	No

Maximum and minimum values and deviations from the nominal values that are defined for equilibrium shear modulus, coefficient of thermal expansion, complex modulus and loss factor of propellant are given in Table 3.4. These ranges are defined using the results of the material characterization tests.

Table 3.4: Material properties as random variables

Parameter	Value
G_∞, Equilibrium Shear Modulus (MPa)	0.189 - 0.630
α, Coefficient of Thermal Expansion (μm/mm/°K)	75 - 115
$E(\omega)$, Complex Modulus	%30 deviation from mean
$\eta(\omega)$, Loss Factor	%20 deviation from mean

3.4 MODELING OF UNCERTAINTIES

In preceding sections, it is explained that the loading and material models have inherent uncertainties. To account these uncertainties, sampling methods can be used. It is known that parameters in the service life model show deviation in a range. Hence, deterministic analysis sets can be constructed using a proper sampling technique, and then the result can be assesses using probabilistic approach.

It is evident that for the reliability assessment, mathematical models for the failure condition are to be formed. These models are utilized using response surface methodology as it is explained in detail in Chapter 5. To have an accurate mathematical model covering the range of deviation, random variables are needed to be sampled. And this sampling must be based on good algorithms for better response surfaces. As the sampling covers the specified ranges better, the response surface models will have better correlation coefficients.

For the utilization of thermomechanical analysis sets, latin hypercube sampling (LHS) method is used. In the vibration analysis, one of the box methods named face-centered cube (FCC) design are used since analysis sets consist less elements.

3.4.1 Face-Centered Cube Design

Face-centered cube design is one of the central composite design techniques which is the most popular class of second order designs and it was first introduced by Box and Wilson in 1951 [45]. When the region of operability and the region of interest is same, the region for the design is called cuboidal region. Face-centered cube design is considered as effective in case of cuboidal regions and it is used in the generation of different analysis sets for obtaining the frequency response functions for the maximum principal stress at critical region. A total of

fifteen design points are utilized as seen in Figure 3.12 and Table 3.5.

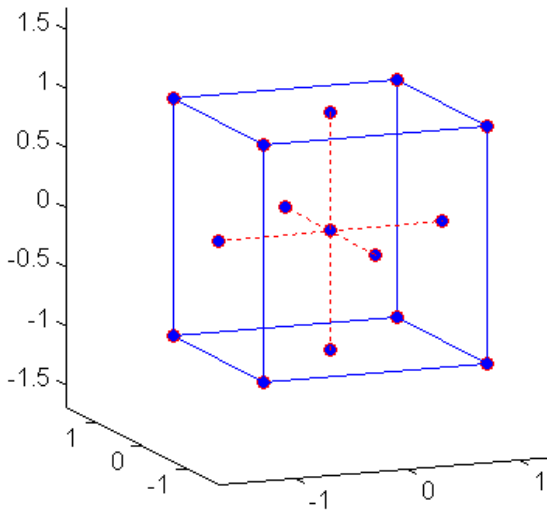

Figure 3.12: Face-centered cube design

Table 3.5: Input data sets for the generation of frequency response function (FRF) for the maximum principal stress at critical region

Set	Propellant Temperature (°C)	Modulus Deviation (%)	Loss Factor Deviation (%)
1	-40	-30	-20
2	-40	-30	20
3	-40	30	-20
4	-40	30	20
5	70	-30	-20
6	70	-30	20
7	70	30	-20
8	70	30	20
9	-40	0	0
10	70	0	0
11	15	-30	0
12	15	30	0
13	15	0	-20
14	15	0	20
15	15	0	0

Apart from the temperature, modulus and loss factor, acceleration spectral densities and calculated cumulative damage due to vibratory load values have deviations as seen in Table 3.6

Table 3.6: Input data sets for the generation of frequency response function (FRF)

Set	FRF	ASD Deviation from the Nominal (%)	Deviation Factor from the Nominal Cumulative Damage (%)
1-15	15 generated FRFs	-30	-50
16-30	15 generated FRFs	-30	50
31-45	15 generated FRFs	30	-50
46-60	15 generated FRFs	30	50
61-75	15 generated FRFs	-30	0
76-90	15 generated FRFs	30	0
91-105	15 generated FRFs	0	-50
106-120	15 generated FRFs	0	50
121-135	15 generated FRFs	0	0

3.4.2 Latin Hypercube Sampling Method

This sampling method is also named as stratified sampling technique. The name of the algorithm comes from ”latin square” array in which symbols or numbers only occur once. The term ”hypercube” denotes the extension of this concept to higher dimensions for many design variables [46]. The main purpose in using this algorithm is to avoid overlapping sampling points and generate multivariate samples of statistical distributions. Steps of the sampling method are listed as follows [46]:

1. Divide the distribution into n overlapping intervals.
2. Select one value at random from each interval with respect to its probability density.
3. Repeat 1 and 2 for all random variables.
4. Associate the n values obtained for each variable at one interval with the n values obtained for the other variable randomly.

In the sampling of deterministic storage analysis sets, latin hypercube sampling tool in MATLAB software is used. Total of 50 analysis sets are created using the proposed method and these sets can be seen in Appendix B. Furthermore, histograms of the sampled variables are given in the same appendix.

CHAPTER 4

DEVELOPMENT AND ANALYSIS OF COMPUTATIONAL MODEL

To predict the response of the system to environmental and transportation loads, a computational model is to be prepared. Failure in solid propellant rocket can only be predicted from the stress-strain response. Hence, finite element method (FEM) is used to predict this particular response.

In the finite element method, a domain is viewed as a collection of subdomains, and over each subdomain the governing equation is approximated by any of the traditional variational methods [47]. Finite element analysis can be done using the readily available commercial FEM tools. In this study, for the storage analysis, MSC.Marc is used as finite element analysis solver and for transportation analysis, MSC.Nastran is used.

MSC.Marc is a nonlinear finite element analysis solution code, and one of the most frequently used tools for obtaining the stress-strain response in viscoelastic materials. Apart from the accurate modeling of viscoelastic materials, it has a large element library including reformulated elements for near-incompressibility [1].

MSC.Nastran is one of the most recognized finite element solvers in predicting the vibration response. Dynamic characteristics of viscoelastic materials can be defined as inputs to code. For the frequency response analysis of the computational model of the system, this tool is used and frequency response functions are obtained.

To make a finite element analysis of the system that has been considered, the domain has to be divided to subdomains first. That is done with meshing the structure. In other words, mathematical discretization of the system is done using finite elements. For storage and trans-

portation, different finite element models are prepared. A general look to the finite element model prepared for the storage analysis is given in Figure 4.3.

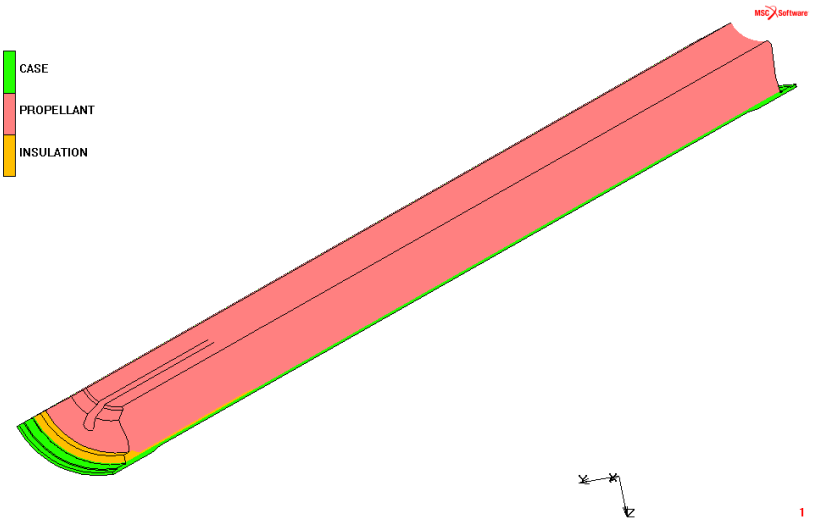

Figure 4.1: General view of finite element model for storage analysis

A more detailed view of the finite element model is illustrated in Figure 4.2. The model consists of 20534 eight nodded hexahedral elements and 26029 grid nodes. Only one seventh of the rocket motor is modeled due to the cyclic symmetry. Steel case, thermal insulation and propellant grain is modeled for the finite element analysis.

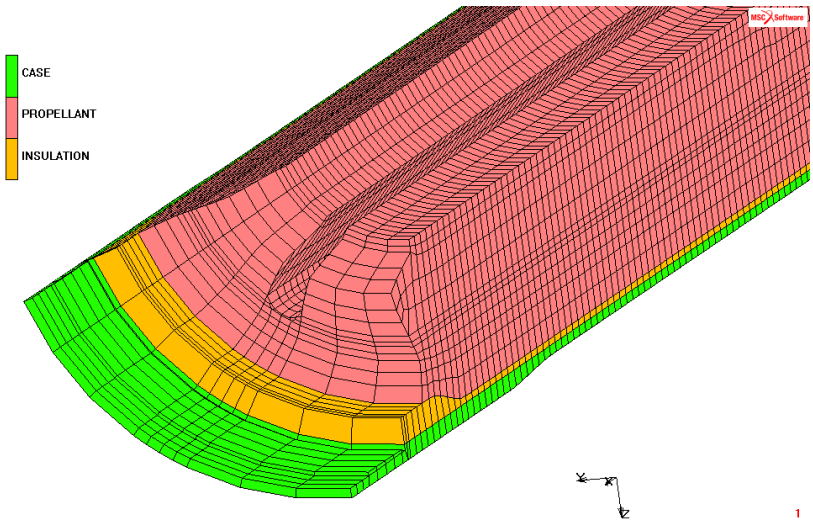

Figure 4.2: Detailed view of finite element model for storage analysis

For transportation, a full finite element model is built, since the problem is not cyclic symmetric in that case. The model has 101772 eight nodded hexahedral elements and 117929 grid nodes. Multi point constraints and point masses are used to include the mass effect of warhead and nozzle.

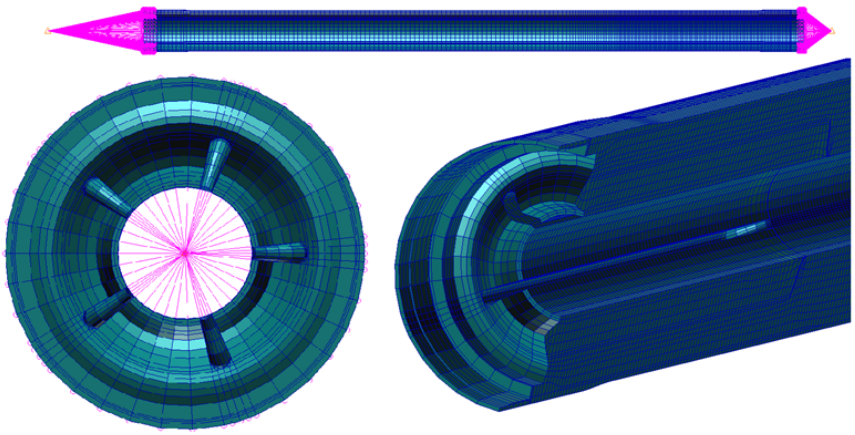

Figure 4.3: General view of finite element model for modal analysis

As mentioned before MSC.Marc has an element library including the reformulated elements for near-incompressibility. These elements are using the variational principles of Herrmann [48]. Hence, for propellant grain, eight-nodded Herrmann reformulated elements with full integration is used which have an element ID of 84. Case and insulation is modeled with using eight-nodded full integration elements which have an element ID of 7 since these materials do not show any incompressibility behaviour [49].

It is explained that using Prony series for representation of relaxation function is a common practice in viscoelastic materials. Relaxation modulus of the viscoelastic materials can be entered to MSC.Marc using Prony series constants directly which are shown in Equation 4.1 with E_i and τ_i. Moreover, constants of Williams-Landel-Ferry (WLF) shift function are given as input to the finite element program.

$$E(t) = E_\infty + \sum_{i=1}^{N} E_i \cdot exp(\frac{-t}{\tau_i}) \tag{4.1}$$

For the modal analysis, MSC.Nastran provides the ability to represent complex frequency dependent material modulus of the form,

$$G(i\omega) = G'(\omega) + iG''(\omega) \tag{4.2}$$

where G' is denoted as the shear storage modulus and G'' is named shear loss modulus. And the ratio of the shear loss modulus to shear storage modulus is denoted as the shear loss tangent as shown in the equation below.

$$\frac{G''(\omega)}{G'(\omega)} = tan(\phi) \tag{4.3}$$

The above formulation of viscoelastic (frequency-dependent) material properties may be used in direct frequency analysis. Solution procedure of the finite element solver is named SOL108 [50].

4.1 BOUNDARY CONDITIONS

For deployment and transportation phenomena, two seperate finite element models have been prepared as mentioned in last section. To formulate a finite element problem, boundary conditions are need to be defined to the system. These boundary conditions for thermomechanical and modal analysis are illustrated in coming sections.

4.1.1 Thermomechanical Analysis

Thermomechanical analysis consists of two problems. One is the thermal problem in the specified domain which needs to be solved in order to find the temperature field of the system. Second is the mechanical part which physically defines the domain. Boundary conditions of these problems are illustrated in Figure 4.4 and Figure 4.5 respectively.

For the initial condition, a constant temperature field which the temperature equals to the stress-strain free temperature of the propellant is given. Stress-strain free temperature of the propellant is an experimentally defined value and it can be found using the formula below.

$$T_{str,free} = T_{cure} + \Delta T \tag{4.4}$$

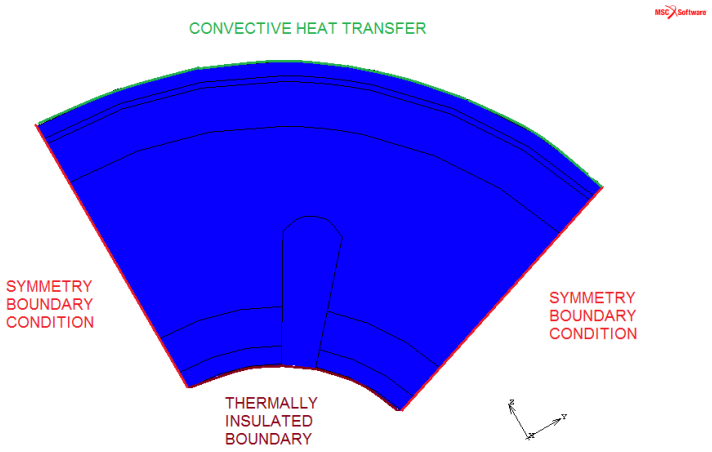

Figure 4.4: Definition of thermal boundary conditions

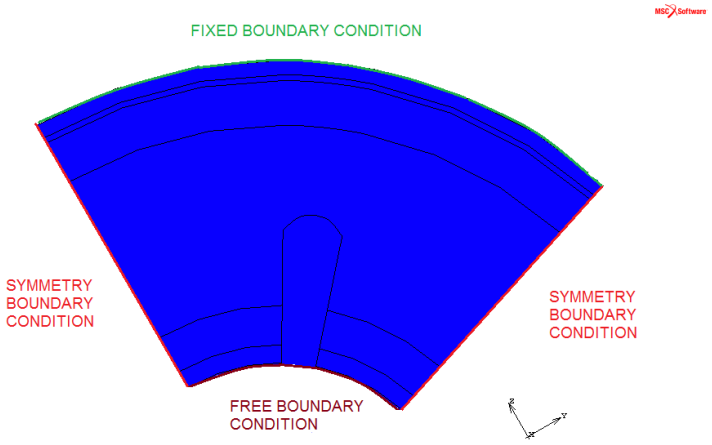

Figure 4.5: Definition of mechanical boundary conditions

A temperature of value ΔT is added to the cure temperature to compensate the cure shrinkage and residual stress effects. This value of ΔT can be in the range of 10-20 °F [10].

Then, as a boundary condition convective heat transfer is defined at the boundary shown in Figure 4.4 in which the film temperature equals to the environmental temperature. The environmental temperature model is explained in detail in Chapter 3.

4.1.2 Vibration Analysis

For the frequency response analysis, the finite element model that is seen in Figure 4.6. Boundary conditions of the acceleration and connection degree of freedoms are illustrated in the figure. For the vertical, transverse and longitudinal excitations, the directions of these boundary conditions are changed accordingly. For connection degree of freedoms, displacement boundary conditions are given to the both ends of rocket motor as in the figure.

In the analysis, acceleration is defined in vertical, transverse and longitudinal axes one at a time and other degrees of freedom of the excitation points are constrained using displacement boundary conditions.Using this assumption, frequency response function of maximum principal stress is obtained in terms of single acceleration input only and the response is superposed in power spectral density analysis since acceleration loads are assumed to be uncorrelated in these three perpendicular axes.

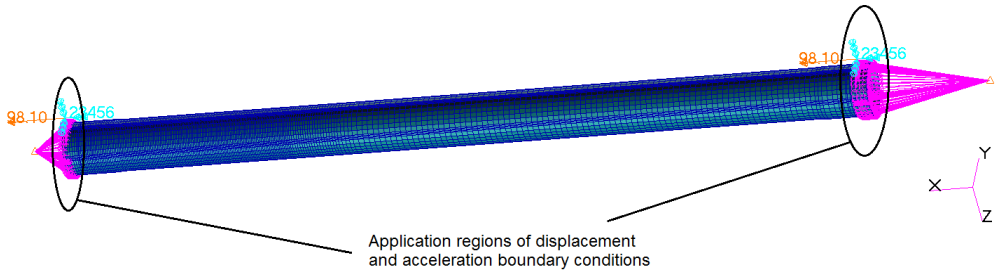

Figure 4.6: Boundary conditions of the frequency response analysis

4.2 FINITE ELEMENT ANALYSIS

With dividing the domain to subdomains, specifying the necessary material models and boundary conditions to define the problem, finite element analysis is ready to be conducted. At later sections, the results of the finite element analysis are given.

4.2.1 Thermomechanical Analysis Results

As part of the thermomechanical analysis, first the thermal problem is solved and temperature gradients are formed. Then, using the temperature field, stress-strain response of the system is calculated.

In Figure 4.7, thermal gradient of the first cooldown cycle is illustrated.

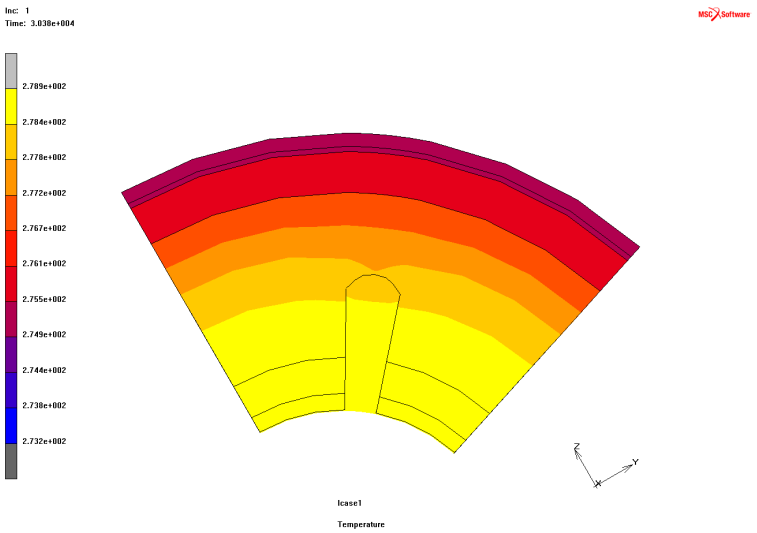

Figure 4.7: Temperature gradient on the solid rocket motor at the first cooldown cycle

Using the temperature field obtained for each load step, stress-strain response of the system is determined. In Figure 4.8 equivalent total strain on the solid rocket motor at an arbitrary time is given. It is seen that the maximum strain region on the motor is found in the fin section. Looking to the stress response in Figure 4.9, it can be concluded that the fin section is the most critical part of the solid rocket motor in thermomechanical fashion.

4.2.2 Vibration Analysis Results

As results of modal analysis, frequency response functions for the maximum principal stress at the stress critical region in the longitudinal, vertical and transverse excitations are obtained. These frequency response functions are illustrated in Figure 4.10, Figure 4.11 and Figure

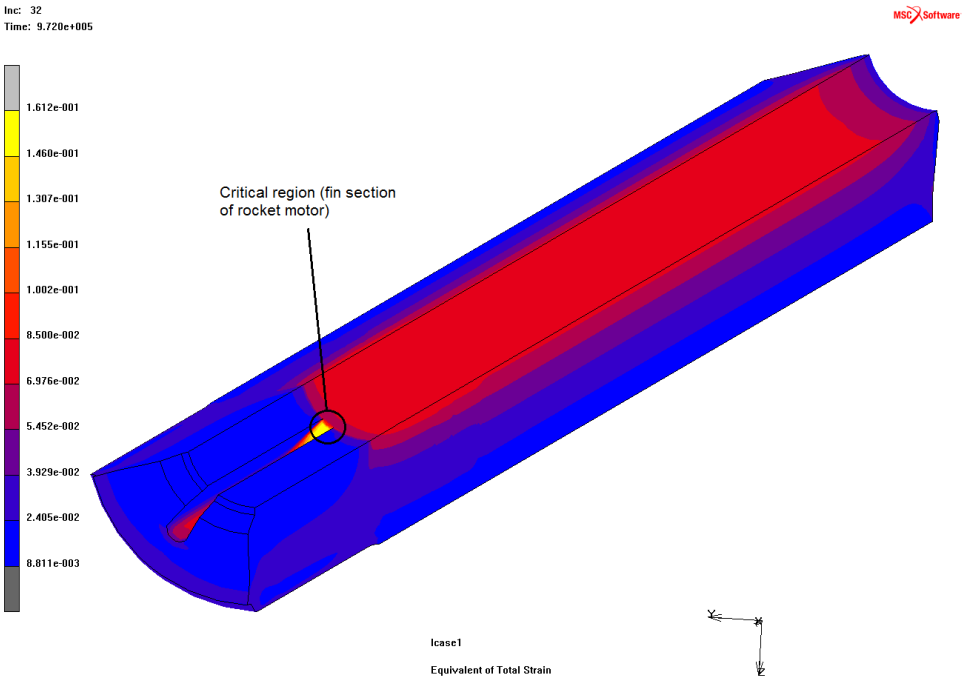

Figure 4.8: Equivalent total strain on the solid rocket motor at an arbitrary time

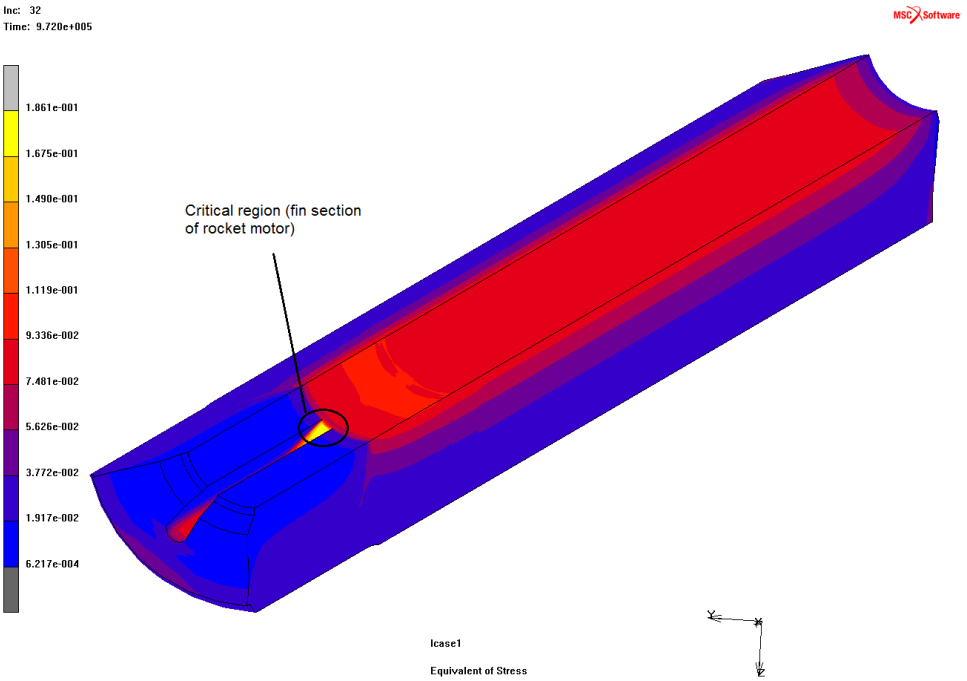

Figure 4.9: Equivalent stress on the solid rocket motor at an arbitrary time (MPa)

4.12, respectively.

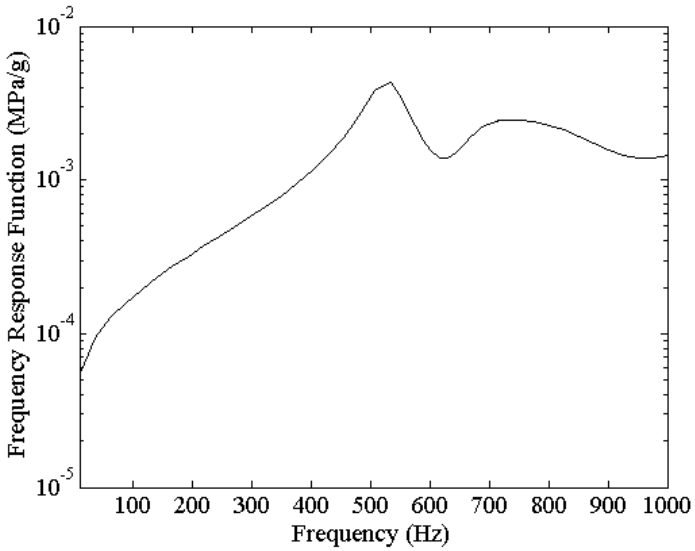

Figure 4.10: Frequency response function for maximum principal stress at the stress critical region (Longitudinal excitation)

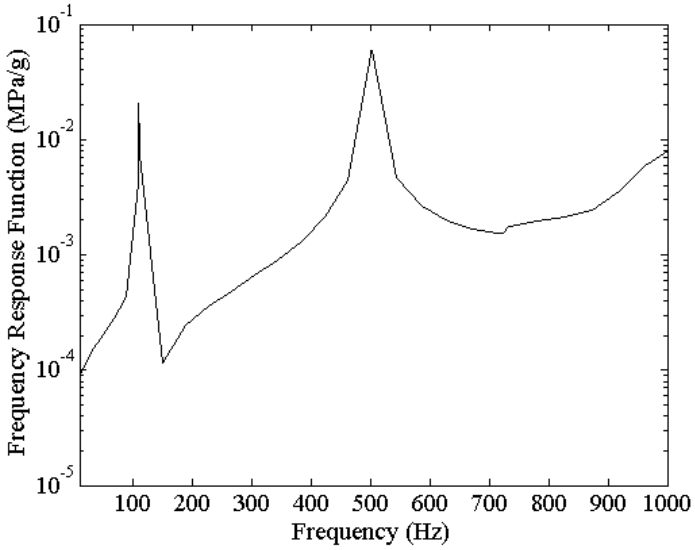

Figure 4.11: Frequency response function for maximum principal stress at the stress critical region (Vertical excitation)

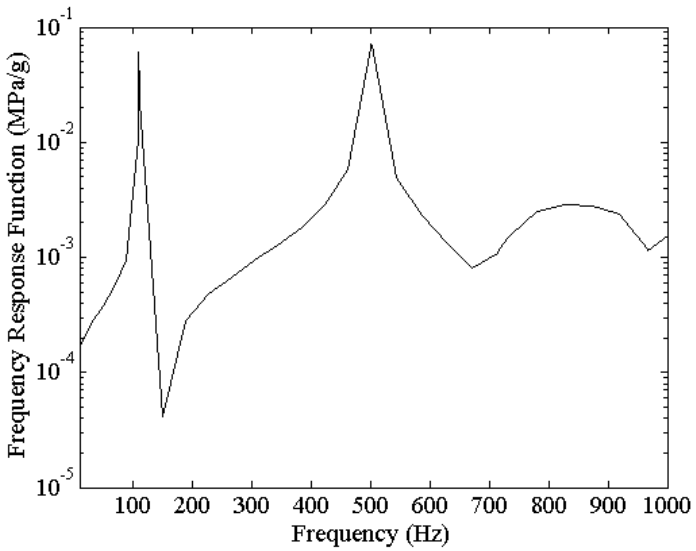

Figure 4.12: Frequency response function for maximum principal stress at the stress critical region (Transverse excitation)

Inspecting the figures, it can be observed that the first resonance frequency of the grain in case of longitudinal excitation is around 530 Hz while the first resonance frequency is around 110 Hz in case of vertical and transverse excitation. These frequency response functions are used to determine the spectral density vectors for the maximum principal stress at stress critical region using the acceleration spectral density values for different types of transportation environments.

4.3 INTERPRETATION OF THE RESULTS

Again, there will be two separate subsections since thermal and vibratory analyses are carried our independently. In the first section using the harmonic nature of temperature input and output, an FFT analysis will be done. And in the next section, a PSD analysis is done to account vibrations.

Flow chart representing the methodology in the finite element part of this study is given in Figure 4.13.

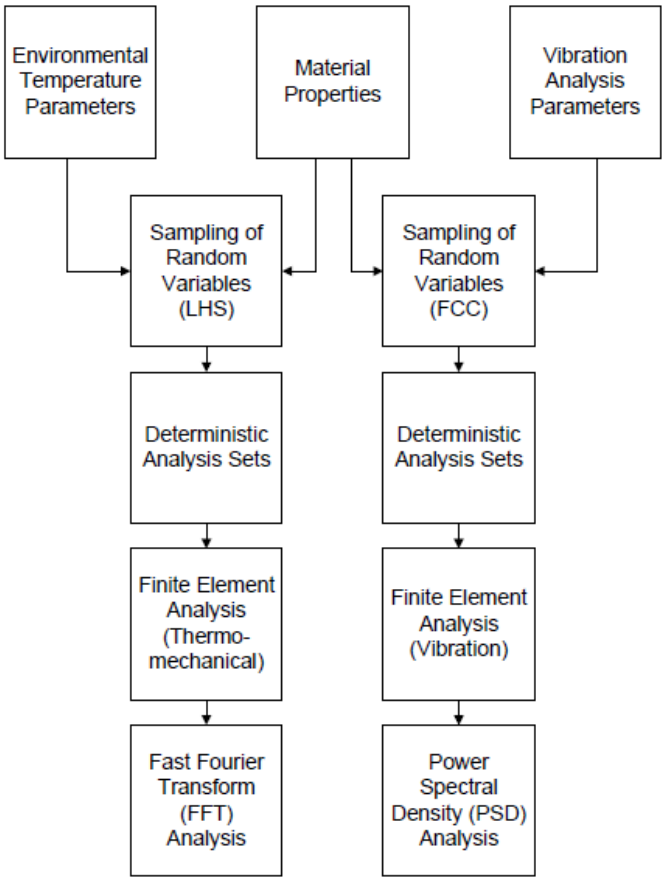

Figure 4.13: Flow chart of finite element analysis part

4.3.1 Thermomechanical Analysis Results

The critical region of the solid rocket motor is determined using with inspecting the results. Now, the strain and stress response of the motor is determined at the critical region, namely the fin section.

The output of equivalent strain at the critical region of the rocket motor for one year is given in Figure 4.14. The response of Set 1 is illustrated in the figure and all analysis sets can be found in Appendix B. Different analysis sets stand for the same finite element analysis routine using different material and environmental temperature model properties. From the figure one can observe that the response is harmonic like the environmental temperature model.

Furthermore, since only first and second cycles can be observed for the yearly frequency

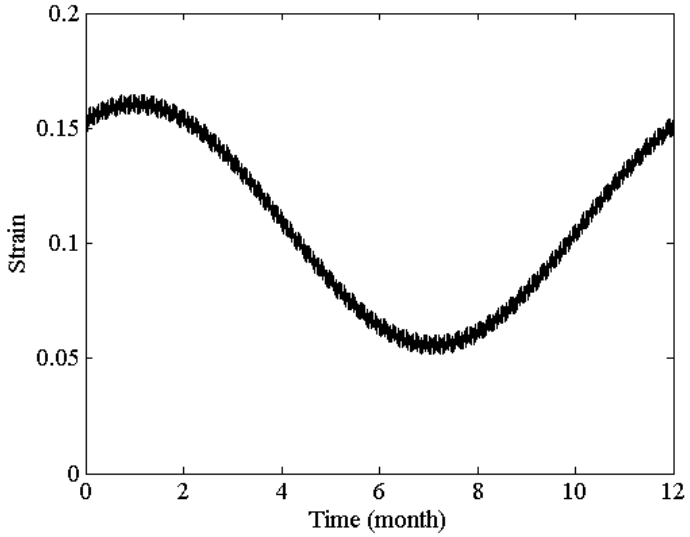

Figure 4.14: Equivalent strain response at the critical section (Set 1)

harmonic, an analysis of the system for five years is done to check for any transient response of the system at this frequency. Daily frequency component is not given to the system for this particular analysis. Strain response at the critical region of the rocket motor is illustrated in Figure 4.15 and it is concluded that no transient response is present in the system.

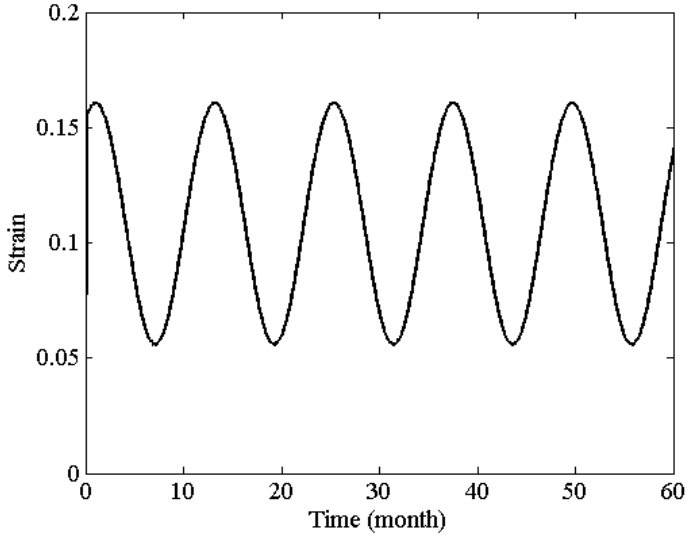

Figure 4.15: Equivalent strain response at the critical section for 5 years excluding daily temperature change (Set 1)

4.3.1.1 Fast Fourier Transform (FFT) Analysis

Harmonic stress and strain outputs are decomposed into amplitudes at mean value, yearly and daily frequencies. For the decomposition fast Fourier transform (FFT) algorithm is used and the decomposition of the equivalent strain response is illustrated in Figure 4.16. The response is and the transform is checked in case of spectral leakage. Amount of leakage is influenced by the sampling period and the sampling of FFT is selected to prevent the phenomenon [51].

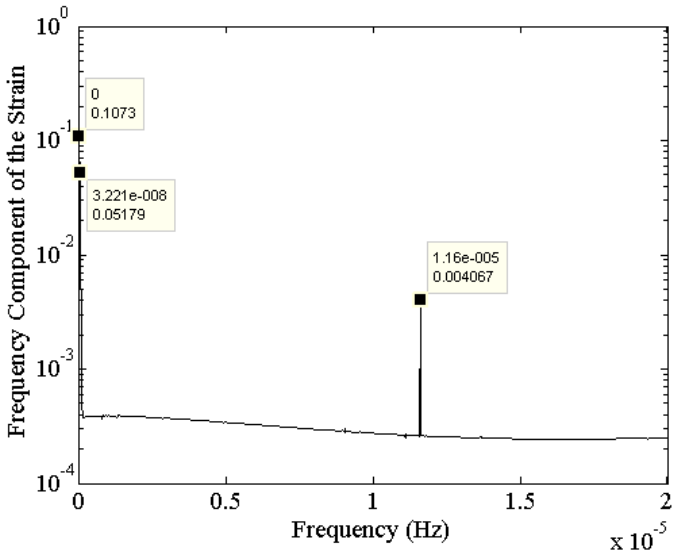

Figure 4.16: FFT of the equivalent strain response at the critical section (Set 1)

With decomposing the amplitudes of the harmonic stress and strain outputs, it is aimed to correlate the inputs to this harmonic amplitudes directly using the response surface method. Fast Fourier transform (FFT) results showed that stress and strain response is harmonic and this harmonic components have the same frequency with the environmental temperature model. Therefore, these responses can be expressed as shown below.

$$\sigma(t) = \sigma_M + \sigma_Y sin\left(\frac{2\pi}{8760}\right)(t - t_0) + \sigma_D sin\left(\frac{2\pi}{24}\right)(t - t_1) \tag{4.5}$$

$$\epsilon(t) = \epsilon_M + \epsilon_Y sin\left(\frac{2\pi}{8760}\right)(t - t_0) + \epsilon_D sin\left(\frac{2\pi}{24}\right)(t - t_1) \tag{4.6}$$

where σ_M is the total mean of the stress, σ_Y is the yearly amplitude of the stress and σ_D is the daily amplitude of the stress. Similar to stress function, ϵ_M is the total mean of the strain, ϵ_Y is the yearly amplitude of the strain and ϵ_D is the daily amplitude of the strain. The formation of the response surfaces for the harmonic amplitude outputs is explained in next chapter.

4.3.2 Vibration Analysis Results

Frequency response functions that has been presented in preceding section are used to find the spectral density vectors for the maximum principal stress vectors as explained in detail below.

4.3.2.1 Power Spectral Density (PSD) Analysis

After the calculation of frequency response functions for the maximum principal stress at the critical region of the rocket motor, spectral density values of the maximum principal stresses at the critical region are utilized using the equation below. The vibration loads are assumed to be stationary and uncorrelated in transverse, vertical and longitudinal axes. Thus, the cross correlation function between any pair of source axes is zero. Using that property, the power spectral density of the total response is found equal to the sum of the power spectral densities of the responses due to individual sources as shown [50].

$$S_j(\omega) = \sum_a |H_{ja}(\omega)|^2 S_a(\omega) \tag{4.7}$$

where $S_j(\omega)$ is the spectral density for maximum principal stress, $S_a(\omega)$ is the input acceleration spectral density, $H_{ja}(\omega)$ is the frequency response function for the maximum principal stress. Frequency responses of maximum principal stress at different axes are denoted by subscript a.

Maximum principal stress spectral densities at critical region of the nominal case for ground, air and sea transportation is given in Figures 4.17, 4.18 and 4.19 respectively.

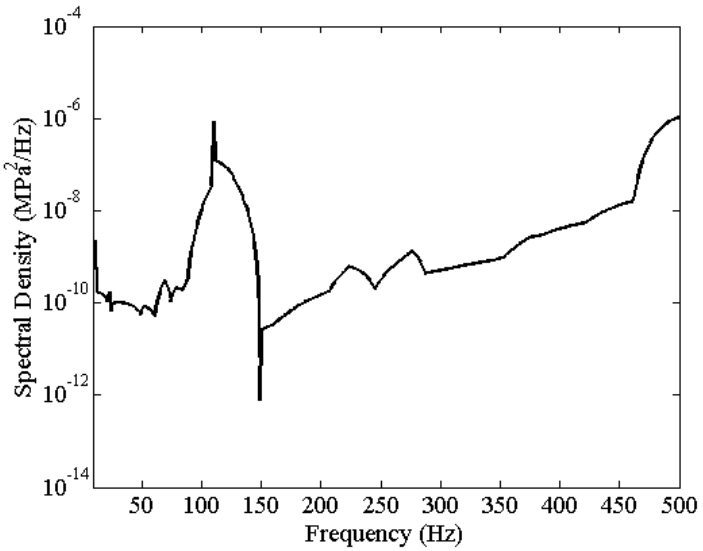

Figure 4.17: Maximum principal stress spectral density at critical region for nominal case (Ground transportation)

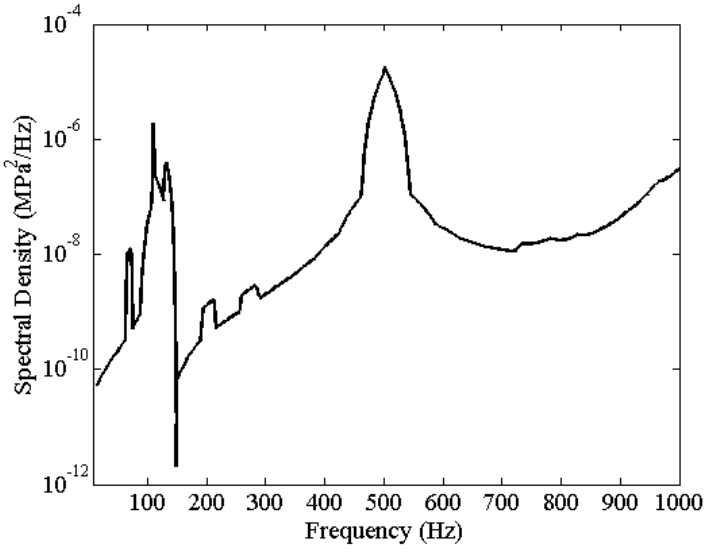

Figure 4.18: Maximum principal stress spectral density at critical region for nominal case (Air transportation)

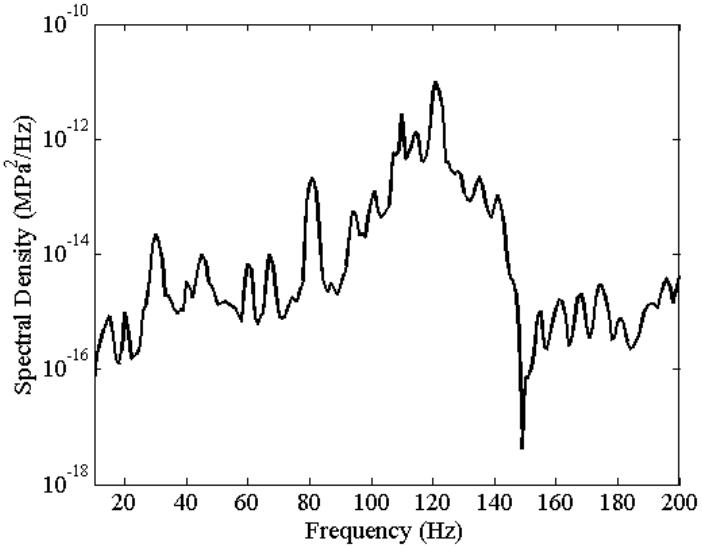

Figure 4.19: Maximum principal stress spectral density at critical region for nominal case (Sea transportation)

Using the stress spectral densities, stress history for each transportation case for a short duration of time is generated. These stress values are illustrated at Figures 4.20, 4.21 and 4.22 respectively.

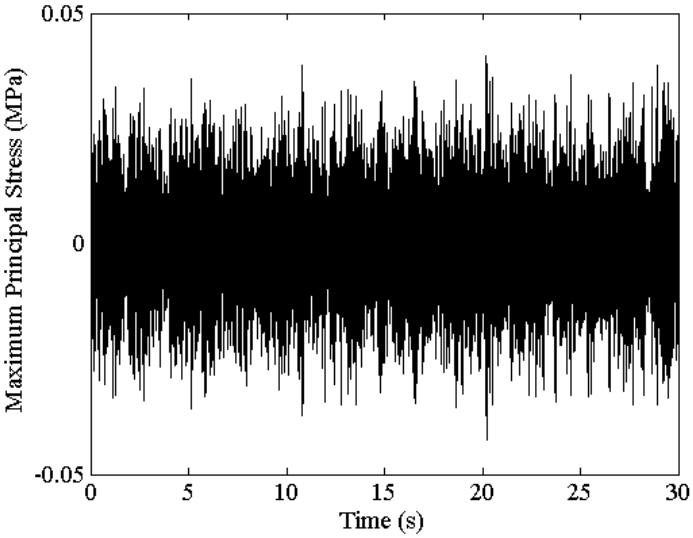

Figure 4.20: Stress history for nominal case (Ground transportation)

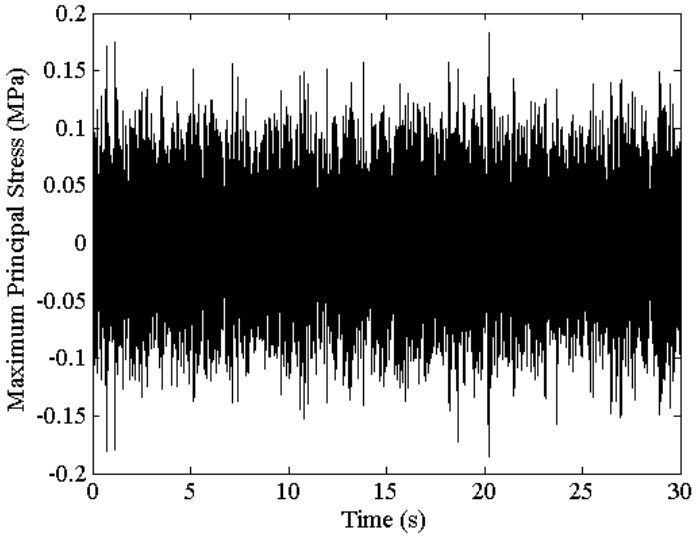

Figure 4.21: Stress history for nominal case (Air transportation)

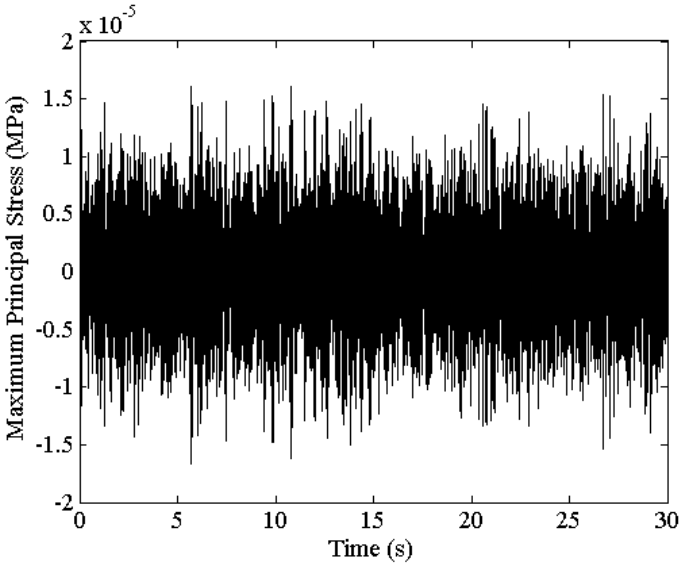

Figure 4.22: Stress history for nominal case (Sea transportation)

The stress history information is used to calculate the cumulative damage for various ways of transportation. Then, the cumulative damage values are used to form the response surfaces. This way, mathematical models are formed for the determination of cumulative damages for different transportation scenarios, material properties and temperatures. Apart from the temperature, modulus and loss factor of the propellant, deviations are given to input acceleration

spectral density (ASD) functions and nominal cumulative damage values. Thus, total of 135 cumulative damage values are calculated for response surfaces. The formation of these response surfaces and assessment of reliability is explained in detail at next chapter of this study.

At next chapter, using the results of thermal and vibration analyses, mathematical models are utilized and then the probability of failure is calculated for the rocket motor.

CHAPTER 5

RELIABILITY ASSESSMENT BASED ON THE RESULTS OF COMPUTATIONAL MODEL

The computational analysis of the system is done and results of finite element analyses are to be used to estimate reliability. For the estimation, first, mathematical models are to be utilized and that is done using response surface method. Hence, first section of this chapter is devoted to explain this method.

A diagram showing the methodology from this point on can be seen in Figure 5.1. The results of power spectral density (PSD) and fast Fourier transform (FFT) analyses are used to build the mathematical response surface models. Then, using this mathematical models of storage and deployment cases, a comprehensive reliability assessment is done using first order reliability method (FORM). This chapter is devoted to explain the mathematical modeling and reliability prediction phases of this study.

5.1 RESPONSE SURFACE METHOD

To determine the response of complex structures like solid rocket propellants, a considerable effort is made as it is presented in last section. Detailed finite element models are prepared and solved using an extensive computational power. With conducting the analysis, a response is obtained for only the predefined set of inputs. To relate the inputs of the structural analysis to the output with a governing mathematical expression, response surface methodology is used. This mathematical model will give the results in terms of the variables considered and from that information, we can conclude how sensitive the results are to input parameters.

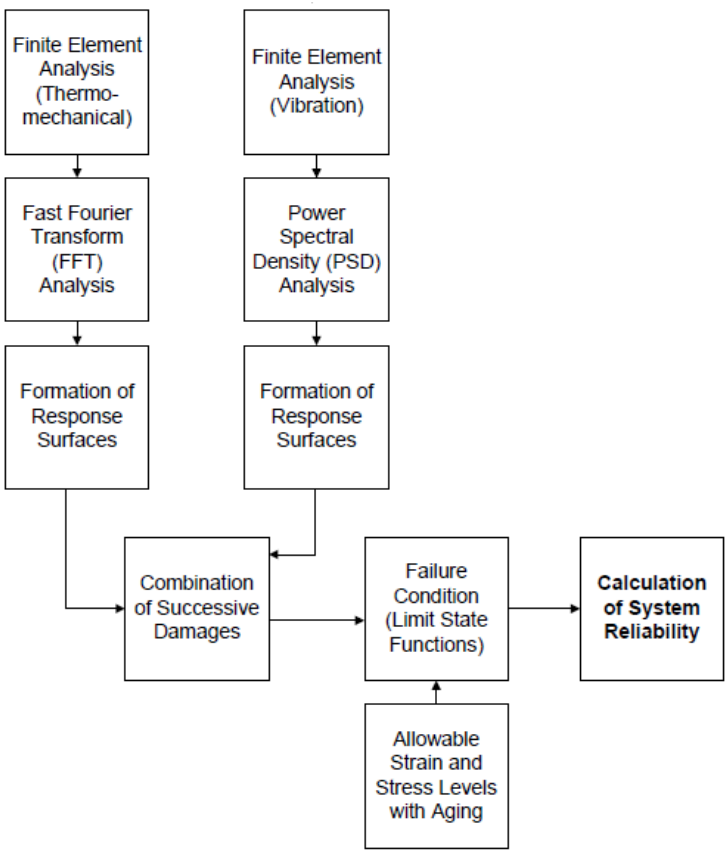

Figure 5.1: Methodology in the reliability assessment part

Response surface method (RSM) is a design of experiments technique in order to determine the behavior of a complex system. Relations between inputs and high order effects can be found with this method. System outputs are calculated from predetermined input parameters to find response of the system.

If the output of system is y and the factors affecting output are X_i (input parameters), the output can be defined as a second order mathematical model shown below.

$$y = a_0 + \sum_{i=1}^{k} a_i X_i + \sum_{\substack{i=1,j=2 \\ i<j}}^{k} a_{ij} X_i X_j + \sum_{i=1}^{k} a_{ii} X_i^2 \tag{5.1}$$

In response surface methodology, main difficulty is to define representative combinations of the random design variables to produce a representative output [52]. Hence, representative inputs must be selected strategically for a better response surface. Experimental design methods

and various sampling algorithms can be used for that purpose which are explained in Chapter 3. The methodology in utilizing the response surfaces is illustrated in Figure 5.2. First, the design parameters that is critical to system response is selected and then, the boundaries need to be specified. After this specification, appropriate sampling algorithm is used and deterministic experiments are conducted in this fashion. Having the results of the experiments, response surface is designed using regression.

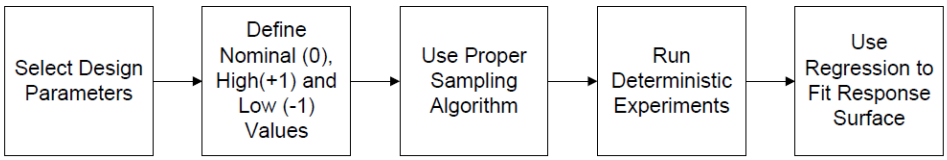

Figure 5.2: Methodology in utilizing the response surfaces

After conducting the experiments in design points, using regression, mathematical expression is formed. The regression equation estimates the output variables accurately as long as the values for all the design variables are somewhere between their low and high values [52].

Linear least squares regression is used in fitting the response surfaces, and correlation coefficients are found to evaluate the quality of fit. A vector of predicted output y_{pr} can also be written in terms of input parameters X and predicted coefficients a as,

$$\{y_{pr}\} = [X] \cdot \{a\} \tag{5.2}$$

To estimate the quality of fit, coefficient of determination, r^2 can be calculated using the formula [53],

$$r^2 = \frac{S_t - S_r}{S_t} \tag{5.3}$$

where S_r is the sum squares of errors and S_t is the sum of squares. These parameters are defined as shown in the equations below.

$$S_r = \sum_{i=1}^{n} (y_i - y_{pr,i})^2 \tag{5.4}$$

$$S_t = \sum_{i=1}^{n} (y_i - \bar{y})^2 \tag{5.5}$$

where $\bar{y}$ is the average of the response values.

Apart from calculating the coefficient of determination values, cross validation can be used to determine the goodness of fit level of response surfaces. For the cross validation, data points in the region of interest which are different than the design points are used. Then, using the actual results, and response surface predictions, a cross validation graph is utilized. Data points lying on the 45°line shows the match between the actual results and prediction of mathematical model. Hence, more points in the vicinity of 45°line, better the response surface is [37].

Response surfaces are formed for determining the strain and stress response in the storage and cumulative damage in transportation. In Figure 5.3, a cross validation graph shows that how the fitted model correlates with the finite element results in the case of yearly strain amplitude. All strain and strain response amplitudes have shown similar regression characteristics. Response surfaces that are utilized for the temperature response has coefficient of determination values in order of 0.999 and 1.

Apart from the storage, for the damage accumulated in vibration analyses, mathematical models are utilized using response surface methodology. The case of ground vibration is illustrated in Figure 5.4 only as the correlation is similar in all cases. Inspecting the figure, it can be said that response surface has predicted the lower damage values poorly. However, a coefficient of determination value of 0.97 is obtained using linear least squares regression. Furthermore, moderate and higher damage values are estimated accurately. Examining the results, the accuracy of the response surface is considered to be good enough.

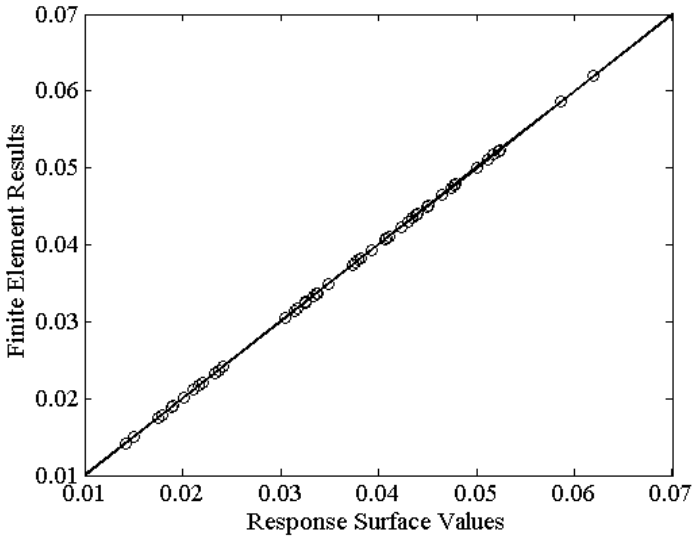

Figure 5.3: Comparison of response surface values with FEA results (Yearly strain amplitude)

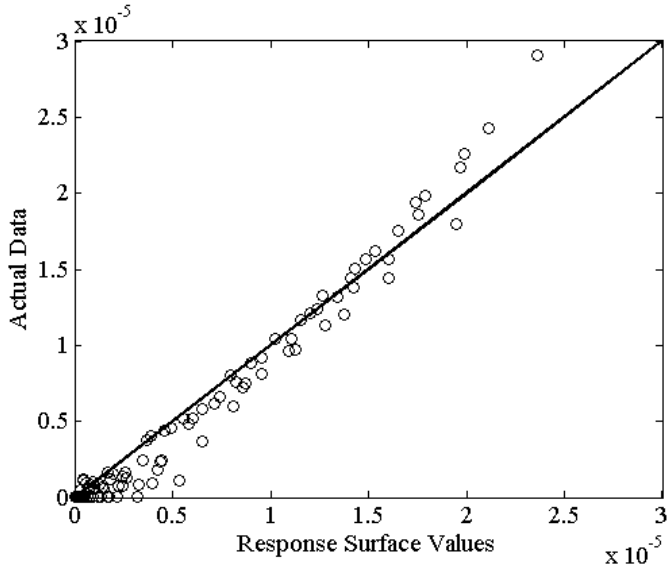

Figure 5.4: Comparison of response surface values with actual damage values of ground transportation

Mathematical models prepared using response surface methodology are going to be used in reliability estimation. Since the response models are built using the input variables that have inherent uncertainty, it is meaningful to estimate reliability in a confidence bound. To estimate reliability in that sense, method proposed by Vittal and Hajela is used in this study [54].

At this point, a confidence interval has to be defined for the calculations. In this study, confidence interval of 95% is used. Using this confidence interval, upper and lower bounds of the response surfaces are determined. If the output is shown as y as the function of input parameters X, upper and lower limits can be expressed as,

$$y(X)^L \leq y(X) \leq y(X)^U \tag{5.6}$$

Upper and lower limits of the response surface can be found using the regression tool in MATLAB. Mathematical expressions for the upper and lower limits of the response surfaces can be seen in Reference [54].

5.2 DEGRADATION MECHANISMS

There are two main degradation mechanisms of propellant grain capability, namely the cumulative damage and chemical aging. Cumulative damage and aging models that are being used are explained in Chapter 2. For the cumulative damage Laheru's linear cumulative damage model based on Miner's law is used and for aging, Layton's aging model is used. In this part, the effect of these mechanisms are illustrated.

5.2.1 Cumulative Damage

Considering the solid rocket motor system, both temperature and vibration loads are the cause of the successive damage. This cumulative damage effect can be superposed assuming the loads are independent of each other. This is considered as a very conservative approach used by United States, United Kingdom and France with different variations and known as damage factor approach or method [1].

According to the method, damage factors coming from thermal and vibration loads are super-

posed as follows.

$$D(t)_{total} = D(t)_{th} + D(t)_{vb} \tag{5.7}$$

where $D(t)_{total}$ denotes the total damage factor, $D(t)_{th}$ is the damage factor coming from thermal loads and $D(t)_{vb}$ is the damage factor accumulated from vibration in the system. Total mean cumulative damage is illustrated in Figure 5.5. As seen in the figure, cumulative damage of 22% is observed in the propellant after 40 years of life cycle.

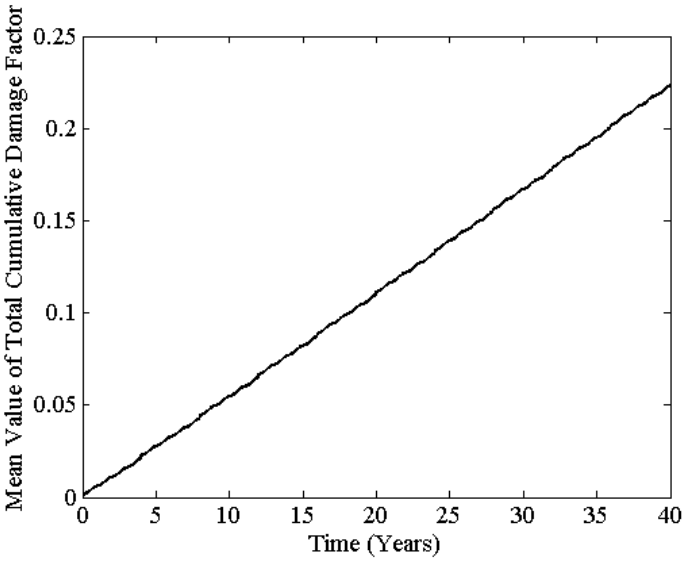

Figure 5.5: Cumulative damage factor vs. time

5.2.2 Aging

Chemical aging is one of the main causes of the deterioration of the mechanical properties of solid propellants as it is explained in detail in Chapter 2. In Figure 5.6, 5.7 and 5.8, rupture strain, rupture stress and instantaneous modulus of the propellant degradation with respect to time is illustrated. It is seen in the figures clearly that rupture strain value decreases with time. Nevertheless, rupture stress and modulus of the propellant increases with time. In this study, it is seen also that aging is dominant in rather high temperature environments than low temperatures. In Figure 5.9, it can be seen that instantaneous modulus of the propellant is

increasing more due to aging at high temperatures. Since the start time of the environmental temperature model is January, it is seen in the figure that the instantaneous modulus increases more in summer conditions.

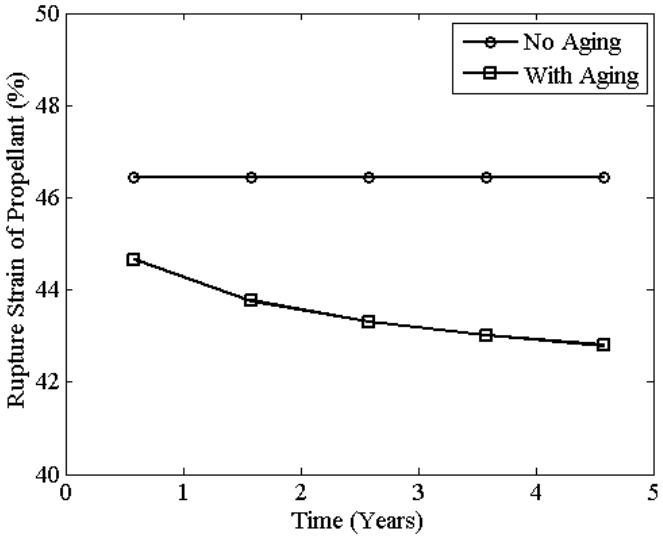

Figure 5.6: Rupture strain vs. time

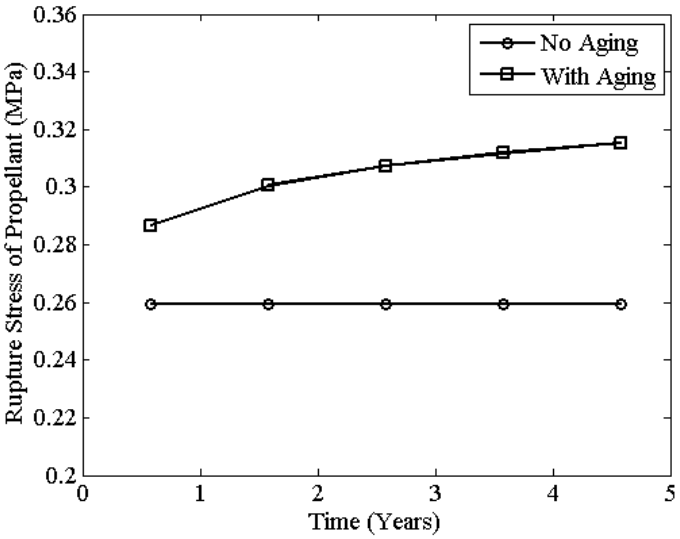

Figure 5.7: Rupture stress vs. time

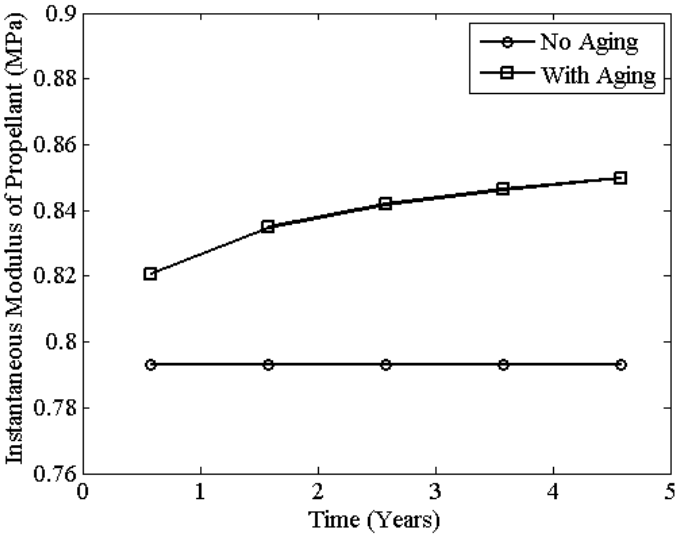

Figure 5.8: Instantaneous modulus of the propellant vs. time

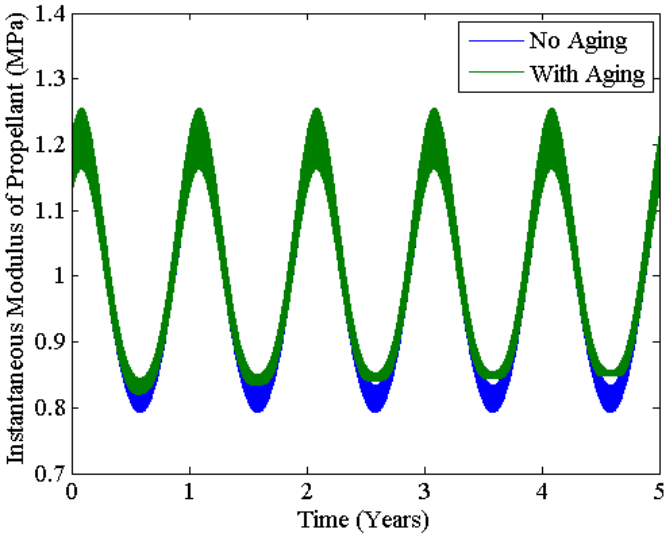

Figure 5.9: Effect of aging to instantaneous modulus of propellant at different temperatures

5.3 LIMIT STATE FUNCTIONS

If a structure or a part of structure exceeds a specific limit, then the structure or a part of structural is unable to perform as required. This specific limit is called as limit-state [46]. The

functions that define this specific limit states are called as limit state or performance functions. These functions are simply defined as,

$$g(X) = R(X) - S(X) \tag{5.8}$$

where g is the limit state function, R is the resistance and S is the loading of the system in where g, R and S are functions of random variables X. Limit state concept is illustrated in Figure 5.10. In the figure, limit state equation, safe and unsafe regions of the design is seen clearly.

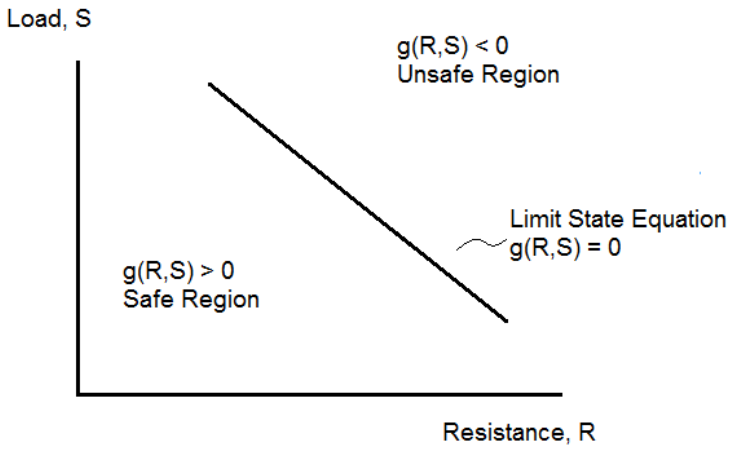

Figure 5.10: Limit state concept (Adapted from [55])

In this fashion, probability of failure can be expressed as the probability of performance function being smaller than zero.

$$P_f = P[g(X) < 0] \tag{5.9}$$

To predict the surface cracks and bondline separation, three limit state functions that are defined for the system. These limit state functions can be listed below as:

- Limit state function for the stress induced in the propellant grain
- Limit state function for the strain induced in the propellant grain

- Limit state function for the stress induced in the propellant-insulation bondline

and denoted with g_1, g_2 and g_3 respectively. These functions are mathematically expressed as follows.

$$g_1 = \sigma_{ind} - \sigma_{all} \tag{5.10}$$

$$g_2 = \epsilon_{ind} - \epsilon_{all} \tag{5.11}$$

$$g_3 = \sigma_{ind}^{bond} - \sigma_{all} \tag{5.12}$$

where in these equations subscript 'ind' denotes the induced strain and stress in the system and 'all' denotes the allowable strain and stress values.

To estimate these limit state functions in the specified confidence interval value, an upper and a lower limit is specified for all of them.

$$g_i = S_{ind} - S_{all} \quad \text{for } i = 1, 2, 3 \tag{5.13}$$

$$g_i^L = S_{ind}^L - S_{all} \quad \text{for } i = 1, 2, 3 \tag{5.14}$$

$$g_i^U = S_{ind}^U - S_{all} \quad \text{for } i = 1, 2, 3 \tag{5.15}$$

where S denotes any property that is being used for the limit state. Induced and allowable values are again denoted with the subscripts 'ind' and 'all'.

5.4 FIRST ORDER RELIABILITY METHOD

In this study, reliability assessment is done by using first-order second-moment (FOSM) reliability method. First order reliability method is selected because of its simple implementation and it is considered as an accurate method at the typical reliability allocation values of solid rocket motors. However, it has been shown that the accuracy of the method is not acceptable for probability of failure values lower than 10^{-5} and highly nonlinear responses [46]. The method is a first order method since it is based on a first-order Taylor series approximation of the performance function linearized at the mean values of the random variables. Also,

the method is called second-moment, because it uses only second-moment statistics (means and covariances) of the random variables [55]. The method is also referred as mean value first-order second-moment (MVFOSM) method since the limit state (performance) function is linearized at the mean values.

Failure condition is being any of the limit state functions to be smaller than zero, namely

$$g_1 \leq 0 \; or \; g_2 \leq 0 \; or \; g_3 \leq 0 \tag{5.16}$$

The probability of failure depends on the ratio of the mean value of the performance function over its standard deviation. This ratio is commonly known as the safety or reliability index [55].

$$\beta = \frac{\mu_g}{\sqrt{Var(g)}} = \frac{\mu_g}{\sigma_g} \tag{5.17}$$

The cumulative distribution function of the safety index gives us the probability of failure as,

$$P_f = \Phi(-\beta) \tag{5.18}$$

To find the variance of the performance function, first order Taylor series approximation is to be used. Carrying out the expansion, one will estimate the variance as:

$$Var(g) \approx \sum_{j=1}^{m} \left(\frac{\partial g}{\partial x_j}\right)^2 Var(x_j) \tag{5.19}$$

A conditional probability function called the hazard rate is defined at this point and denoted by $\lambda(t)$ [34]. This parameter is simply the probability of failure at time interval dt of the component that has survived to time t. It can be expressed mathematically as in the equation below.

$$\lambda(t) = \frac{P_f(t_i)}{1 - \sum_{j=1}^{i-1} P_f(t_j - 1)} \tag{5.20}$$

Mean value of the hazard rate of the first limit state, stress induced in the propellant grain is illustrated in Figure 5.11. It is observed that with the increasing cumulative damage value over time, the hazard rate value is increasing. Furthermore, hazard rates of the second and third limit states, namely the strain induced in the propellant grain and stress induced in propellant insulation bondline is illustrated in Figures 5.12 and 5.13. It is seen in the calculations that the hazard rates of second and third limit states are zero. Hence, reliability of these limit states are calculated as unity using Equation 5.21.

Using the hazard rate, time dependent progressive reliability can be expressed as,

$$R(t) = exp\Big(- \int_0^t \lambda(\zeta) d\zeta \Big) \tag{5.21}$$

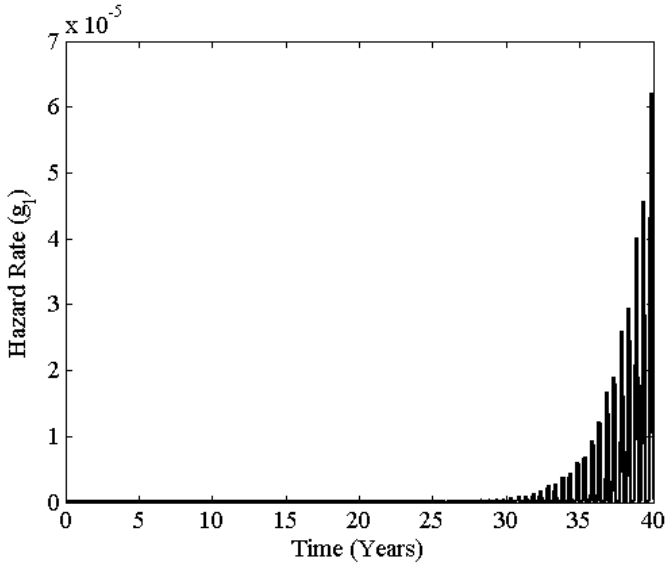

Figure 5.11: Hazard rate of the stress induced in the propellant grain

And the reliability can be related to the probability of failure with a simple formula shown as,

$$R(t) = 1 - P_f(t) \tag{5.22}$$

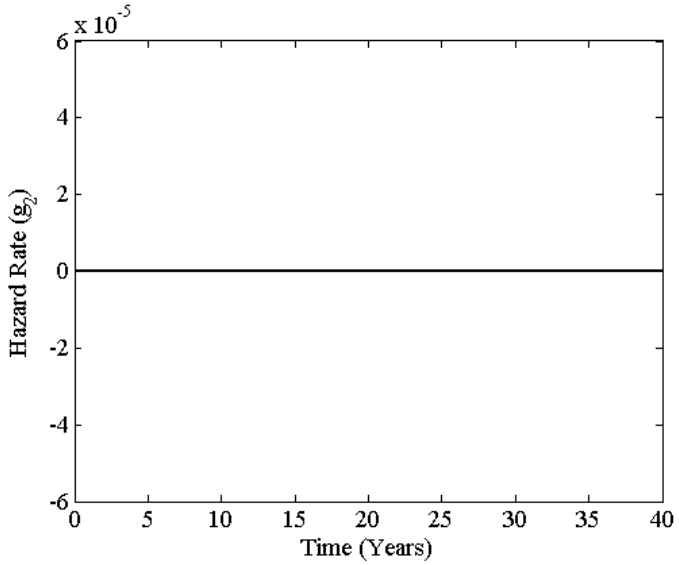

Figure 5.12: Hazard rate of the strain induced in the propellant grain

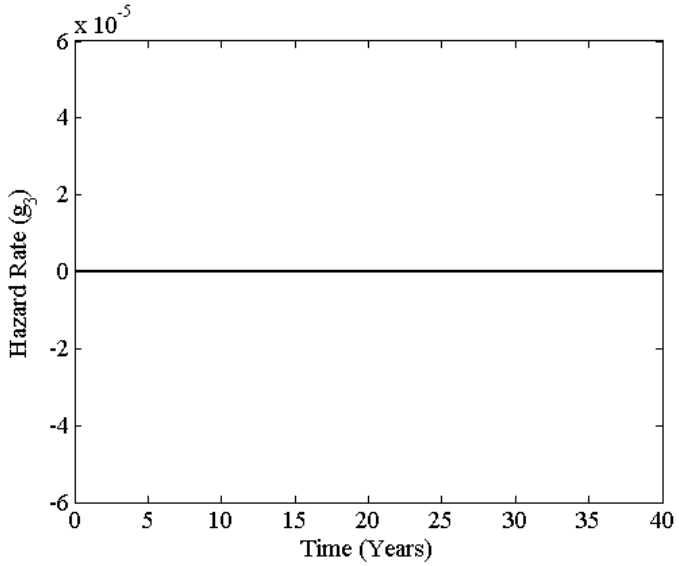

Figure 5.13: Hazard rate of the stress induced in the propellant insulation bondline

5.5 PROBABILITY OF FAILURE AND RELIABILITY OF THE SYSTEM

Probability of failure can be expressed as the likelihood of the system malfunction to occur. In this study, every limit state function represents a different failure criteria. Using three limit states, failure in the propellant grain is calculated as the union of three independent events.

Independent events may be approximated by the sum of probabilities [41].

$$P_{f,total}(t) = \sum_{i=1}^{n} P_{fi} = P_{f1} + P_{f2} + P_{f3} \tag{5.23}$$

Total system reliability can be found similarly using the multiplication rule of the reliabilities.

$$R_{total}(t) = \prod_{i=1}^{n} (1 - P_{fi}) = (1 - P_{f1})(1 - P_{f2})(1 - P_{f3}) \tag{5.24}$$

To find this reliability value in a specified confidence interval, first order reliability method (FORM) calculations are carried out using lower bound, mean and upper bound of the all limit state functions. Hence, reliability is calculated using a confidence bound of 95%.

In Figure 5.14, total instantaneous reliability of the system in a confidence interval of 95% is illustrated. Furthermore, total probability of failure of the system in a confidence interval of 95% is shown in Figure 5.15.

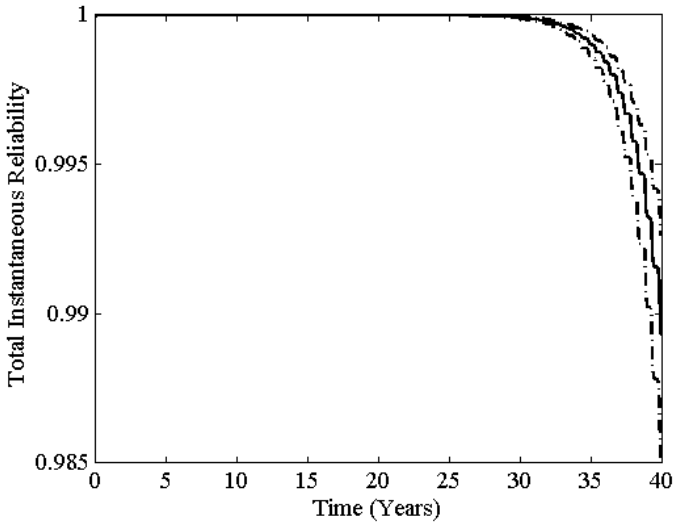

Figure 5.14: Total instantaneous reliability of the system (95% confidence interval)

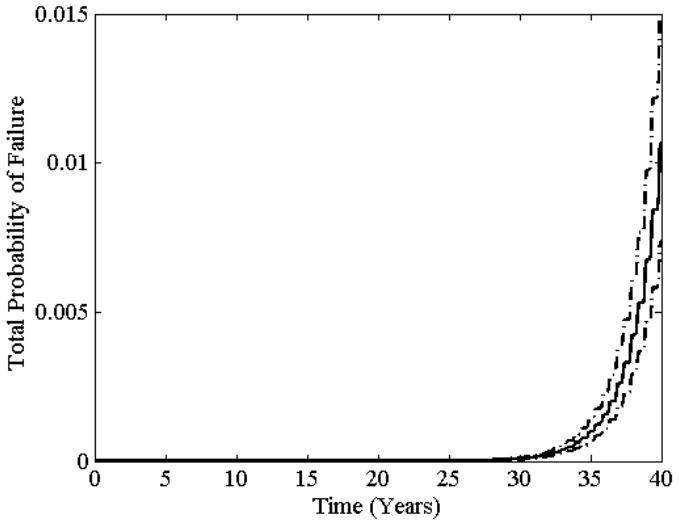

Figure 5.15: Total probability of failure (95% confidence interval)

Using these reliability and probability of failure expressions, a service life assessment of proposed solid rocket motor design can be made with defining an acceptable level of reliability. To set an example, typical reliability values taken from Reference [10] is used and listed in Table 5.1.

Table 5.1: Rocket reliability allocations [10]

System element	Reliability allocation
Rocket motor	0.985
Warhead structure	0.998
Explosive core assembly	0.993
Electrical	0.998
Fuse	0.995
Fin assembly	0.995
Fin release system	0.995

Using the typical reliability allocation value for the rocket motor, service life of the proposed design can be estimated as 40 years considering the lower bound value of the confidence interval. However, the reliability allocation values can change from design-to-design. More conservative allocations will give shorter service life estimations.

CHAPTER 6

DISCUSSION AND CONCLUSION

6.1 SUMMARY AND DISCUSSION

In this study, a methodology for the service life assessment of a solid rocket motor is presented. Using this methodology, it is aimed to assess the life of a solid rocket motor under environmental thermal and vibratory loads at the early design phases.

First, an introduction is made to explain the general characteristics of solid rocket motor systems and to state the motivation and scope of this study in detail. After this brief introduction, material behavior of solid propellants are explained in detail. Linear viscoelastic material models are used extensively for the solid propellants in literature, and several material characterization tests are made for utilizing this material models. Material tests that has been done for the characterization are explained in this study with giving references to test standards prepared from STANAG and ASTM. Strain outputs in the thermomechanical analyses are in the vicinity of %15-20, and comparing this strain level with the stress-strain curve of the propellant at room temperature shown in Figure 6.1, it is concluded that the linear material behavior assumption will not be true for the strain levels above %20-25.

Not only the constitutive stress-strain relationships, but the dynamic behavior is explained in detail as well. Using the outputs from the test data, master curves are utilized for the material properties which are used as inputs to finite element analyses. Master curves are utilized for the solid propellant since it is a thermorehologically simple material. Apart from the material behavior of viscoelastic solids, main degradation mechanisms in the solid propellants, namely the cumulative damage and aging phenomena are explained in detail. In this study, a linear cumulative damage model based on Miner's law is used for the representation of cumulative

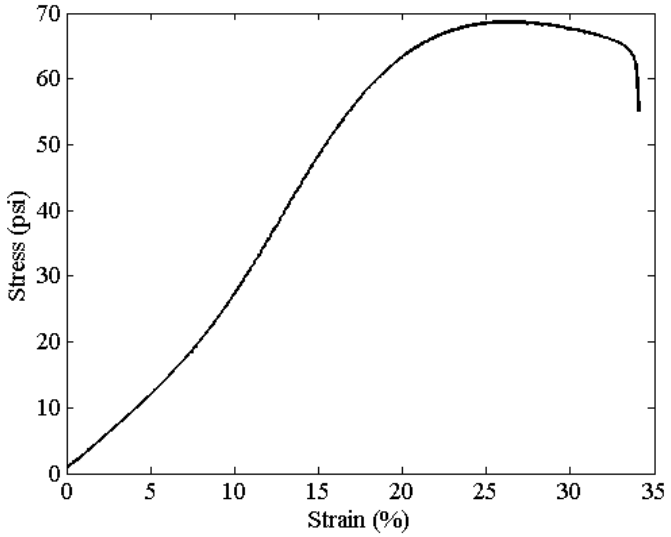

Figure 6.1: Stress-strain curve of the solid propellant at room temperature

damage and Layton model is used to account the aging. At the end of this chapter, a detailed survey summarizing the service life studies of solid rocket motors is given.

After explaining the nature of the solid propellant behavior, physical properties of the system are explained. Failure modes in propellant grain are explained and illustrated. In this study, formation of surface cracks and debonding of case-insulation-propellant bondlines are considered as failure modes. Then, thermal and vibratory loads that the solid rocket motor experience during its life and their random nature are mentioned. To account the statistical variability in these loads, random variables of the loading model are sampled and deterministic finite element analysis sets are utilized for the formation of mathematical models. The finite element analyses are conducted using commercial software tools, MSC.Marc and MSC.Nastran and results are illustrated. Critical sections in the propellant grain are determined using stress-strain output of finite element analyses.

Since the output of thermomechanical analyses have a harmonic response, fast Fourier transform is used in decomposing the harmonic amplitudes. These amplitudes are later used in formation of mathematical models using response surface methodology. To account the vibratory loads, power spectral density analysis is done and cumulative damage values for the different transportation scenarios are obtained. Using the outputs of fast Fourier transform and power spectral density analyses, response surfaces are utilized in a specified confidence

interval. Cumulative damages obtained from the thermal and vibratory loads are combined using damage factor approach and three limit state functions are considered to detect the failure in propellant grain. Using first order reliability method (FORM), hazard rates for the limit state functions are calculated, and instantaneous reliability for the system is obtained. Reliability of the system is calculated with a specified confidence limit interval. With specifying a reliability allocation limit, life of the solid rocket motor is estimated.

As mentioned, solid rocket motors indeed are very complicated designs. Hence, a methodology assessing the service life of such a design combines approaches from various disciplines. In the study presented, such a comprehensive methodology is carried out.

In this study, it is seen that cumulative damage due to environmental temperature is larger than the cumulative damage due to transportation loads and as time passes, cumulative damage effect of environmental temperature becomes dominant. It is also seen that the damage accumulated in sea transportation scenarios are negligible compared to ground and air transportation scenarios. To evaluate the total damage in the propellant grain, it is necessary to superpose the damage effects from thermal and vibratory loads. In Table 6.1, a comparison between the accumulated damages resulting from thermal and vibration loads are made.

Table 6.1: Total damage after 40 years of life cycle

Loading Type	Total Damage (%)
Thermal	20.79
Vibration	1.55

Inspecting the response surfaces that are prepared for storage and transportation response, it is observed that the correlation of the mathematical models that are prepared for storage analysis are better than the mathematical models prepared for the cumulative damage of transportation scenarios. One of the reasons is using a space filling technique in the sampling of storage analysis variables, namely latin hypercube sampling instead of box methods. Especially, lower damage values in transportation are predicted poorly, nevertheless, moderate and higher damage values are estimated accurately and the mathematical model is considered to be good enough. To increase the correlation in the response surfaces of transportation scenarios, nonlinear regression methods like artificial neural networks may be used in the formation of of response surfaces of transportation analyses.

It is also seen in this study that chemical aging is dominant at higher temperatures rather than lower temperatures. However, at lower temperatures, stress and strain is increasing in propellant grain which increases the cumulative damage. In other words, storing the rocket motor in a colder environment will decrease the effect of chemical aging but the cumulative damage will increase since the induced stress and strain in the propellant grain will be larger. Hence, to evaluate the contradicting effects of storage environment, developing a comprehensive methodology for the service life assessment becomes a need.

Final service life prediction is done using a reliability allocation value. This value specifies the reliability limit for the design and practically a design limitation. Higher reliability allocation values will give shorter but more conservative service life estimations.

6.2 RECOMMENDATIONS FOR FUTURE WORK

The methodology presented in this study gives an overview for the service life assessment of solid rocket motors. However, the approach can be further improved with additional efforts. Improvements that can be made are listed as follows.

- Throughout the study, a linear viscoelastic material model is used for the solid propellant and linear elastic material models are used for case and insulation. To predict the stress and strain response better in the propellant grain, a nonlinear viscoelastic material model can be used especially for high elongation solid propellants. To characterize the propellant as a nonlinear viscoelastic material, additional material tests are needed to be carried out like biaxial tensile and shear tests. Furthermore, a hyperelastic model can be utilized for the thermal insulation for a better prediction of stresses and strains in bondline of insulation and propellant. To use this methodology in composite case solid rocket motors, necessary tests are needed to perform to model the case as a composite material.

- A dilatation model can be utilized with a nonlinear viscoelastic material model as it is a common material behavior seen in solid propellants. Although, solid propellants are treated as incompressible materials in the literature with a Poisson ratio in order of 0.49 to 0.5 which is done for convenience, no measurement is performed generally [1]. It is the case in this study also. However, volume dilatation can be measured in uniaxial

tensile tests to determine the actual Poisson ratio of the material. Studies show that even small changes in Poisson ratio can vary the stress and strain response of propellant grain [56].

- Several failure criteria are used in this study to predict the crack formation and bondline separation. However, this is a conservative approach as not all the cracks mean failure in solid propellant grains. To assess the crack behavior in a more comprehensive way, fracture mechanics principles may be used which will require additional material testing to determine the stress concentration factors of the propellant. Several fracture mechanics approaches in determining the failure of solid rocket motors and material testing are given in References [57], [58] and [59].

- A rather recent technique in service life studies in the world is using stress sensors placed in the bondline of case, thermal insulation and propellant. With that, an experimental data is obtained and service life estimations are further improved using this data. Although, the sensors are expensive and several damage motors are needed to be utilized, assessment can be improved. One of the most recent study using this experimental approach can be found in Reference [60].

- Accelerated aging data is used for the propellant in this study and using the results of aging tests, Layton model is used for aging. Although accelerated aging models have a widespread usage in the literature, it is known that aging is a more complicated mechanism. Hence, to improve the aging model and service life assessment, natural aging data can be used especially in long lasting projects since natural aging tests takes time.

REFERENCES

[1] Advisory Group for Aerospace Research and Development (AGARD), *Structural Assessment of Solid Propellant Grains*, AGARD-AR-350, Dec. 1997.

[2] Davenas, A., et al., *Solid Rocket Propulsion Technology*, Pergamon Press, 1993.

[3] Advisory Group for Aerospace Research and Development (AGARD), *Design Methods for Solid Rocket Motors*, AGARD-LS-150, 1988.

[4] Caveny, L.H., Geisler, R.L., Ellis, R.A., Moore, T.L., *Solid Rocket Enabling Technologies and Milestones in the United States*, Journal of Propulsion and Power, Vol. 19, No. 6, pp. 1038-1066, 2003.

[5] Sutton, G.P., Biblarz, O., *Rocket Propulsion Elements, 7th Ed.*, John Wiley and Sons, 2001.

[6] Advisory Group for Aerospace Research and Development (AGARD), *Service Life of Solid Propellant Systems*, AGARD-CP-586, May 1996.

[7] Lakes, R.S., *Viscoelastic Solids*, CRC Press, 1999.

[8] Özgen, G.O., *ME 708 Techniques for Vibration Control and Isolation Lecture Notes*, Middle East Technical University, Fall 2010.

[9] Jones, D.I.G., *Handbook of Viscoelastic Vibration Damping*, John Wiley and Sons, 2001.

[10] Duerr, T.H., Marsh, B.P., *Solid Propellant Grain Structural Behavior and Service Life Prediction*, , Progress in Astronautics and Aeronautics, AIAA, Vol. 170, pp. 115-135, 1996.

[11] NATO Standardization Agency, *STANAG 4507 PCS (Ed. 1) Explosives, Physical/Mechanical Properties Stress Relaxation Test in Tension*, Jan. 2002.

[12] NATO Standardization Agency, *STANAG 4506 PPS (Ed. 1) Explosives, Physical/Mechanical Properties Uniaxial Tensile Test*, Mar. 2000.

[13] ASTM Standard E 831-03, *Standard Test Method for Linear Thermal Expansion of Solid Materials by Thermomechanical Analysis*, 2003.

[14] ASTM Standard E 1269-01, *Standard Test Method for Determining Specific Heat Capacity by Differential Scanning Calorimetry*, 2001.

[15] NATO Standardization Agency, *STANAG 4540 (Ed. 1) Explosives, Procedures for Dynamic Mechanical Analysis (DMA) and Determination of Glass Transition Temperature*, Aug. 2002.

[16] Ferry, J.D., *Viscoelastic Properties of Polymers, 2nd Edition*, John Wiley and Sons, 1970.

[17] National Aeronautics and Space Administration (NASA), *Solid Propellant Grain Structural Integrity Analysis, Space Vehicle Design Criteria SP-8073*, June 1973.

[18] Miner, M.A., *Cumulative Damage in Fatigue*, Journal of Applied Mechanics, Vol. 12, pp. 159-164, 1945.

[19] Bills, K.W., Herrmann, L.R., *Applications of Non-Linear Viscoelasticity and Cumulative Damage*, Aerojet Solid Propulsion Company, Report No: 1565-26-Q-1, 1970.

[20] Kunz R.K., *Characterization of Solid Propellant for Linear Cumulative Damage Modeling*, 45th AIAA/ASME/SAE/ASEE Joint Propulsion Conference and Exhibit, Denver, Colorado, AIAA 2009-5257, Aug 2009.

[21] Laheru, K.L., *Development of a Generalized Failure Criterion for Viscoelastic Materials*, Journal of Propulsion and Power, Vol. 8, No. 4, pp. 756-759, 1992.

[22] Layton, L.H., *Chemical Structure Aging Effects*, Air Force Rocket Propulsion Laboratory, Report No: AFRPL-TR-73-27, 1973.

[23] Christiansen, A.G., Layton, L.H., Carpenter, R.L., *HTPB Propellant Aging*, Journal of Spacecraft and Rockets, Vol. 18, p:211, 1981.

[24] Kivity, M., Hartman, G., Achlama, A.M., *Aging of HTPB Propellant*, AIAA/ASME/SAE/ASEE Joint Propulsion Conference, AIAA 2005-3802, 2005.

[25] Chappell, R.N., Jensen, F.R., *Statistical Service Life Prediction: Minuteman Third-Stage Propellant Grain*, ICRPG/AIAA Solid Propulsion Conference, Anaheim, Jun. 1967.

[26] Heller, R.A., Kamat, M.P., Singh, M.P., *Probability of Solid Propellant Motor Failure Due to Environmental Temperatures*, Journal of Spacecraft and Rockets, Vol. 16, No.3, pp. 140-146, 1979.

[27] Thrasher, D.I., Hildreth, J.H., *Structural Service Life Estimate for a Reduced Smoke Rocket Motor*, Journal of Spacecraft and Rockets, Vol. 19, No.6, pp. 564-570, 1981.

[28] Heller, R.A., Singh, M.P., *Thermal Storage Life of Solid-Propellant Motors*, Journal of Spacecraft and Rockets, Vol. 20, No.2, pp. 144-149, 1983.

[29] Zibdeh, H.S., Heller, R.A., *Rocket Motor Service Life Calculations Based on the First-Passage Method*, Journal of Spacecraft and Rockets, Vol. 26, No. 4, pp. 279-284, 1989.

[30] Janajreh, I.M., Heller, R.A., Thangjitham, S., *Safety Index Approach to Predicting the Storage Life of Rocket Motors*, Journal of Spacecraft and Rockets, Vol. 31, No.6, pp. 1072-1078, 1994.

[31] Heller, R.A., Thangjitham, S., Janajreh, I.M., *Probabilistic Service Life Prediction for Solid Propellant Motors Subjected to Environmental Thermal Loads*, AGARD CP-586, No.34, 1996.

[32] Margetson, J., Wong, F.C., *Service Life Prediction of Solid Rocket Propellant Motors Stored in a Random Thermal Environment*, AGARD CP-586, No.36, 1996.

[33] Collingwood, G. A., Clark, L. M., Becker, E. B., *Solid Rocket Motor Service Life Prediction Using Nonlinear Viscoelastic Analysis and a Probabilistic Approach*, AGARD CP-586, No.29, 1996.

[34] Akpan, U.O., Wong, F.C., *The Role of Probabilistic Sensitivity Analysis in Assessing the Service Life of Solid Rocket Motors*, 43rd AIAA/ASME/ASCE/AHS/ASC Structures, Structural Dynamics and Materials Conference, Apr 2002.

[35] Akpan, U.O., Dunbar, T.E., Wong, F.C., *Probabilistic Risk Assessment of Solid Propellant Rocket Motors*, Journal of Spacecraft and Rockets, Vol. 40, No. 3, 2003.

[36] Marotta, S.A., et. al., *Predicting Reliability of Tactical Missiles Using Health Monitoring Data and Probabilistic Engineering Analyses*, 5th International Workshop, Structural Health Monitoring, Stanford University, 2005.

[37] Hasanoğlu, M.S., *Storage Reliability Analysis of Solid Rocket Propellants*, M.Sc. Thesis, Middle East Technical University, Aug 2008.

[38] Kuran, B., Taşkınoğlu, E. E., Çiçek, B. C., *Effects of Vibration Loads on the Service Life of Solid Rocket Propellants*, SAVIAC, 81st Shock and Vibration Symposium, 2010.

[39] Yıldırım, H.C., *Stress Analysis of a Solid Propellant Rocket Motor*, M.Sc. Thesis, Bosphorus University, 2009.

[40] Yıldırım, H.C., Özüpek, Ş, *Structural Assessment of a Solid Propellant Rocket Motor: Effects of Aging and Damage*, Aerospace Science and Technology, 2011.

[41] Gligorijevic, N., et. al., *Structural Analysis Procedure for a Case Bonded Solid Rocket Propellant Grain*, Scientific Technical Review, Vol. 61, No. 1, 2011.

[42] MIL-STD-810G, *Environmental Engineering Considerations and Laboratory Tests*, Department of Defense, United States of America, 2008.

[43] Turkish State Meteorogical Service, http://mgm.gov.tr/veridegerlendirme/il-ve-ilceler-istatistik.aspx last viewed on 20.07.2012.

[44] AECTP 200, *Environmental Conditions (Ed. 3)*, NATO Standardization Agency, 2006.

[45] Myers, H.M., Montgomery, D.C., *Response Surface Methodology, Process and Product Optimization Using Designed Experiments, 2nd Ed.*, John Wiley and Sons, 2002.

[46] Choi, S., Grandhi, R.V., Canfield, R.A., *Reliability-based Structural Design*, Springer-Verlag London Limited, 2007.

[47] Reddy, J.N., *An Introduction to the Finite Element Method, 3rd Edition*, McGraw Hill, 2006.

[48] Herrmann, L.R., *Elasticity Equations for Incompressible and Nearly Incompressible Materials by a Variational Theorem*, AIAA Journal, Vol. 3, No. 10, pp. 1886-1900, 1965.

[49] MSC.Software Corporation, *MARC 2010 User's Manual Volume B: Element Library*, 2010.

[50] MSC.Software Corporation, *MSC.Nastran Version 70 Advanced Dynamic Analysis User's Guide*, 2004.

[51] Harris, F.J., *On the Use of Windows for Harmonic Analysis with the Discrete Fourier Transform*, Proceedings of the IEEE, Vol. 66, No. 1, pp. 51-83, 1978.

[52] Long, M.W., Narciso, J.D., *Probabilistic Design Methodology for Composite Aircraft Structures*, U.S. Department of Transportation Federal Aviation Administration, Report No: DOT/FAA/AR-99/2, 1999.

[53] Chapra, S.C., Canale, R.P., *Numerical Methods for Engineers, 5th Ed.*, McGraw Hill, 2006.

[54] Vittal, S., Hajela, P., *Confidence Intervals for Reliability Estimated Using Response Surface Methods*, 9th AIAA/ISSMO Symposium on Multidisciplinary Analysis and Optimization, AIAA 2002-5475, 2002.

[55] Haldar, A., Mahadevan, S., *Probability, Reliability and Statistical Methods in Engineering Design*, John Wiley and Sons, 2000.

[56] Chu, H.T., Chou, J.H., *Poisson Ratio Effect on Stress Behavior of Propellant Grains Under Ignition Loading*, Journal of Propulsion and Power, Vol. 27, No. 3, pp. 662-667, 2011.

[57] Francis, E.C., Jacobs, H.R., *Fracture Considerations for Surveillance Programs*, Journal of Spacecraft and Rockets, Vol. 13, No. 8, pp. 451-455, 1976.

[58] Ho, S.Y., Care, G., *Modified Fracture Mechanics Approach in Structural Analysis of Solid-Rocket Motors*, Journal of Propulsion and Power, Vol. 14, No. 4, pp. 409-415, 1998.

[59] Tussiwand, G.S., Saouma, V.E., Terzenbach, R., De Luca, L.T., *Fracture Mechanics of Composite Solid Rocket Propellant Grains: Material Testing*, Journal of Propulsion and Power, Vol. 25, No. 1, pp. 60-73, 2009.

[60] Brouwer, G.C.R., Tenden, S., Sollien, I., Ninive, A., Weterings, F.P. *Structural Assessment AP/HTPB Propellant Grains*, AVT - Symposium on Technical Advances and Changes in Tactical Missile Propulsion for Air, Sea and Land Application, RTO-MP-AVT-208, 2012.

APPENDIX A

MATERIAL PROPERTIES

Material properties that do not have any statistical variations are listed in Table A.1. In the table, properties of case, insulation and propellant are available.

Table A.1: Material properties

Parameter	Value
Case	
E_c, Young's Modulus	210000 MPa
ν_c, Poisson's Ratio	0.3
ρ_c, Density	7.85 g/cm^3
α_c, Coefficient of Thermal Expansion	10.8 μm/mm/°K
$C_{p,c}$, Specific Heat	0.46 J/g/°K
k_c, Thermal Conductivity	42.5 W/m^2/°K
Thermal Insulation	
E_t, Young's Modulus	11000 MPa
ν_t, Poisson's Ratio	0.3
ρ_t, Density	1.6 g/cm^3
α_t, Coefficient of Thermal Expansion	225.8 μm/mm/°K
$C_{p,t}$, Specific Heat	3.68 J/g/°K
k_t, Thermal Conductivity	0.36 W/m^2/°K
Propellant	
ν_p, Poisson's Ratio	0.5
ρ_p, Density	1.73 g/cm^3
$C_{p,p}$, Specific Heat	0.83 J/g/°K
k_p, Thermal Conductivity	0.61 W/m^2/°K

APPENDIX B

LATIN HYPERCUBE SAMPLING POINTS AND HISTOGRAMS

Sampled analysis sets for the thermomechanical finite element analyses that are being created using latin hypercube sampling method are given in Table B.1 and Table B.2. The values presented in tables are normalized values bounded in [-1,1].

Results of latin hypercube sampling algorithm can be further illustrated by utilizing histograms for each sampling variable are given in Figures B.1-B.5. For meaningful histogram graphs, an empirical relationship is used as shown [55].

$$k = 1 + 3.3log_{10}n \tag{B.1}$$

where k is the number of intervals and n is the number of samples which is fifty in this case. As a result of this empirical relationship, seven intervals are used for the histograms.

Table B.1: Sampled 50 analysis input sets (1-25).

Set	T_M	T_Y	T_D	E_0	CTE
1	-0.7264	-0.3142	-0.1588	-0.1256	0.8412
2	0.6342	0.2338	0.4556	0.5386	0.3984
3	-0.4826	0.2696	0.1642	0.4796	0.3524
4	-0.4742	0.6932	0.5122	-0.1768	-0.9008
5	-0.9990	0.9510	0.9604	0.1512	-0.5056
6	-0.1172	0.4070	-0.9296	0.8534	0.7864
7	-0.2564	-0.0130	-0.3290	0.2198	0.6140
8	-0.7160	-0.8196	0.0640	-0.3842	0.6658
9	0.4206	-0.7106	-0.6312	0.3118	0.0860
10	-0.1388	0.5304	-0.3136	-0.0054	-0.7418
11	-0.5268	0.7346	0.7836	0.9192	-0.7070
12	-0.3234	0.3500	-0.8560	-0.3174	0.4298
13	-0.5854	-0.1494	-0.7908	-0.0680	0.8352
14	-0.0524	0.7864	-0.5300	-0.3424	0.3184
15	-0.8986	-0.7322	0.2854	-0.8120	-0.0356
16	0.0316	-0.3250	-0.4272	-0.6818	0.1698
17	-0.9200	-0.9204	0.4010	-0.7942	-0.5920
18	0.8082	0.1630	-0.3674	0.9760	0.5424
19	-0.3748	0.0836	0.5514	0.0790	0.5170
20	-0.8006	-0.9752	-0.4526	0.4026	0.1538
21	-0.0286	0.1320	0.3300	0.5994	-0.1698
22	0.1912	-0.3868	-0.6948	0.4942	0.0368
23	0.6524	-0.8852	0.8958	0.8086	-0.3542
24	0.5902	0.8720	-0.0954	-0.9008	0.9938
25	0.7094	-0.6362	-0.2620	-0.6518	-0.2646

Table B.2: Sampled 50 analysis input sets (26-50).

Set	T_M	T_Y	T_D	E_0	CTE
26	0.2348	0.0444	-0.6554	0.3350	0.8988
27	0.8662	0.5848	0.0934	0.6230	-0.9676
28	0.0498	0.3900	-0.0406	-0.2620	0.4496
29	0.5244	-0.8642	-0.9126	-0.4476	-0.1446
30	0.4916	-0.2250	0.7460	0.0102	0.2740
31	0.3902	-0.2408	0.8114	-0.9286	-0.4182
32	0.9020	0.4872	0.5616	-0.8442	0.7328
33	0.9628	0.9792	-0.0202	0.7642	-0.6112
34	-0.4246	-0.4764	0.6534	-0.2330	-0.2250
35	-0.8504	0.6752	0.7028	0.3648	-0.4776
36	0.7348	-0.7978	0.3660	-0.4036	-0.9426
37	0.3322	-0.4370	-0.8262	0.0918	0.2122
38	-0.6562	0.4762	-0.7402	0.6734	0.5608
39	-0.1678	-0.0566	-0.1748	0.1666	0.0440
40	0.9478	0.0270	0.6126	0.7310	-0.3060
41	-0.7878	-0.5138	0.2360	0.9288	-0.7994
42	0.2948	-0.6780	0.0380	-0.5906	-0.8066
43	-0.6100	-0.1092	-0.9948	-0.9620	0.9396
44	0.1582	0.6126	-0.5860	0.6956	-0.0650
45	0.0988	0.2944	0.8556	-0.6358	-0.8720
46	-0.2870	-0.1726	0.2632	-0.7406	-0.5368
47	0.2592	-0.5892	0.1398	0.2596	-0.6422
48	-0.2348	-0.5264	-0.4866	-0.4902	-0.3808
49	0.7754	0.8896	0.9562	-0.5588	0.7146
50	0.4692	0.8364	-0.2274	-0.1032	-0.0946

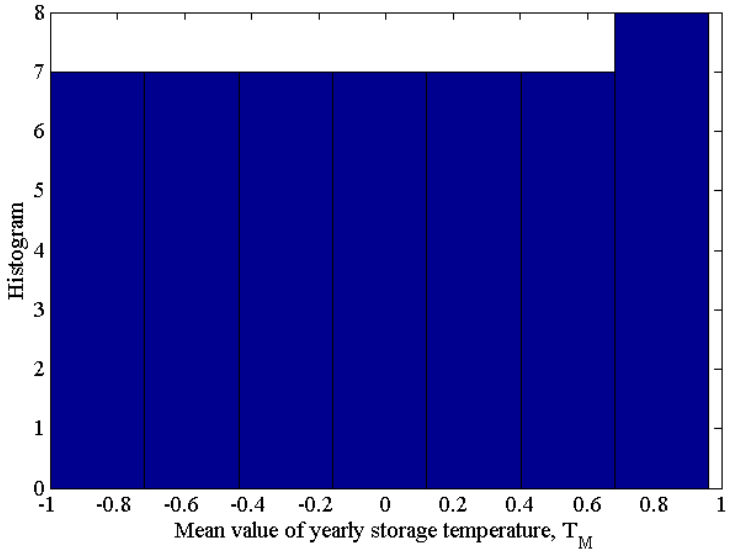

Figure B.1: Histogram of the mean temperature, T_M

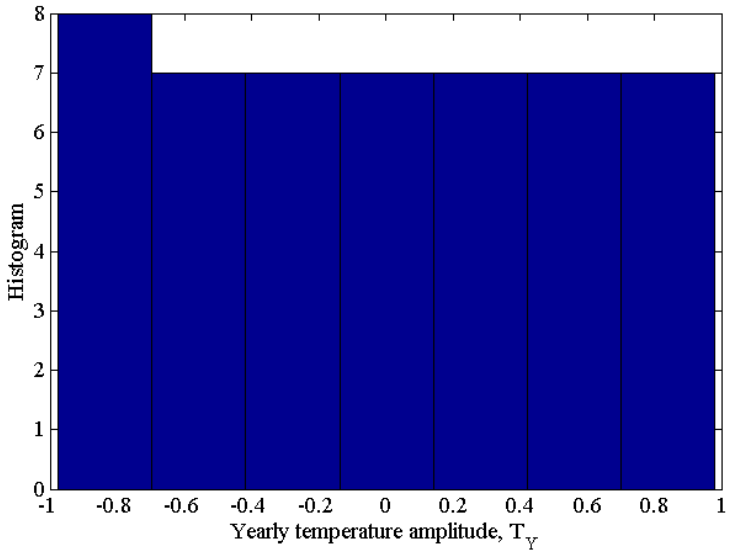

Figure B.2: Histogram of the yearly temperature amplitude, T_Y

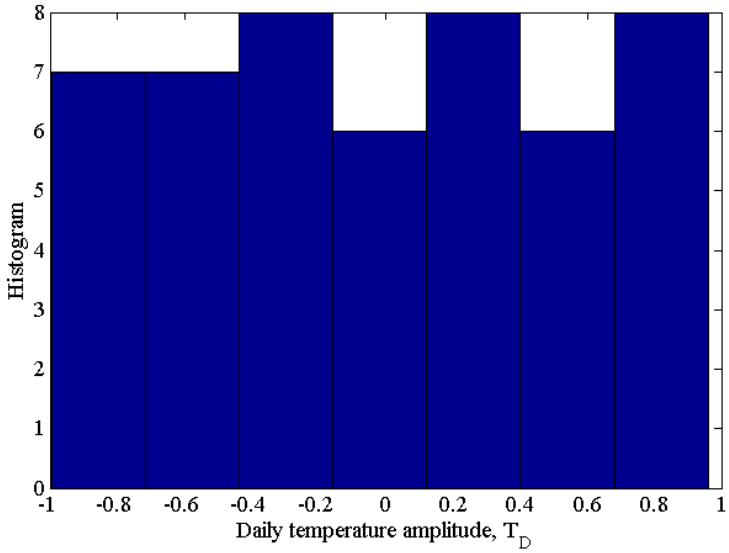

Figure B.3: Histogram of the yearly temperature amplitude, T_D

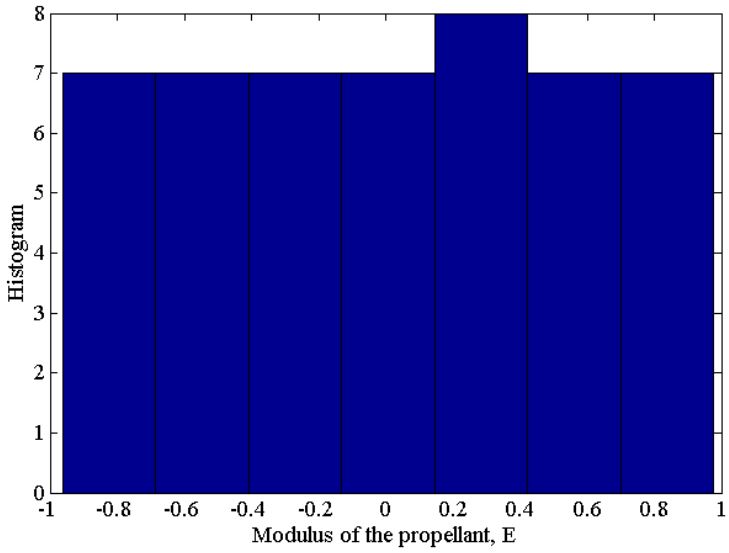

Figure B.4: Histogram of the modulus of the propellant, E

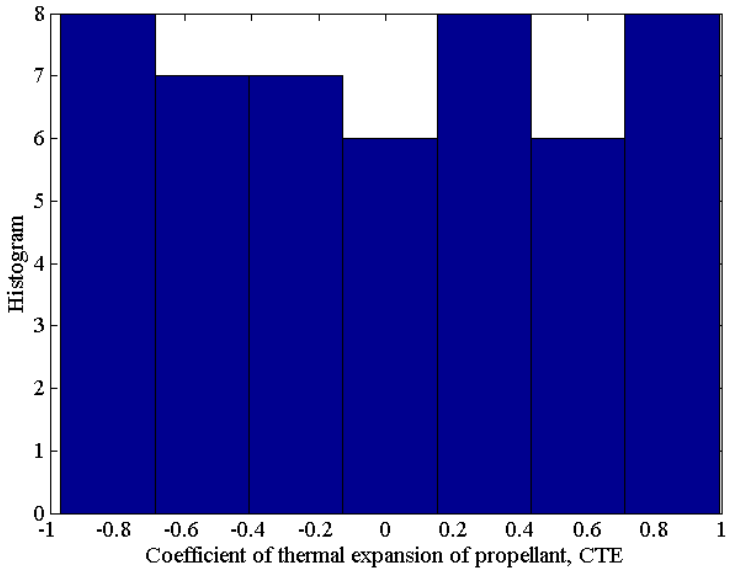

Figure B.5: Histogram of the coefficient of thermal expansion of the propellant, CTE